

AD-A154 074

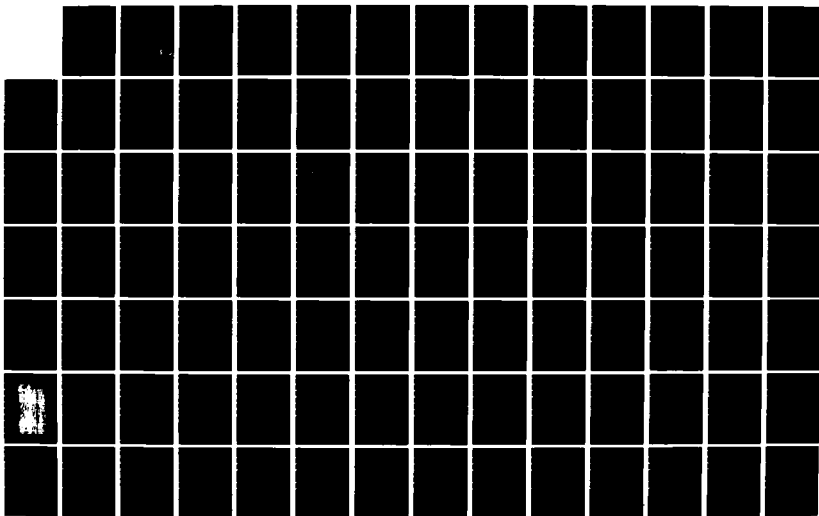
PHYSIOLOGICAL INFLUENCES ON TISSUE ELECTRICAL  
PROPERTIES IN SITU(U) GEORGIA INST FOR RESEARCH ATHENS  
E C BURDETTE ET AL. SEP 81 DAND17-78-C-8044

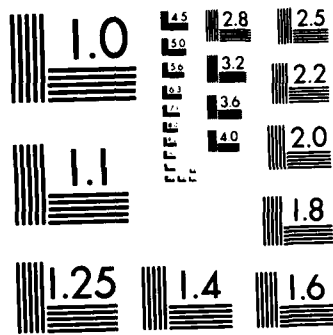
1/4

UNCLASSIFIED

F/G 6/16

NL





MICROCOPY RESOLUTION TEST CHART  
NATIONAL BUREAU OF STANDARDS-1963-A

Physiological Influences on Tissue Electrical Properties  
In Situ

①

Annual Report

E. C. Burdette  
P.G. Friederich  
A. R. Moser

September 1981

Supported by

U.S. ARMY MEDICAL RESEARCH AND DEVELOPMENT COMMAND  
Fort Detrick, Frederick, Maryland 21701-5012

Contract No. DAMD17-78-C-8044

Georgia Institute of Technology  
Georgia Tech Research Institute  
Atlanta, Georgia 30332

DTIC  
ELECTE  
MAY 22 1985  
S A D

DOD DISTRIBUTION STATEMENT

Approved for public release; distribution unlimited

The findings in this report are not to be construed as  
an official Department of the Army position unless so  
designated by other authorized documents

AD-A154 074

DTIC FILE COPY

| REPORT DOCUMENTATION PAGE  |                       | READ INSTRUCTIONS<br>BEFORE COMPLETING FORM   |
|--|-----------------------|---|
| 1. REPORT NUMBER   | 2. GOVT ACCESSION NO. | 3. RECIPIENT'S CATALOG NUMBER   |
| 4. TITLE (and Subtitle)<br>Physiological Influences on Tissue Electrical Properties In Situ  |                       | 5. TYPE OF REPORT & PERIOD COVERED<br>Annual Report<br>(1 July 80 - 30 Sept. 81)          |
| 7. AUTHOR(s)<br>E. C. Burdette<br>P. G. Friederich<br>A. R. Moser  |                       | 6. PERFORMING ORG. REPORT NUMBER  |
| 9. PERFORMING ORGANIZATION NAME AND ADDRESS<br>Georgia Institute of Technology<br>Georgia Tech Research Institute<br>Atlanta, Georgia 30332  |                       | 8. CONTRACT OR GRANT NUMBER(s)<br>DAMD17-78-C-8044  |
| 11. CONTROLLING OFFICE NAME AND ADDRESS<br>U.S. Army Medical Research and Development Command<br>Fort Detrick, Frederick, Maryland 21701-5012  |                       | 10. PROGRAM ELEMENT, PROJECT, TASK AREA & WORK UNIT NUMBERS<br>62777A.3E162777A878.BB.013 |
| 14. MONITORING AGENCY NAME & ADDRESS (if different from Controlling Office)  |                       | 12. REPORT DATE<br>September 1981   |
|  |                       | 13. NUMBER OF PAGES<br>96   |
|  |                       | 15. SECURITY CLASS. (of this report)<br>Unclassified                                      |
|  |                       | 15a. DECLASSIFICATION/DOWNGRADING SCHEDULE  |
| 16. DISTRIBUTION STATEMENT (of this Report)<br>Approved for Public Release; Distribution Unlimited   |                       |   |
| 17. DISTRIBUTION STATEMENT (of the abstract entered in Block 20, if different from Report)   |                       |   |
| 18. SUPPLEMENTARY NOTES  |                       |   |
| 19. KEY WORDS (Continue on reverse side if necessary and identify by block number)<br><u>In-Vivo</u> probe<br>Dielectric properties<br><u>In-Situ</u> tissues<br>Antemortem/Postmortem studies, Renal blood flow,<br>Electromagnetic energy,<br>Monopole antenna   |                       |   |
| 20. ABSTRACT (Continue on reverse side if necessary and identify by block number)<br>The overall objectives of this research investigation are to further develop and extend the capabilities of the recently-developed <u>in-vivo</u> probe measurement technique and to use this technique to study the possible effects of induced physiological changes on tissue dielectric properties. During the third year of the program, the research investigations performed included (1) dielectric measurement of renal tissue under controlled perfusion conditions, both <u>in-vitro</u> and <u>in-vivo</u> , (2) preliminary investigation of the |                       |   |

UNCLASSIFIED

SECURITY CLASSIFICATION OF THIS PAGE(When Data Entered)

(3) influence on these properties of  $\alpha$ -blocking drugs added to the perfusate, (3) characterization of renal pressure/flow relationship, (4) design and development of hardware for a fully automated data acquisition and processing system, and (5) development of software for statistical analysis of experimental results.

In addition to these investigations, a  $3/4\lambda$  monopole antenna over a ground plane designed for underwater operation was developed for use by Army personnel at the Walter Reed Army Institute of Research.

The in-vitro renal studies which were performed consistently showed a relationship between decreased renal flow and increased relative permittivity and conductivity, whereas increased renal flow produced the opposite effect on the dielectric properties. Cortex and medulla tissues exhibited changes in the same direction, although cortical changes were generally greater. Similar results were indicated by in-situ studies.

The data acquisition and logging system was upgraded to include 15 channels of signal-conditioning buffer amplifiers and a 10-position event marker, the output of which is routed through a multiplexing A/D converter capable of 20 kHz sampling to a Zenith-Heath WH-89 microcomputer with 300 kbytes available disk storage. Software will be developed to allow the WH-89 microcomputer to control the network analyzer system and to provide preliminary processing of experimental data. The system will also have a provision for communication between the microcomputer and the Georgia Tech Cyber 70/74 computer system.

Programs were developed on the Cyber 70/74 computer system to perform data processing and analysis, including baseline subtraction, averaging, and computation of linear correlation coefficients and correlation probabilities for pairs of variables. These programs were used for analysis of the measured physiological and dielectric data.

UNCLASSIFIED

SECURITY CLASSIFICATION OF THIS PAGE(When Data Entered)

Physiological Influences on Tissue Electrical Properties  
In Situ

Annual Report

E. C. Burdette  
P.G. Friederich  
A. R. Moser

September 1981

Supported by

U.S. ARMY MEDICAL RESEARCH AND DEVELOPMENT COMMAND  
Fort Detrick, Frederick, Maryland 21701-5012

Contract No. DAMD17-78-C-8044

Georgia Institute of Technology  
Georgia Tech Research Institute  
Atlanta, Georgia 30332

DOD DISTRIBUTION STATEMENT

Approved for public release; distribution unlimited

The findings in this report are not to be construed as  
an official Department of the Army position unless so  
designated by other authorized documents

|            |                                     |
|------------|-------------------------------------|
| SEARCHED   | <input checked="" type="checkbox"/> |
| SERIALIZED | <input type="checkbox"/>            |
| INDEXED    | <input type="checkbox"/>            |
| FILED      | <input type="checkbox"/>            |
| A-1        |                                     |



## FOREWORD

Research during the third year of this four-year program was conducted by personnel of the Biomedical Research Division of the Electronic and Computer Systems Laboratory of the Engineering Experiment Station at the Georgia Institute of Technology, Atlanta, Georgia 30322. Mr. F. L. Cain served as the Principal Investigator and Mr. E. C. Burdette served as the Associate Principal Investigator through 30 June 1981, and E. C. Burdette became Principal Investigator 1 July 1981. The program, which is sponsored by the U.S. Army Medical Research and Development Command, Fort Detrick, Frederick, Maryland 21701, under Contract No. DAMD17-78-C-8044, is designated by Georgia Tech as Project A-2171.

This Annual Technical Report covers work performed from 1 July 1980 through 30 September 1981. This work was made possible through the combined efforts of many people at the Walter Reed Army Institute of Research (WRAIR), at the Emory University School of Medicine, and at the Georgia Institute of Technology. The authors would especially like to thank Dr. L. E. Larsen and J. H. Jacobi at WRAIR and Dr. V. P. Popovic at the Emory University School of Medicine, all of whom contributed significantly to this research program.

In conducting the research described in this report, the investigator(s) adhered to the "Guide for the Care and Use of Laboratory Animals," prepared by the Committee on Care and Use of Laboratory Animals of the Institute of Laboratory Animal Resources, National Research Council (DHEW Publication No. (NIH) 78-23, Revised 1978).

## SUMMARY

The overall objectives of this research investigation are to further develop and extend the capabilities of the recently-developed in-vivo probe measurement technique and to use this technique to study the possible effects of induced physiological changes on tissue dielectric properties.

During the third year of this program, research investigations included (1) dielectric measurement of renal tissue under controlled perfusion conditions both in-vitro and in-vivo, (2) preliminary investigations of the influence of  $\alpha$ -blocking drugs added to the perfusate on renal dielectric properties, (3) characterization of renal pressure flow relationships, (4) design and development of hardware for a fully automated data acquisition and processing system, and (5) development of software for statistical analysis of experimental results.

In addition to these investigations, a  $3/4\text{-}\lambda$  monopole antenna over a ground plane designed for underwater operation was developed in response to a request from Army personnel at the Walter Reed Army Institute of Research.

Results of the in-vitro renal studies consistently showed a relationship between decreased renal flow and increased relative permittivity and conductivity, whereas increased renal flow produced the opposite effect on the dielectric properties. Cortex and medulla tissues exhibited dielectric changes in the same direction, although cortical changes were generally greater. Similar results were indicated by in-situ studies. However, the in-situ measurement results were less conclusive, due in part to a smaller data base and in part to less-refined experimental protocols.

The data acquisition and logging system was upgraded to include 15 channels of signal-conditioning buffer amplifiers and a 10-position event marker, from which the output signals are routed through a multiplexing A/D converter capable of a 20 kHz sampling rate and to a Zenith/Heath WH-89 microcomputer having 300 kbytes disk storage. Software will be developed during the fourth year research efforts to allow the WH-89

microcomputer to control the network analyzer system and to provide initial processing of measured data. The system will also have a provision for communication between the microcomputer/controller system and the Georgia Tech Cyber 70/74 computer system.

Programs were developed on the Cyber 70/74 computer system to perform most data processing functions, including baseline subtraction, averaging, and computation of linear correlation coefficients and correlation probabilities for pairs of variable. These programs were used for the analysis of the measured renal physiological and dielectric property data.

TABLE OF CONTENTS

| <u>Section</u>  | <u>Page</u> |
|---|-------------|
| I. INTRODUCTION. . . . .  | 1           |
| A. Research Objectives . . . . .  | 1           |
| B. Summary of Research Performed . . . . .                                    | 2           |
| II. MONOPOLE ANTENNA DEVELOPMENT. . . . .                                     | 12          |
| A. Prototype Scale Model Design. . . . .                                      | 12          |
| B. Fabrication and Performance Testing of Final<br>Antenna . . . . .          | 26          |
| III. DATA ACQUISITION AND ANALYSIS . . . . .                                  | 29          |
| A. Data Acquisition - Technical Considerations . . . . .                      | 29          |
| B. Microcomputer-Based Data Acquisition System<br>Investigation . . . . .     | 30          |
| C. Current Data Acquisition System Design. . . . .                            | 31          |
| D. Data Analysis . . . . .  | 36          |
| IV. EXPERIMENTAL INVESTIGATIONS . . . . .                                     | 42          |
| A. Surgical Procedures . . . . .  | 42          |
| B. Perfusion Pressure, Renal Flow, and Kidney Weight<br>Measurements. . . . . | 49          |
| C. Renal Dielectric Property Studies . . . . .                                | 55          |
| V. CONCLUSIONS AND RECOMMENDATIONS . . . . .                                  | 78          |
| A. Conclusions from Results. . . . .  | 78          |
| B. Recommended Future Efforts. . . . .  | 81          |
| VI. REFERENCES. . . . .   | 83          |

## LIST OF FIGURES

| <u>Figure</u>   | <u>Page</u> |
|---|-------------|
| 1. Simplified diagram of instrumentation for amplitude and phase measurements of small antennas. . . . .  | 14          |
| 2. Antenna configuration for experimental measurements on phase center range showing directions of position adjustments . . . . .   | 16          |
| 3. Theoretical results of principal plane elevation cuts taken from ideal $3/4\text{-}\lambda$ monopoles over an infinite ground plane (solid line) and a finite ground plane of several $\lambda$ diameter (broken line). The phase patterns are identical . . . . . | 18          |
| 4. Principal plane elevation cut at 3.06 GHz of $3/4\text{-}\lambda$ monopole over $8\lambda$ diameter ground plane . . . . .   | 19          |
| 5. Principal plane elevation cut for three axial displacements at 3.06 GHz . . . . .  | 20          |
| 6. Principal plane elevation cut for three lateral displacements at 3.06 GHz . . . . .  | 21          |
| 7. Principal plane elevation cuts at three different frequencies. . . . .   | 22          |
| 8. Schematic illustration of $3/4\text{-wavelength}$ ( $3/4\lambda$ ) monopole antenna designed for underwater operation showing configuration of $1/4\lambda$ impedance-matching transformer . . . . .   | 25          |
| 9. Measured reflection coefficient magnitude of $3/4\text{-wavelength}$ monopole antenna in water plotted as a function of frequency. . . . .   | 28          |
| 10. Block diagram of the new Zenith/Heath WH89-based data acquisition and processing system to be used in subsequent experiments . . . . .  | 32          |
| 11. Typical input signals to be monitored during an experiment with the new data acquisition system. . . . .  | 33          |
| 12. Block diagram of the signal conditioning hardware used to convert various transducer outputs into uniform inputs to the data processing system. . . . .   | 35          |

LIST OF FIGURES

Continued

| <u>Figure</u>   | <u>Page</u> |
|---|-------------|
| 13. Example printout of results computed using the averaging program discussed in text. . . . .   | 39          |
| 14. Example printout of results from linear correlation program.  | 41          |
| 15. Diagrammatic illustration of experimental setup used for perfusion during <u>in-vitro</u> renal dielectric measurements. . .                            | 44          |
| 16. Two anatomical views of kidney . . . . .  | 46          |
| 17. Diagram of extracorporeal perfusion circuit used for control of renal blood flow during <u>in-situ</u> renal dielectric property measurements . . . . . | 48          |
| 18. Flow rate vs. perfusion pressure and vs. pump speed for Kidney #1. . . . .  | 50          |
| 19. Flow rate vs. perfusion pressure and vs. pump speed for Kidney #3. . . . .  | 51          |
| 20. Flow rate vs. perfusion pressure and vs. pump speed for Kidney #4. . . . .  | 52          |
| 21. Flow rate vs. perfusion pressure and vs. pump speed for Kidney #5. . . . .  | 53          |
| 22. Flow rate vs. perfusion pressure and vs. pump speed for Kidney #6. . . . .  | 54          |
| 23. Relative dielectric constant and conductivity of renal tissue measured as a function of perfusion pressure. . . . .                                     | 56          |
| 24. Amplitude and phase of complex reflection coefficient of medulla tissue measured <u>in-vitro</u> in isolated, perfused kidney . . . . .                 | 57          |
| 25. Averaged, baseline-subtracted dielectric properties as a function of flow rate in Kidneys 1-4 . . . . .   | 61          |
| 26. Averaged, baseline-subtracted dielectric properties as a function of perfusion pressure in Kidneys 1-4. . . . .   | 62          |

LIST OF FIGURES

Concluded

| <u>Figure</u> |  | <u>Page</u> |
|---------------|--|-------------|
| 27.           | Average changes in perfusion pressure and kidney weight as functions of flow rate while measuring dielectric properties of cortex and medulla tissues in Kidneys 1-4. . . . .        | 63          |
| 28.           | Baseline-subtracted dielectric properties as a function of flow rate in Kidney #6. . . . .   | 69          |
| 29.           | Baseline-subtracted dielectric properties as a function of perfusion pressure in Kidney #6 . . . . .   | 70          |
| 30.           | Changes in perfusion pressure and kidney weight as functions of flow rate while measuring dielectric properties of cortex and medulla tissues in Kidney #6. . . . .                  | 71          |
| 31.           | Comparison of baseline-subtracted dielectric properties of renal cortex in Kidney #5 under varying flow conditions, before and after administration of phenoxybenzamine . . . . .    | 73          |
| 32.           | Comparison of baseline-subtracted dielectric properties of renal cortex in Kidney #5 under varying perfusion pressures before and after administration of phenoxybenzamine . . . . . | 74          |
| 33.           | Changes in perfusion pressure and kidney weight as functions of flow rate in Kidney #5, before and after administration of phenoxybenzamine . . . . .                                | 75          |

LIST OF TABLES

| <u>Table</u> |  | <u>Page</u> |
|--------------|--|-------------|
| I.           | RENAL CORTEX PROPERTIES VS. FLOW RATE . . . . .  | 59          |
| II.          | RENAL MEDULLA PROPERTIES VS. FLOW RATE . . . . .   | 60          |
| III.         | CORRELATION COEFFICIENT AND PROBABILITIES FOR CORRELATION . .                            | 65          |
| IV.          | <u>IN-SITU</u> RENAL DIELECTRIC PROPERTIES UNDER VARIED PERFUSION<br>CONDITIONS. . . . . | 77          |

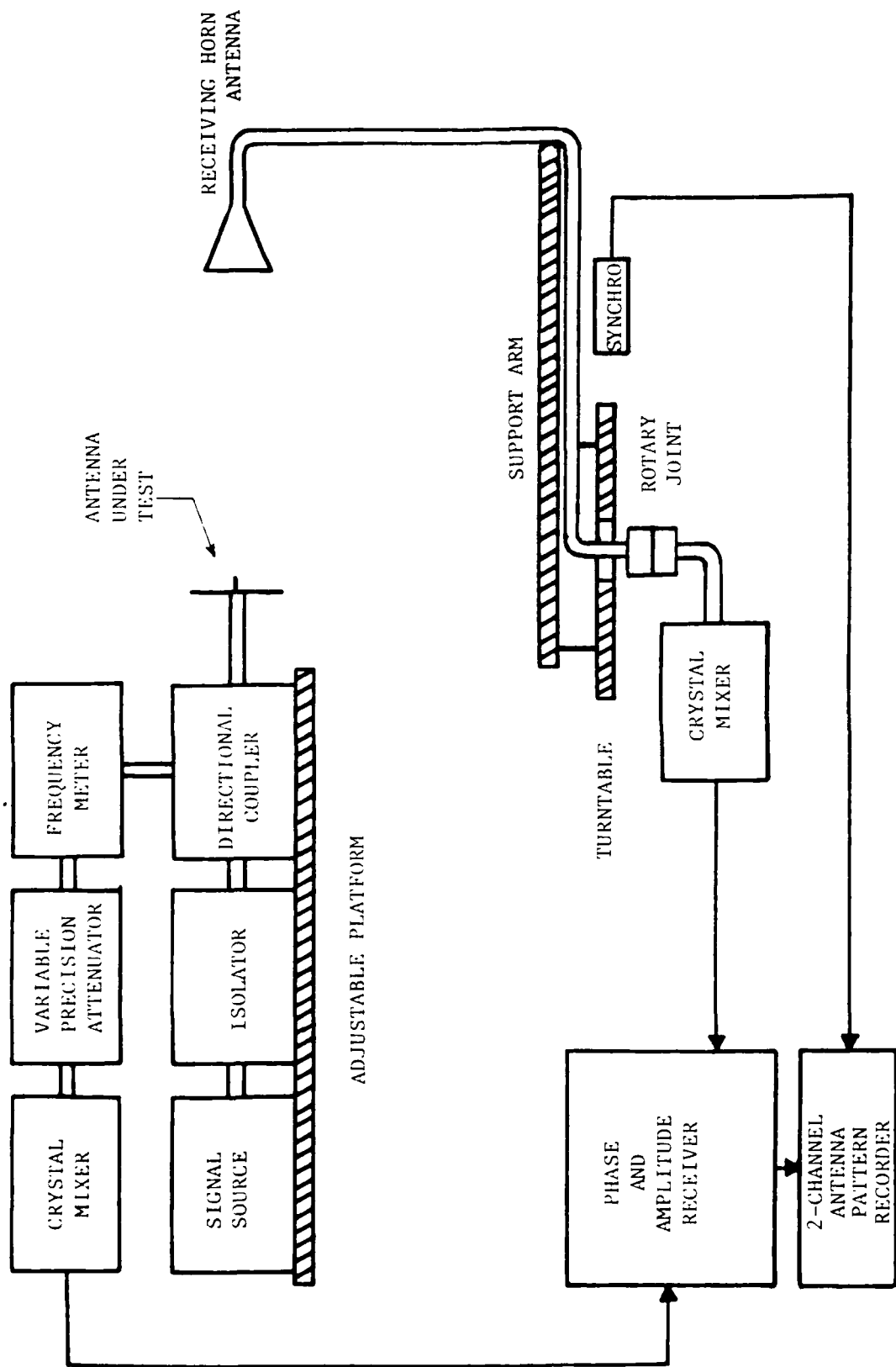


Figure 1. Simplified diagram of instrumentation for amplitude and phase measurements of small antennas.

a length of the cable's center conductor exposed by removing the copper outer conductor and Teflon dielectric. The first model measured had 2.5 cm of center conductor exposed ( $1/4 \lambda$  at 3.0 GHz), and no ground plane was attached. A 24-cm radius circular ground plane was fashioned from tin-plated steel, which was then welded to a brass sleeve that fit tightly around the outer conductor of the cable. This arrangement constituted the second version. The center conductor was trimmed to adjust the resonant frequency to a value near 3.0 GHz, as determined with a HP-8410S Network Analyzer. A third version of the antenna consisted of the second version with the ground plane extended to a 40-cm radius. In both the second and third versions, the ground plane was flush with the junction of the antenna feed and the exposed center conductor (at the base of the monopole).

The instrumentation arrangement which was used to record the antenna amplitude (radiation) and phase patterns is shown in Figure 1. As shown in the figure, part of the signal from the power source is routed to the phase-amplitude receiver as a required reference signal for the receiver, and the other part is routed to the transmitting antenna under test. The signal from the receiving horn is routed through a rotary joint to the other input port of the phase-amplitude receiver.

The radiation pattern of the transmitting antenna is recorded by rotating the receiving horn in a circular arc around the transmitting antenna in the horizontal plane. The received signal is amplified by the phase-amplitude receiver, and the output signal is recorded on a rectangular antenna pattern recorder.

The phase center of the transmitting antenna is located by adjusting the position of the antenna to obtain the best response possible. This response is obtained when the rotating receiving horn antenna is on a constant phase surface of the transmitting antenna; consequently the comparison of the two signals by the phase-amplitude receiver produces an output signal which is proportional to any phase difference between the two input signals. The receiver phase output signal is recorded on an X-Y recorder. The recorder is driven in synchronism with the rotating receiving horn; therefore, the phase pattern is recorded as a function

## SECTION II

### MONOPOLE ANTENNA DEVELOPMENT

In ongoing research efforts being conducted at the Walter Reed Army Institute of Research, Army personnel identified a need for a small antenna, suitable for operation underwater, whose radiation pattern was well characterized in amplitude and phase. Ideally, a point source antenna would be utilized because of its omnidirectional radiation pattern and uniform spherical phase. In practice, it is not possible to fabricate an antenna with point-source characteristics. However, it is possible to design and fabricate an antenna with known radiation characteristics which can be accurately documented. It was determined that a 3/4-wavelength monopole over a finite ground plane would have a radiation pattern which would be a reasonable compromise with respect to the desired radiation characteristics. If the amplitude and phase characteristics of a 3/4-wavelength monopole were sufficiently documented, such an antenna would likely be a suitable substitute.

#### A. Prototype Scale Model Design

The monopole antenna was designed for operation in an aqueous medium. Since adequate test facilities for antenna radiation pattern and phase characterization in an aqueous medium were not available, it was decided to build a scale model to be characterized in air. The patterns obtained from the scale model could then be applied to the antenna designed for operation in water. The scale factor for such a model depends on the ratio of wavelengths in the two media being compared, which in turn depends on the square root of the ratio of the relative permittivities (assuming that both media are non-magnetic). If a value of 77.4 is accepted for the relative permittivity of water at 22°C [7,10], and air is equated with free space, one obtains a scaling factor of 8.8. Thus, dimensions of the scaled model in the air medium should be 8.8 times the equivalent dimensions of the working antenna in the water medium.

Scale models for measurement in air were constructed from 0.141-inch diameter semi-rigid coaxial cable. The coaxial cable comprised both the antenna feed and the antenna itself, which consisted simply of

a good cortical response to the sensory stimuli. The use of a different anesthetic agent (halothane gas anesthesia or  $\alpha$ -chloralose plus ethane) and improved auditory stimulation (possibly loud clicks) should correct the problem, thus permitting evaluation of the effect of sensory stimulation on the dielectric properties of canine cortex.

In the following sections of this report, the investigations performed during the period 1 July 1980 through 30 September 1981 are detailed. Section II describes the design of a monopole antenna for use under water. Section III describes the development of a microcomputer-based 16-channel data acquisition system and the algorithms developed for data analysis. In Section IV, the experimental investigations are described and results therefrom presented. Conclusions from results and recommendations for future studies are presented in Section V.

controlled conditions of flow rate and arterial pressure. A  $K^+ - Mg^{2+}$  rich solution (composition in mM: NaCl, 96.2; KCl, 40.3;  $CaCl_2$ , 1.7;  $MgSO_4$ , 12.5;  $NaHCO_3$ , 11.9; glucose, 11.1; hydroxyethyl starch 30g/liter) was used as the perfusate for all in-vitro experiments. The data collected during this reporting period from in-vitro measurements of isolated, perfused kidneys indicated that the quantities of flow rate/perfusion pressure have an inverse relationship with the electrical properties of conductivity and relative permittivity.

The inverse dielectric/flow relationship observed during our in-vitro measurements of dog kidneys appears contrary to what one would expect from simple bulk water effects. That is, if increased renal flow caused an increased presence of bulk water, one would expect a corresponding rise in the measured components (and in the computed dielectric properties) rather than the decrease which actually occurred. Thus, these results obtained using the probe measurement technique suggest that the pressure-flow-volume relationship in the kidney is not a simple one, and that redistribution of flow within the renal vasculature would likely influence local renal dielectric properties. Therefore, it is important that techniques be developed for multiplexing dielectric information measured simultaneously using multiple probes in different spatial locations. Further, bulk water shifts may not be the only influencing factor in the measured dielectric changes. The use of the probe measurement technique offers the advantage that measurements could be performed at both RF and microwave frequencies, possibly elucidating effects due to changes in protein conformation or fluid compartment shifts.

In a limited study of the effects of acoustical stimulation on dielectric properties of the auditory cortex in dogs, no correlation between acoustic stimuli and dielectric property changes was observed. However, this lack of effect does not necessarily mean that no correlation exists because the cortical EEG recordings taken during auditory stimulation showed no change in the electrical activity of the auditory cortex. It is believed that the problem was due to the CNS depressant effects of anesthesia used (pentobarbital sodium in most trials) on higher cortical centers and to the use of non-optimal auditory stimulation, thus preventing

vein. All dielectric and cardiovascular physiological parameters were monitored for 90 minutes postmortem, with death being defined to be the time at which all systemic pressures were zero. A comparison of results obtained with KCl sacrifice to those obtained with  $\text{CaCl}_2$  sacrifice can be found in Tables II and III in Section III of Annual Technical Report No. 2 [9]. The overall trend in both groups is similar. Both conductivity and dielectric constant gradually decrease as a function of time postmortem. However, in cases of  $\text{CaCl}_2$  sacrifice, the values peak immediately upon intravenous injection and change more than in the KCl cases. While nominal values for the dielectric constant are about 57 in both cases, the  $\text{CaCl}_2$  sacrifice results in an increase to about 62.3, or a change of approximately 10%. This peak occurs from 6-10 seconds before systemic pressures reach zero. This indicates that the  $\text{CaCl}_2$  injection causes a stronger and more abrupt change in blood flow to the brain, as would be expected from the different mechanisms by which the  $\text{K}^+$  and  $\text{Ca}^{2+}$  ions cause death.

Studies of the effects of changing renal blood flow on the dielectric properties of kidney cortex and medulla were performed during this reporting period. A decrease in total renal flow consistently produced an increase in both relative dielectric constant and conductivity, and an increased renal flow produced the opposite results. Measurements on renal tissue were performed both in-situ in living dogs and in-vitro using isolated, perfused kidneys. Measured renal dielectric changes were usually in the same direction in both the cortex and medulla, with the greater change being observed in the cortex. The procedure for measuring dielectric properties of renal tissue was outlined in Annual Technical Report No. 2 [9]. The kidneys were surgically removed and placed on an in-vitro perfusion circuit. Care was taken to minimize the time between cessation of the normal blood flow and initiation of in-vitro perfusion. In most cases, this time was five minutes or less, and the greatest interval was ten minutes. Following initiation of in-vitro perfusion, the kidney's dielectric properties were measured using the probe dielectric measurement technique. The dielectric properties were measured under varying

In order to meet the expense constraint, three systems in the prospective price range were considered; the PET, APPLE II, and Zenith-Heathkit WH-89 microcomputers. In addition, an existing Intecolor 8052 microcomputer previously purchased with internal funds, and which could be shared with other projects, was considered.

Among the microcomputers considered, the Zenith/Heathkit WH-89 appeared to be the best choice. Its advantages included two Z-80 microprocessors (as opposed to a single MCS-6502 in the PET and APPLE and an 8080A in the Intecolor computer). One of the Z-80s in the WH-89 is used as the CPU, the other is used as the controller for a "smart" terminal. In addition, the WH-89 has the most versatility for input/output functions. However, the PET and APPLE computers do have commercially available IEEE interfaces, whereas the Heathkit WH-89 and Intecolor do not. During the latter portion of the third year of this research program, internal funds were made available for purchasing the Zenith/Heathkit WH-89 microcomputer system. Funds from this program were used to purchase external dual floppy disk drives for use with the microcomputer system. This computer system is presently being interfaced to the network analyzer system.

Studies of antemortem/postmortem dielectric property changes in dog brain were conducted during the second year, and a limited investigation of vascular effects on measured in-situ tissue impedance was performed. Each of the antemortem/postmortem experiments involved measurement of the in-situ dielectric properties of dog brain with the dura mater and arachnoid removed and the probe placed directly on the pia mater over the ectosylvian gyrus. All dielectric measurements were performed as a function of time at a frequency of 2450 MHz using a 2.1-mm diameter probe.

In-situ dielectric measurements were performed over a two-hour period. Both dielectric property data and physiological data were recorded for 30 minutes prior to sacrificing the animal. This ensured physiological stability of the animal and permitted recording in-situ dielectric data under conditions of homeostasis. Sacrifice was performed by injecting a 25 cc bolus of saturated KCl or CaCl<sub>2</sub> into the femoral

physiological parameters were also recorded in analog form. Recording data in this manner permitted both on-line digital dielectric property computations and continuous monitoring of dielectric parameters during periods of rapid physiological change. Further, it was not necessary to time-lock the digital sampling of dielectric data to the respiratory cycle of the animal because of the correlated continuous analog recording of dielectric property data.

The method described above for acquiring and storing data involves recording the physiological signals on a strip chart recorder and recording the measured dielectric property information in digital form using a Hewlett-Packard semi-automated network analyzer system. In order to analyze the data and correlate the different signals, data must be tabulated on a point-by-point basis and then transcribed to data cards for a computer analysis. This manual method of data logging was found to be both time consuming and tedious, and thus formed a practical limitation to the extent of the actual analysis of the data (and to the number of experiments which could be performed and analyzed).

The improvement to the data acquisition and logging system investigated during the third year involved the implementation of a microcomputer-controlled multiplexing A/D system and storage of the data on magnetic disks. The system has sixteen (16) data channels capable of being sampled at a variable, computer-controlled rate. These 16 analog signals along with a time frame marker will be recorded on magnetic disk. The data stored on disk will be in the proper form for detailed correlation analyses by the microcomputer or, if necessary, for transfer to a large mainframe computer where a more detailed analysis may be undertaken. An additional feature considered for incorporation within this system was an IEEE-STD-488 interface to allow control of the network analyzer used for acquiring dielectric data.

The primary constraints on the system were (1) the ability to sample data at rates up to 20 kHz, (2) data storage for the duration of one experiment (300 kBytes disk storage), (3) enough computing power to implement some real-time data reduction, and (4) the funds limitation under the present contract. The final system configuration is presented and discussed in Section III.

The first approach involved the use of an active filter to remove high frequency noise from the phase signal. However, filtering of noise in this manner both added complexity to the measurement system and reduced the maximum data sampling rate. The second approach utilized a software filtering technique in which the reflection coefficient phase data were multiply sampled at each frequency of interest and the statistical mean of these samples was computed and stored. In this manner, the actual data sample rate was not affected and no additional hardware was required. The software filter greatly reduced the noise present in the phase measurement of small complex reflection coefficients.

The Commodore PET microcomputer initially used with the probe dielectric measurement system for control and data acquisition purposes lacked sufficient memory to permit storage of computed dielectric property data for the duration of an experiment. Several possible solutions to the need for an increased data storage capability were examined, and the necessity for time-locking data sampling to the respiratory cycle of the animal was evaluated. The primary question concerned selection of a digital sampling frequency high enough to record the rapid dielectric and physiological changes which occurred immediately upon terminating the animal. However, it was also noted that throughout most of the period during which experimental data were recorded, those changes took place very slowly. Although the optimal solution would be the use of a digital recording system which automatically increased sampling frequency at the onset of a physiological change, it was determined that by recording the dielectric property data in both analog and digital form, it was possible to record the more rapid dielectric property changes in analog form, permitting the use of a slower digital sampling rate. Two modifications to the recording methodology were incorporated. The Commodore PET microcomputer (8 kBytes memory) was replaced by a Hewlett-Packard 9835A Desktop Computer (48 kBytes memory). The additional memory in the HP-9835A provided adequate data storage for sampling dielectric property data at a rate of one point per minute during a ninety-minute experiment. Simultaneous with digital recording of dielectric property data, the amplitude and phase of the complex reflection coefficient and various

time after death were performed both in brain and on the pial surface in separate experiments.

During studies of antemortem/postmortem dielectric changes in dog brain, it was determined that probe contact pressure on the tissue was also a factor in the accuracy and repeatability of measured results. Following cessation of blood flow, the brain receded slightly into the skull, resulting in a change in probe contact pressure and a concomitant change in measured dielectric properties. A six percent maximum change in dielectric constant was measured between the conditions of initial probe contact with the pia and an applied pressure producing a 0.4-cm depression of the pia using a 2.1-mm diameter probe. An approximate change of four to five percent in conductivity was also observed under the above stated probe contact conditions. To minimize these effects of probe contact pressure on measured tissue dielectric characteristics, in the second year of the program a mechanical "spring-loaded in-situ probe holder" was designed to maintain the probe contact on the tissue at a constant or nearly constant pressure. The contact force and therefore, contact pressure of the probe with the tissue is determined by the spring constant. Springs were selected which provided sufficient tension for maintaining consistent uniform probe/tissue contact over a probe travel distance of one inch. Using the spring-loaded probe holder, the probe contact induced variations in measured in-situ dielectric properties were on the order of one percent. During the third (current) year's efforts, the spring-loaded probe holder design was modified to permit the use of a single spring. The ability to follow tissue movements either pushing against or moving away from the in-situ probe was maintained.

Methods for further reducing systemic measurement errors associated with the microwave network analyzer were investigated during the second year [9]. Following implementation of the vector measurement error correction model during the first year of the program, the only remaining systemic measurement error source of significance was noise present in the measurement of the phase angle of small-magnitude reflection coefficients. Two approaches to the solution of this problem were examined.

through measurements of terminations (short circuits, open circuit, and a sliding matched load) for which the reflection coefficients are known. From these measurements, the error terms are computed using the error correction model and the measured tissue sample data are corrected to account for the systemic measurement errors.

The semi-automated microprocessor-based dielectric property data acquisition system was upgraded during the first year of the program [5]. Specifically, a digital frequency locking capability was added to the system, an external keyboard/printer was interfaced, and the computer algorithm was rewritten to increase system flexibility and to accommodate additional system hardware. Reflection coefficient data from test samples measured by the probe are automatically collected and processed, and corrected dielectric property information outputted. Measurements may be made either over swept frequency bands between 0.11 GHz and 10 GHz or as a function of time at a single frequency.

Effort was also directed toward the evaluation of the effects of fluid accumulation in the vicinity of the probe. Excessive fluid accumulation affects both the accuracy of the dielectric measurements and the repeatability of the measurements. It was determined that fluid accumulation around the probe did not appreciably effect the results of dielectric measurements of high-loss tissues (muscle, kidney). However, significant effects of fluid accumulation were observed in the results of measurements on relatively low-loss tissues (fat). After investigating several methods of preventing the fluid accumulation, a simple approach was developed which yielded accurate and consistent results.

Preliminary in-situ measurements of living and non-living brain and of in-vivo dielectric properties of brain under conditions of induced physiological change were also performed as a part of the first-year efforts. All measurements were performed at a frequency of 2450 MHz using a probe having a diameter comparable to that of a 16-gauge hypodermic needle. In-situ dielectric measurements of both living and non-living canine brain were performed on the dura, on the pia, and in gray and white matter. Measurements of dielectric properties as a function of

investigation of renal dielectric properties under conditions of altered renal blood flow, and initial studies of acoustical stimulation effects on auditory cortex dielectric properties were performed.

The first year of the present 3-year effort was largely devoted to refinement of the in-situ probe measurement technique. Under previous research efforts [5,9], it was determined that probe positioning was a critical factor in the performance of accurate in-vivo dielectric measurements. Further, it was determined that positioning of the probe needed to be made more compatible with measurement conditions associated with animals larger than mice or rats, which were positioned beneath a fixed measurement probe. Several alternative methods involving the use of semi-rigid or flexible coaxial cable attached to the in-vivo measurement probe were evaluated. The technical requirements of a suitable cable for use with the probe were the following: a length adequate to allow the probe to be positioned on a large experimental animal (dog) and still permit convenient location of the network analyzer, adequate cable flexibility for ease in repositioning, introduction of minimal phase variations due to cable movement, low attenuation and VSWR, and the ability to withstand sterilization. Following an examination of cables from nearly a dozen manufacturers, it was determined that the best-suited cable was the Gore-Tex® flexible cable. A three-foot length cable, including connectors, was tested and found to perform satisfactorily over the frequency range examined (2-4 GHz).

An investigation of the accuracy of the results obtained from measurements of standard dielectric materials indicated a need to evaluate the residual systemic errors associated with the network analyzer measurement system [10]. An existing model [9] for reduction of microwave measurement errors (directivity, source match, frequency tracking) associated with the network analyzer, reflectometer, and interconnecting cables was further developed to include multiple-load data in the determination of the directivity error. Also, the systemic error correction model was incorporated in a microprocessor-based data acquisition/data processing system. The error correction is performed

(1) extending the capabilities of the recently developed in-vivo probe measurement technique [5-9], (2) elucidating differences between the in-situ dielectric properties of living tissue and dielectric properties of tissue determined in-vitro, (3) studying renal dielectric characteristics under changing blood flow conditions, and (4) correlating changes in the in-vivo dielectric properties of brain with physiological changes (regional cerebral blood flow) due to hypercapnic and anoxic conditions and to non-noxious sensory stimuli. A longer-term objective is the extension of the probe technique as a method for quantitative determination of local changes in tissue perfusion and blood flow, and for examining spatial distribution changes in kidney and brain without the need for radioactive tracers and tissue excision.

#### B. Summary of Research Performed

During the present 3-year program, under Army Medical Research and Development Command support, the measurement capabilities of the in-situ dielectric probe have been significantly improved. The versatility of the probe was increased through the use of a high-quality flexible probe cable, and systemic and cable/connector measurement errors were accounted for through the development and application of a data correction and processing program which corrects the impedance data measured by the probe for those errors. Methods were developed to eliminate fluid accumulation at the tip of the measurement probe, and an investigation to determine the minimum sample volume necessary for accurate dielectric measurement results was performed. Techniques for rapid data acquisition and processing were studied and developed, and a spring-loaded probe holder which maintains the probe contact pressure on the tissue being measured at a nearly constant value was developed and tested. In-situ measurements of different locations within dog brain were performed which yielded information about the existence of significantly different electrical properties for the various types of brain matter, which in turn impacts EM-hazards dosimetry determination. Studies of antemortem/postmortem dielectric characteristics of the pial surface of dog brain,

SECTION I  
INTRODUCTION

The electrical properties of a biological system largely determine the interaction between that system and an applied electromagnetic (EM) field. Accurate knowledge of in-situ tissue electrical property information would be of significant benefit in many ways. Real-time in-situ measurement of living tissues could be used for the detection of pathophysiological conditions in tissues, for measuring changes in normal physiological processes (such as changes in local perfusion), for differentiating between normal and diseased tissues, and for elucidating pharmacophysiological effects due to drugs. Also, it is important to note that tissue electrical properties play a key role in electromagnetic imaging, both dosimetric and diagnostic in nature. Specific differences or changes in in-situ electrical properties within a single tissue type or among tissues are reflective of the ability of EM imaging methods to discern the existence of pathophysiological conditions in intact tissues, organs, or organisms. Differences between in-situ living tissue properties and in-vitro properties are of key importance in dosimetry determinations (in both magnitude and distribution) via EM imagery [1-4]. Finally, in dosimetry determinations with respect to potential EM radiation hazards and in treatment planning for cancer patients using hyperthermia induced by electromagnetic fields, an accurate knowledge of the respective in-situ tissue electrical properties is essential to an accurate determination of absorbed power.

A. Research Objectives

The objectives of this research program are to further develop and extend the in-vivo probe measurement technique for determining tissue dielectric characteristics, to use this technique to study possible changes in dielectric properties (electrical properties at HF and microwave frequencies) resulting from physiological changes, and to investigate differences between tissue dielectric properties determined in-vivo versus those determined in-vitro. Specific areas of investigation include

of angle. After the best phase response is obtained, the effective phase center is on the axis of rotation of the receiving horn.

A standard-gain S-band horn (manufactured by Scientific-Atlanta) was mounted on the rotating end of the boom and used as a horizontally-polarized directional receiving antenna. In the same horizontal plane as the horn, the monopole was mounted with its base directly over the center of rotation of the boom. This was determined by hanging a small plumb line from the monopole at its junction with the ground plane and adjusting the position of the antenna until the plumb bob pointed directly at the center of boom rotation. Adjustments were easy because the monopole assembly was fixed to an "X-Y" table, that is, one which could be manually adjusted through a continuous range of positions in either of two orthogonal, horizontal directions. Thus, a continuous range of positions in an area of several square centimeters in the horizontal plane was achievable with the proper adjustments. The monopole antenna was mounted such that position could be varied in directions parallel or orthogonal to the antenna's boresight direction. The receiving horn could be rotated 180° in azimuth through the monopole's polar angle as illustrated in Figure 2.

A signal was fed to the antenna from a Watkins-Johnson 1252 microwave synthesizer, and the receiving horn was connected to a Scientific-Atlanta 1773 Receiver. Patterns were recorded on a Scientific-Atlanta Series 1540 (two-channel) pattern recorder, with relative amplitude information displayed on one channel and relative phase information on the other. The boom, table, and surrounding walls were covered as much as possible with absorbing material to reduce the effect of reflections on the recorded pattern.

Patterns from the first scale model with no ground plane showed numerous lobes and nulls. Since the transmission line was apparently contributing to the radiated power, it was determined that the addition of a ground plane was necessary. The second scale model yielded a pattern much closer to the expected monopole characteristics. With the addition of an extended ground plane in the third scale model, further improvement was obtained. The amplitude pattern exhibited broader lobes and the phase pattern had less variation and a sharper transition at boresight.

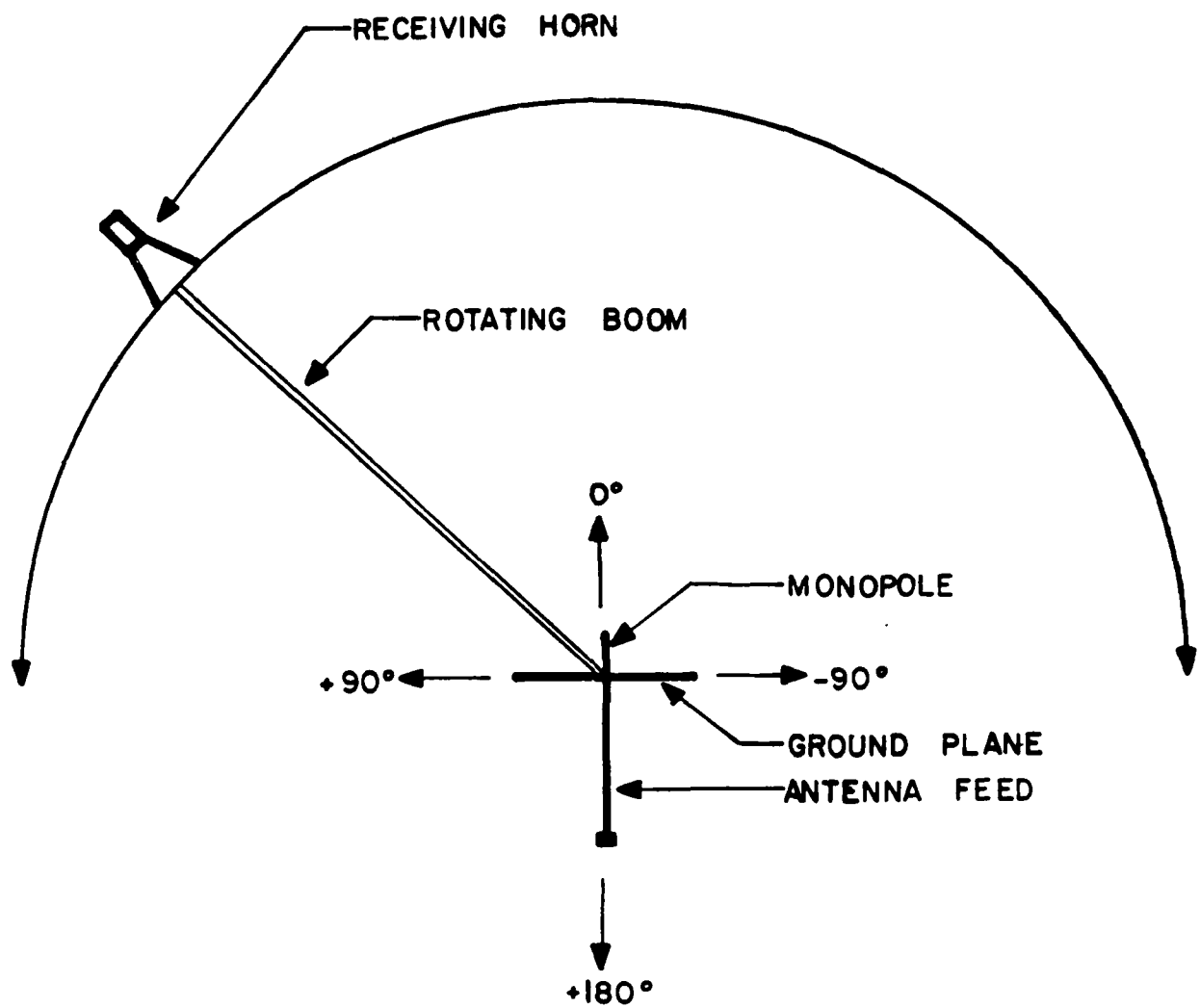


Figure 2. Antenna configuration for experimental measurements on phase center range showing directions of position adjustments.

Antenna radiation patterns of the third scale model were recorded on the phase-center range facility. In Figures 3-7, the upper recording displays relative phase information and the lower recording displays relative amplitude, measured in dB. If an isotropic radiator were measured on this facility, both recordings (phase and amplitude) would exhibit a flat trace over the entire 180° polar cut. Figure 3 illustrates the pattern one would obtain from an ideal 3/4-wavelength monopole over an infinite ground plane. Note that the phase is flat, with the exception of a 180° phase shift at boresight along the axis of the monopole. The amplitude is relatively flat, varying less than 10 dB except in the region  $\pm 6^\circ$  from boresight, where a deep null occurs. In the same figure, the effects of a finite ground plane on the radiation pattern are also illustrated. An ideal monopole over a ground plane several wavelengths in diameter would have the same relative phase pattern, but the amplitude pattern would be different, as shown by the broken-line trace. The amplitude pattern is more uniform over a wider angular region; however, additional nulls begin to form at large angles from boresight (along and below the plane of the ground plane) as its diameter is decreased to less than one wavelength [11].

Figure 4 shows the elevation cut taken at 3.06 GHz. A reasonably good approximation to the ideal case (Figure 3) was exhibited. In the flat region of the phase trace (from about 8° to about 64° off boresight) the phase remains constant to within  $\pm 4^\circ$ . Over approximately the same range (10° - 66° from boresight) the amplitude variations are less than 10 dB. Note also the minor null on each side of the amplitude trace. This null is probably due to edge effects from the finite ground plane. Other small variations in both amplitude and phase were caused by imperfections in the scaled monopole and ground plane and by unavoidable reflections at the antenna test facility.

Figures 5 and 6 show the effects of test antenna position changes on the resultant pattern. Figure 5 displays the results of patterns taken with the feedpoint of the monopole directly over the center of rotation, and with the feedpoint moved 0.5 cm in either direction parallel to the axis of the antenna (0° and 180° from boresight). The amplitude

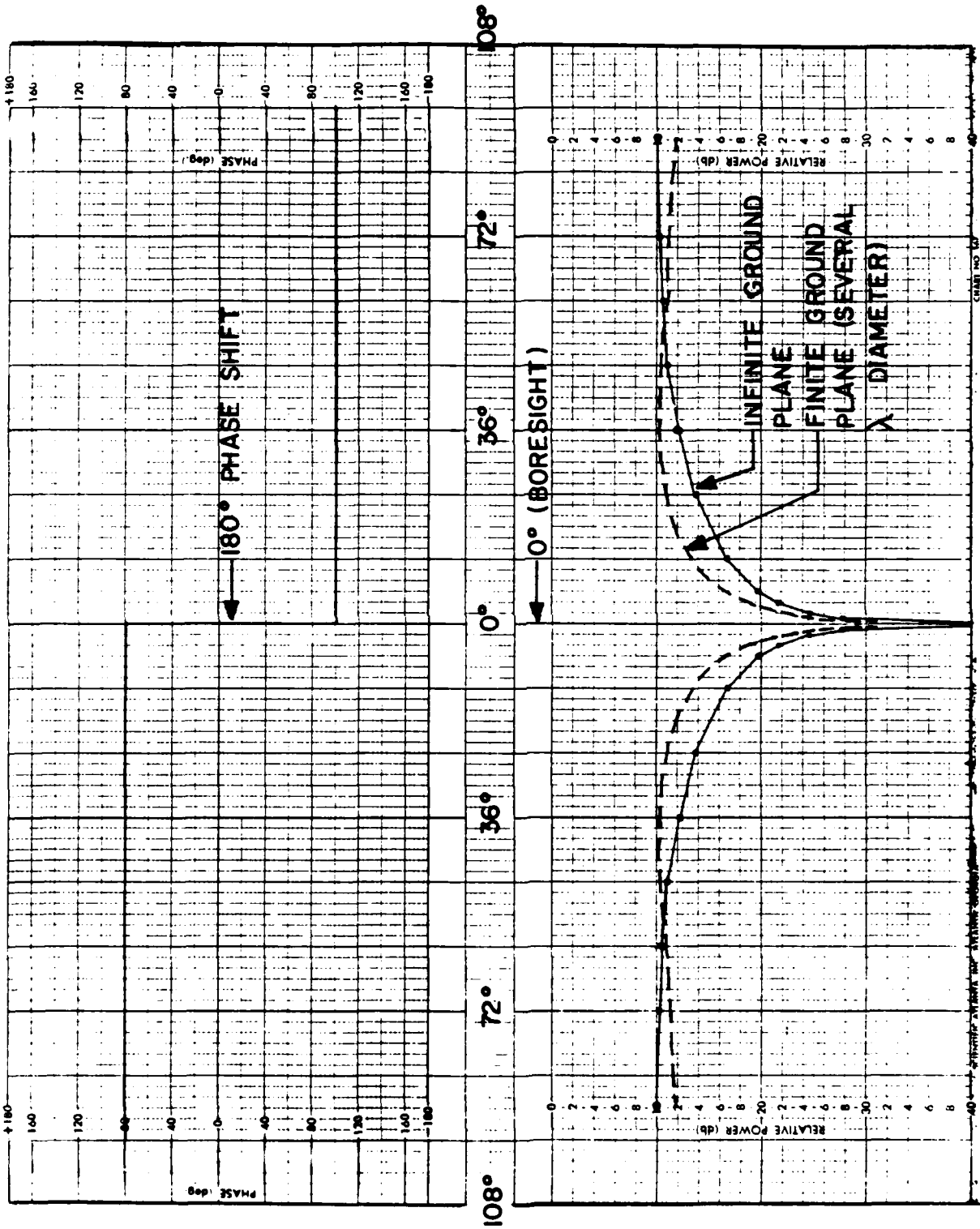


Figure 3. Theoretical results of principal plane elevation cuts taken from ideal  $3/4\lambda$  monopoles over an infinite ground plane (solid line) and a finite ground plane of several  $\lambda$  diameter (broken line). The phase patterns are identical.

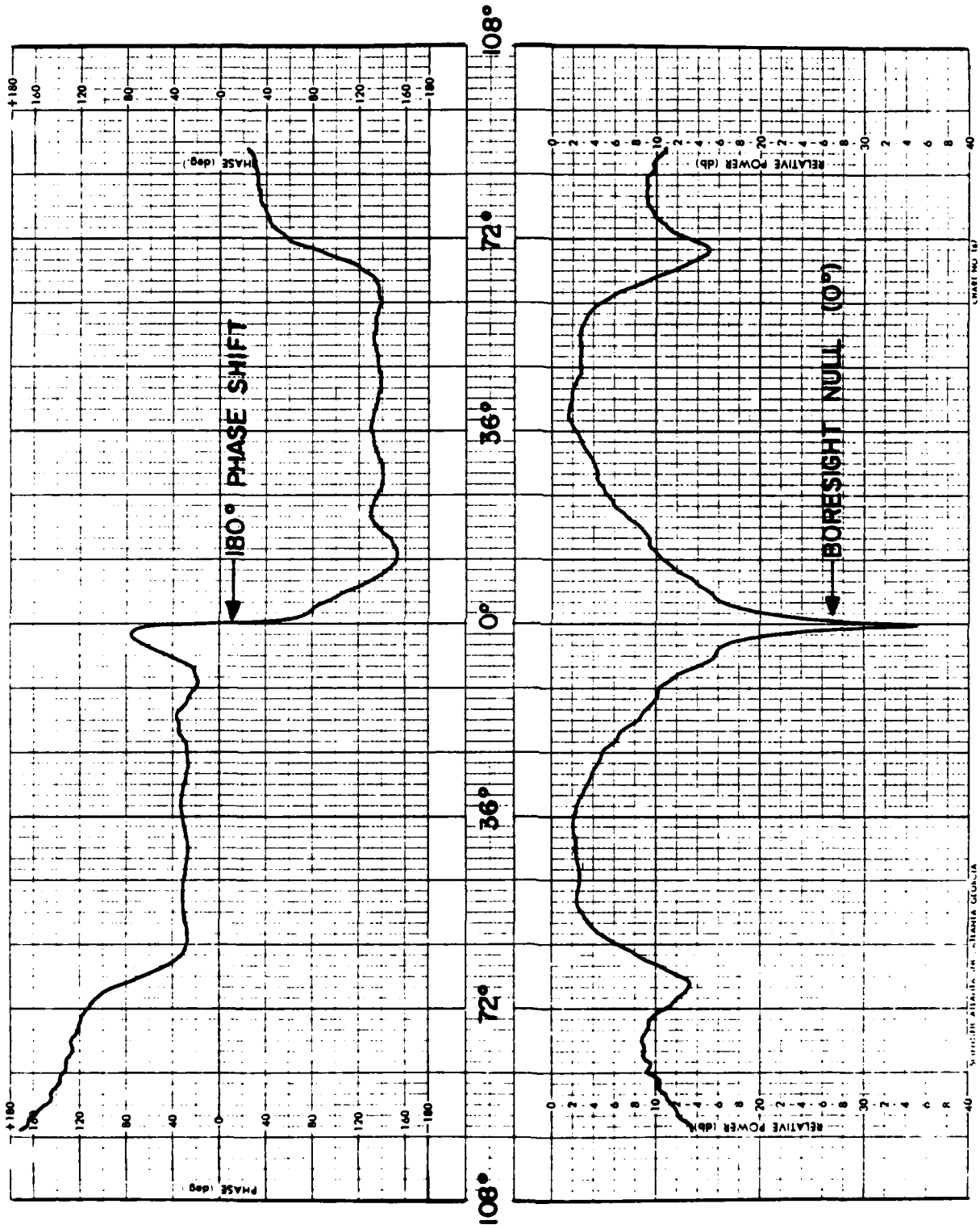


Figure 4. Principal plane elevation cut at 3.06 GHz of  $3/4-\lambda$  monopole over  $8 \lambda$  diameter ground plane.

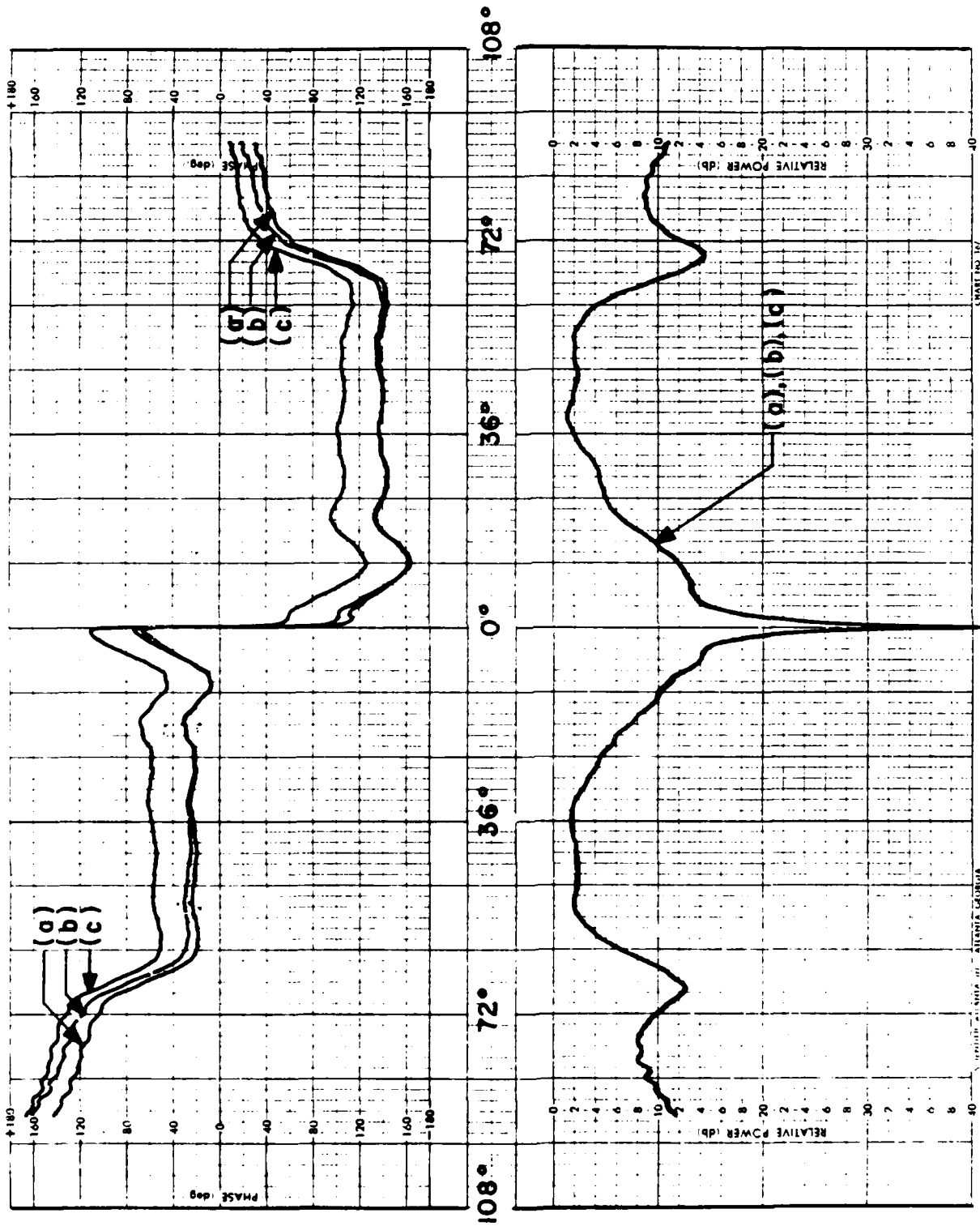


Figure 5. Principal plane elevation cut for three axial displacements at 3.06 GHz.  
 (a) Zero displacement—monopole phase center over center of rotation. (b) Axial displacement of 0.5 cm  $\angle 0^\circ$ . (c) Axial displacement of 0.5 cm  $\angle 180^\circ$ .

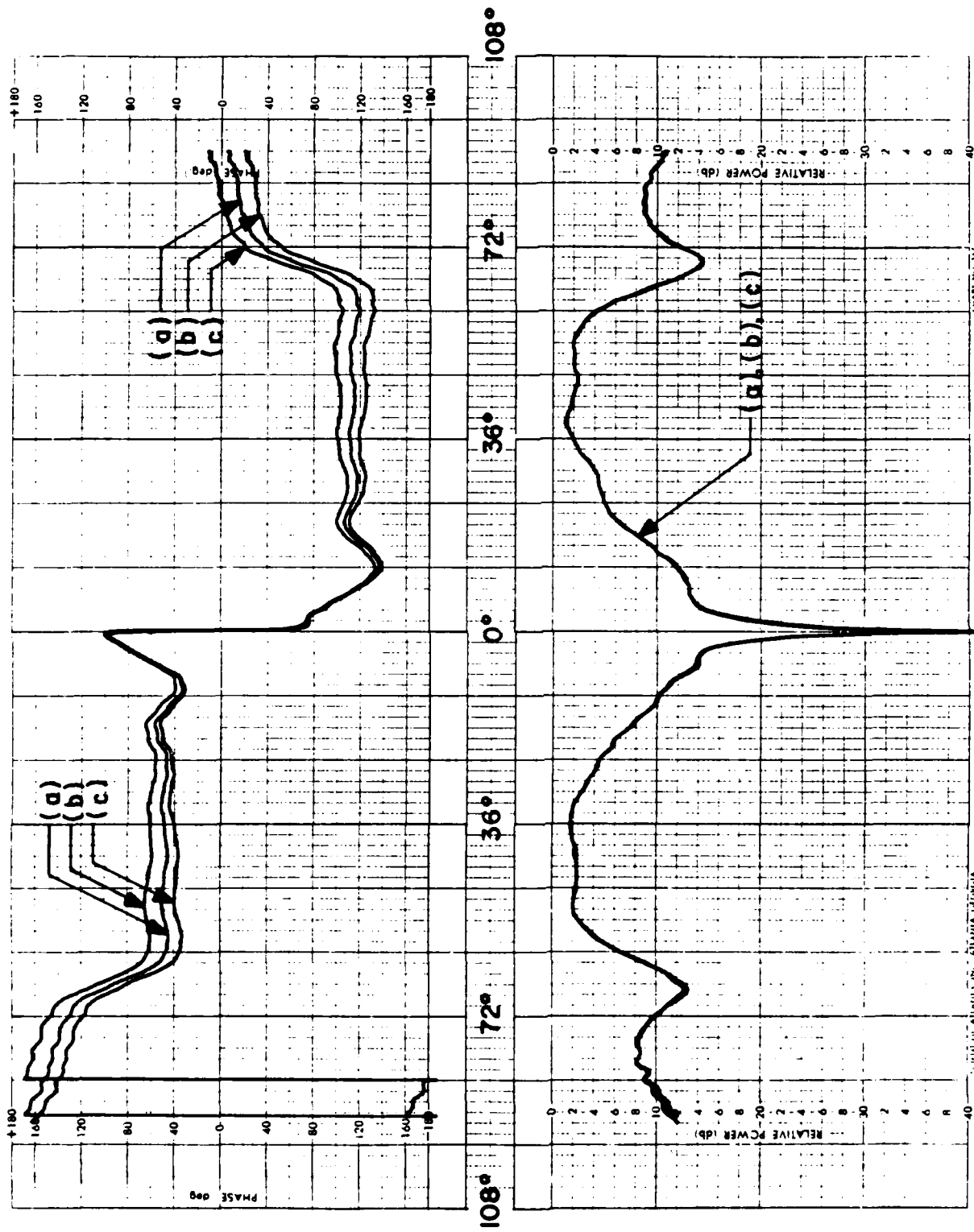


Figure 6. Principal plane elevation cut for three lateral displacements at 3.06 GHz.  
 (a) Zero displacement—monopole phase center over center of rotation. (b) Lateral displacement of 0.5 cm  $\angle +90^\circ$ . (c) Lateral displacement of 0.5 cm  $\angle -90^\circ$ .

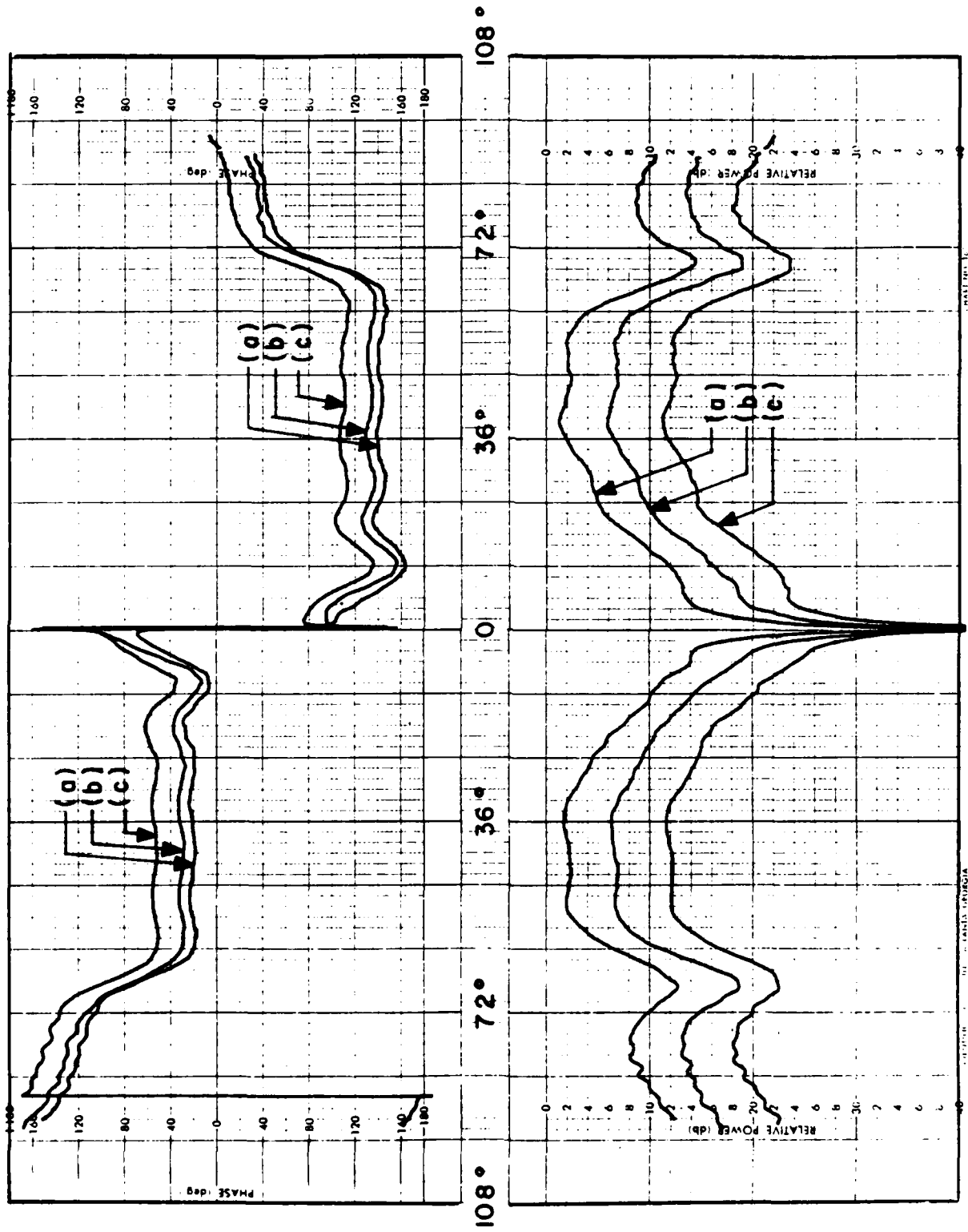


Figure 7. Principal plane elevation cuts at three different frequencies. (a) 3.06 GHz. (b) 3.07 GHz. Amplitude is offset -5 dB from the trace in (a). (c) 3.05 GHz. Amplitude is offset -10 dB from the trace in (a).

is unaffected by these movements, but the phase is shifted slightly depending on the direction of test antenna displacement. Similarly, Figure 6 shows the effects of a 0.5 cm displacement in either direction perpendicular to the axis of the antenna ( $\pm 90^\circ$  from boresight). Again, the amplitude is unaffected, but in this case the phase is rotated about boresight either clockwise or counterclockwise, depending on the direction of displacement. Figures 5 and 6 show the importance of locating the "phase center" of the antenna, which in this case is the base (feedpoint) of the monopole, directly over the center of rotation of the receiving probe. The flatness of each side of the phase trace is thus optimized, and a true measure of the antennas' radiation pattern characteristics is obtained.

In Figure 7, radiation patterns recorded at 3.05, 3.06, and 3.07 GHz are displayed. Note that the amplitude patterns are offset from one another. The only significant difference in the phase traces occurs during the  $180^\circ$  phase shift at boresight ( $0^\circ$ ), with the pattern recorded at 3.06 GHz exhibiting the smoothest transition. The major difference in the amplitude patterns at these three frequencies occurs in the boresight null. As the frequency is decreased, the beginning of new lobes forming in the pattern can be seen as "shoulders" on either side of the null. As the frequency is increased, the boresight null gets broader. The optimum boresight null for the scaled test antenna occurred at 3.06 GHz, where it was sharpest without pronounced shoulders. This is one indication that 3.06 GHz is close to the resonant frequency of the antenna.

Once the patterns exhibited by the scale model were deemed acceptable, the problem of impedance matching in water was considered. The free-space terminal impedance,  $Z_T$ , of the monopole antenna was approximately 37 ohms, which presented a reasonably good impedance match to a 50-ohm semi-rigid coaxial transmission line. However, in water, the terminal impedance is reduced by a factor equal to the square root of the relative dielectric constant of that medium. The intrinsic impedance of the medium (water) is given by

$$\eta_{H_2O} = (\epsilon^*)^{-1/2} \eta_0, \quad (1)$$

where  $\eta_0 = 377 \text{ ohms } (\Omega)$  is the intrinsic impedance of free space and  $\epsilon^* = \epsilon' - j\epsilon''$  is the complex permittivity of the medium. In water at  $23^\circ\text{C}$ ,  $\epsilon^* = 76.7 - j 12.04$  or equivalently,  $\epsilon^* = 77.6 \angle -8.92^\circ$ . Thus, the intrinsic impedance of water is  $\eta_{H_2O} = 42.8 \Omega \angle -4.46^\circ$ . The magnitude of the terminal impedance  $Z_T$  is known as the radiation resistance,  $R_r$ , of the antenna. In air,  $R_r$  equals the free-space terminal impedance. In water,

$$R_{r_{H_2O}} = (\epsilon_r)^{-1/2} R_{r_{air}}, \quad (2)$$

where  $R_{r_{(air)}} = 377 \Omega$  and  $\epsilon_r = \epsilon'/\epsilon_0$  is the relative dielectric constant. Thus,  $R_{r_{(H_2O)}} = 4.2 \Omega$ . Because the phase angle of the terminal impedance is small at the monopole's resonant frequency, the reactive component of  $Z_T$  is nearly zero and  $R_r \sim Z_T$ . The impedance mismatch resulting when the  $3/4$ -wavelength antenna in water is fed with a  $50 \Omega$  transmission line is greater than 10:1 and most of the energy received by the monopole is not coupled to the transmission line. One solution to this problem is to incorporate a quarter-wave impedance transformer at the antenna feedpoint. The quarter-wave transformer impedance required to match an element of impedance  $Z_1$  to an element of impedance  $Z_2$  is given by

$$Z_{\text{Transformer}} = (Z_1 Z_2)^{1/2}, \quad (3)$$

with an effective electrical length of  $1/4$  wavelength. In this particular case, the transformer must have an impedance of  $14.5 \Omega$  in order to exactly match the monopole's terminal impedance to the  $50 \Omega$  transmission line.

The required impedance transformation was accomplished by modifying the ground plane attachment as illustrated in Figure 8. The quarter-wave transformer used was a short coaxial section with the radius of the inner conductor being that of the monopole itself. Thus, the characteristic

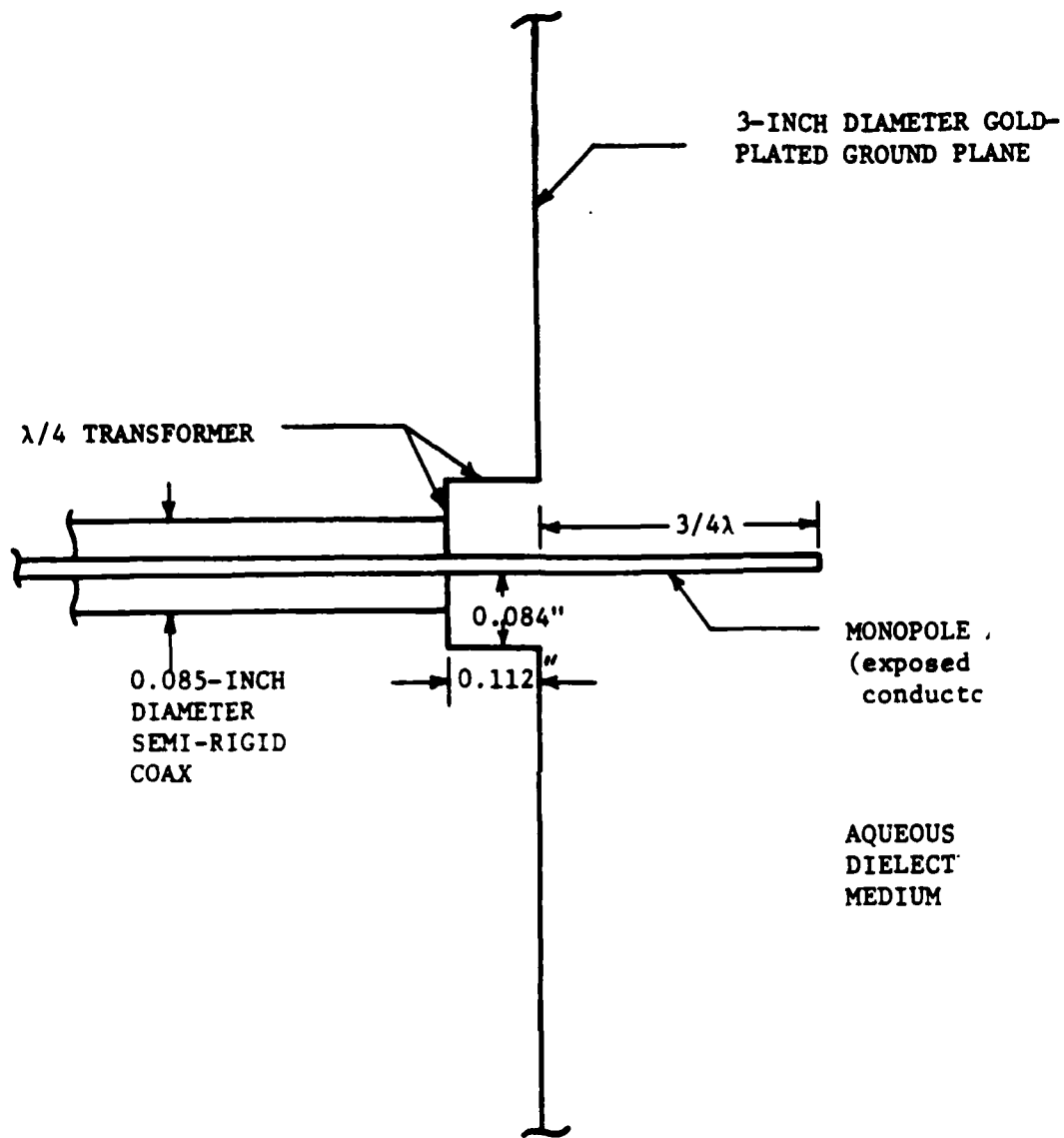


Figure 8. Schematic illustration of 3/4-wavelength monopole antenna designed for underwater showing configuration of  $1/4\lambda$  impedance transformer.

impedance of this coaxial section was determined by its outer radius and the dielectric material located between the inner and outer conductors. As shown in Figure 8, water was selected as the dielectric material to be located between the inner and outer conductors of the coaxial section comprising the impedance transformer. Therefore, the impedance of the transformer becomes a function of only the outer conductor's radius. The characteristic impedance of this coaxial section is given by

$$Z_c = Z_{\text{Transformer}} = \frac{\ln\left(\frac{r_o}{r_i}\right)}{2\pi} n_{\text{H}_2\text{O}} \quad (4)$$

where  $r_o$  and  $r_i$  are radii of the outer and inner conductors, respectively, and other symbols are as previously defined.

#### B. Fabrication and Performance Testing of Final Antenna

The final antenna was fabricated from 0.085-inch diameter semi-rigid coaxial cable in a manner similar to that used for the construction of the scaled models. The radius  $r_i$  of the inner conductor was 0.01005 inch, and the water medium was used as the dielectric material for the coaxial section transformer. Thus, the desired characteristic impedance of 14.5 was obtained by making the outer conductor radius  $r_o = 0.084$  inch. The length of the quarter-wave transformer was determined by dividing the free-space quarter wavelength by  $(\epsilon_r)^{1/2}$ , yielding a value of approximately 0.112 inch. These dimensions are illustrated in Figure 8.

The ground plane and quarter-wave transformer were fashioned from a three-inch diameter brass disk, mounted on a short brass sleeve which formed a tight physical connection with the outer conductor of the coaxial cable. The ground plane diameter was thus 6.8 wavelengths in water at 3.0 GHz. Although this was slightly less than the equivalent dimension of the scaled model, it was felt that a larger ground plane on the working antenna would prove unwieldy. The radiation efficiency of a monopole over a ground plane is somewhat compromised by impedance mismatches introduced by the presence of a finite ground plane (as opposed to an infinite ground plane). However, a ratio of ground plane radius-to-free

space wavelength greater than 0.2, when used in a water medium, results in negligible effects on the monopole antenna [12]. The working antenna produced by this effort has a ground plane radius to free space wavelength ratio of 0.38; thus, the presence of a finite ground plane did not significantly affect its impedance.

Following exposure of approximately one centimeter of the center conductor, the ground plane was affixed to the antenna and the entire unit was gold-plated. The center conductor of the semi-rigid coaxial cable was trimmed to the computed  $3/4$ -wavelength dimension at 3.0 GHz, and then the actual resonant frequency of the monopole antenna was determined by measuring the antenna's reflection coefficient in deionized water at 22°C with a Hewlett-Packard 84105 semi-automated Network Analyzer System.

The results of this measurement over the swept-frequency band from 2.3 GHz to 3.9 GHz are presented in Figure 9. The resonant frequency of the monopole antenna (i.e., the frequency at which the smallest reflection coefficient was measured) was determined to be 2.7 GHz. Since the antenna radiation patterns measured on the scale model antenna in air (Figures 4-7) were for the resonant frequency of that antenna, those patterns were indicative of the patterns which would be obtained at the resonant frequency of the final antenna intended for operation underwater. The finished antenna and its associated documentation were shipped to personnel at the Walter Reed Army Institute of Research for further evaluation and use.

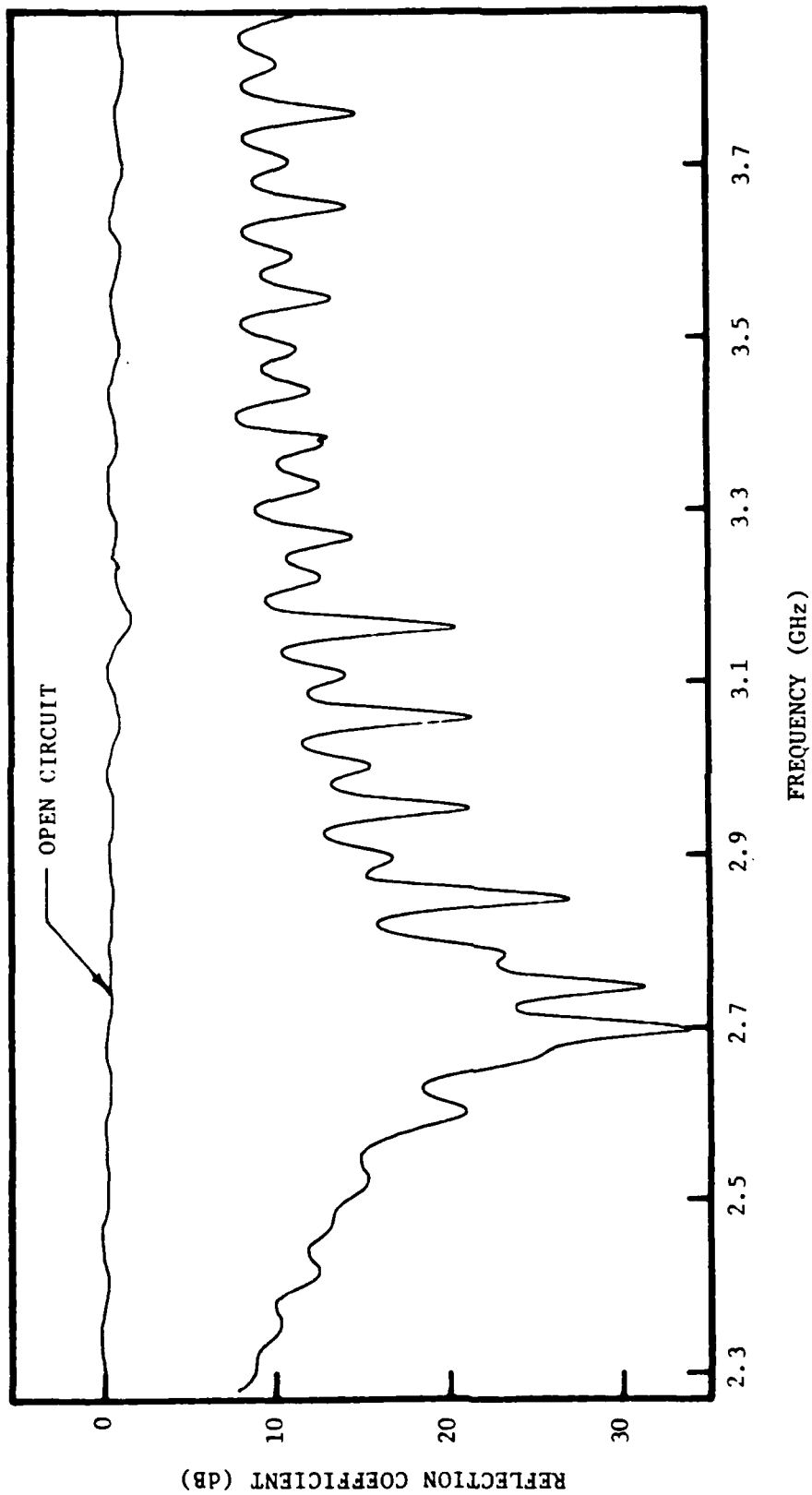


Figure 9. Measured reflection coefficient magnitude of 3/4-wavelength monopole antenna in water plotted as a function of frequency. Best impedance match is obtained at an operating frequency of 2.7 GHz.

SECTION IV  
EXPERIMENTAL INVESTIGATIONS

This section summarizes the experimental investigations of physiological influences on tissue dielectric properties conducted during this reporting period. These investigations consisted of (1) in-vitro renal flow/dielectric property studies, wherein isolated canine kidneys were placed on an external perfusion circuit and renal dielectric properties were measured under various controlled flow conditions; (2) in-situ renal flow/dielectric property studies, wherein measurements were performed in-situ and renal flow was controlled via an extracorporeal pump circuit, and (3) investigations of drug-elicited effects on renal dielectric properties for different total renal flow conditions. For each investigation, laboratory procedures are outlined and experimental results are presented. Surgical procedures and experimental methods are described first. Measurements of renal pressure and weight for various flow rates are next presented, followed by results from complex permittivity measurements.

A. Surgical Procedures

Dogs were used as the experimental subjects for the renal dielectric studies. Surgical procedures used were similar to those reported in Annual Technical Report No. 2 [9]. These are reviewed and changes noted below. Subject dogs weighing 15-20 kg were obtained from Emory University Department of Physiology, and surgical and measurement procedures were performed in the animal surgery laboratory at Georgia Tech. Each dog was anesthetized initially with 30 mg/kg body weight of pentobarbital sodium (Nembutal) intravenously (IV) and maintained at Geudel's Stage II, Level 3 of anesthesia with supplemental doses of 30-60 mg administered as needed. Three in-situ preparations used anesthesia of 50 mg/kg body weight  $\alpha$ -chloralose administered IV.

With the dog in a supine position, the right femoral triangle and both left and right sides of the abdomen were shaved and scrubbed. The right femoral vessels were cannulated to provide a site for IV injections (femoral vein) and a site for continuous monitoring of systemic pressure (femoral artery). The cannulae were filled with heparinized saline to prevent clotting.

PROG2B,A1T4MS1

THIS PROGRAM CALCULATES THE LINEAR CORRELATION  
COEFFICIENT FOR TWO VARIABLES.

VARIABLE NUMBERS ARE:

|                  |                  |
|------------------|------------------|
| 1 - TIME         | 2 - PUMP SPEED   |
| 3 - FLOW RATE    | 4 - PRESSURE     |
| 5 - WEIGHT       | 6 - TEMPERATURE  |
| 7 - PERMITTIVITY | 8 - CONDUCTIVITY |
| 9 - AMPLITUDE    | 10 - PHASE       |
| 11 - PROBE FORCE |                  |

ENTER THE DATA SET NUMBER

? 1

ENTER THE VARIABLE NUMBERS

(INDEPENDENT VARIABLE FIRST)

? 3 7

DO YOU WANT TO USE THE ERRORS ASSOCIATED  
WITH THE VARIABLES IN THE CALCULATION (Y OR N)?

? N

AVERAGE OF 1 TO 4 MEDULLA BASELINE SUBTRACTED (PUMP SPEED 1)

INDEPENDENT VARIABLE = 3      DEPENDENT VARIABLE = 7  
6 POINTS                      4 DEGREES OF FREEDOM

A = 6.298E-02      B = -1.162E-01  
( 8.149E-01)      ( 2.128E-02)

CORRELATION COEF. = -.939  
PROBABILITY FOR CORRELATION = .995

DO YOU WISH TO LOOK AT MORE  
CORRELATIONS (Y OR N)?

? Y

IN THIS DATA SET (Y OR N)?

? Y

ENTER THE VARIABLE NUMBERS

? 3 8

DO YOU WANT TO USE THE ERRORS ASSOCIATED  
WITH THE VARIABLES IN THE CALCULATION (Y OR N)?

? N

AVERAGE OF 1 TO 4 MEDULLA BASELINE SUBTRACTED (PUMP SPEED 1)

INDEPENDENT VARIABLE = 3      DEPENDENT VARIABLE = 8  
6 POINTS                      4 DEGREES OF FREEDOM

A = -1.768E-02      B = -6.823E-02  
( 5.157E-01)      ( 1.347E-02)

CORRELATION COEF. = -.930  
PROBABILITY FOR CORRELATION = .993

Figure 14. Example printout of results from linear correlation program. Variables within a data point vector may be paired as desired. The value of the linear correlation coefficient, the probability for correlation, and linear fit parameters are printed.

coefficient, the probability that the value of  $r$  obtained does not come from an uncorrelated parent population is obtained as follows [18]. The probability that a sample of  $N$  data points for  $(X,Y)$  with linear correlation coefficient  $r$  is obtained from normal bivariate sample space with correlation coefficient equal to zero is:

$$\text{Pr}(r, \nu) = \frac{1}{\sqrt{\pi}} \frac{\Gamma(\nu+1)/2}{\Gamma(\nu/2)} (1-r^2)^{\frac{\nu-2}{2}}, \quad (8)$$

where  $\nu = N-2$  and  $\Gamma$  is the Gamma function. Thus, the probability that a random sample of  $N$  uncorrelated data points yields a linear correlation coefficient greater than or equal to  $|r|$  is

$$P_c(r, N) = 2 \int_{|r|}^1 P_r(\rho, \nu) d\rho. \quad (9)$$

This can be evaluated using equation 8 yielding

$$P_c(r, N) = 1 - \frac{2}{\sqrt{\pi}} \frac{\Gamma\left(\frac{\nu+1}{2}\right)}{\Gamma(\nu/2)} \left\{ \sum_{i=0}^I (-1)^i \binom{I}{i} \frac{|r|^{2i+1}}{(2i+1)} \right\} \quad (10a)$$

for  $\nu$  even where  $I = \frac{\nu-2}{2}$

$$= 1 - \frac{2}{\pi} \left\{ \sin^{-1}(|r|) + |r| \sum_{i=1}^I (1-r^2)^{i/2} \frac{(i-1)!!}{i!!} \right\} \quad (10b)$$

for  $\nu$  odd, where  $I = \nu-2$ .

Since this is the probability that the  $N$  data points having a correlation coefficient of  $|r|$  or greater come from an uncorrelated sample space, one minus this is the probability that  $N$  data points do not come from an uncorrelated parent population (in short, this value is referred to as the probability of correlation, although as can be seen from the above explanation this is not really a proper term). The linear correlation coefficient, probability for correlation, and slope and intercept (with errors) for the linear fit are printed out by this program. An example printout is presented in Figure 14.

AVFG2B.D1T4M51.A1T4M01

THIS PROGRAM AVERAGES DATA FROM SEVERAL EXPERIMENTS.

DO YOU WANT THE WEIGHT CORRECTED FOR THE PROBE CONTACT FORCE? (Y OR N)

? N

DO YOU WANT TO SUBTRACT A BASELINE VECTOR? (Y OR N)

? N

ENTER THE NUMBER OF DATA SETS THAT YOU WANT TO AVERAGE.

? 4

ENTER THE DATA SET NUMBERS TO BE AVERAGED

? 1 2 3 4

ENTER AN ALPHANUMERIC DESCRIPTION FOR THE AVERAGED DATA SET (70 CHARACTERS MAX)

? AVERAGE OF 1 TO 4 MEDULLA BASELINE SUBTRACTED (PUMP SPEED 1)

|  | 1      | 1000   | 6       |        |       |
|--|--------|--------|---------|--------|-------|
| AVERAGE OF 1 TO 4 MEDULLA BASELINE SUBTRACTED (PUMP SPEED 1) |        |        |         |        | 1     |
| DATA POINT 1   |        |        |         |        |       |
| 58525.000  | 1.000  | 8.450  | 0.000   | 0.000  | 0.000 |
| 0.000  | 0.000  | 0.000  | 0.000   | 0.000  | 0.000 |
| 19753.623  | 0.000  | 1.379  | 0.000   | 0.000  | 0.000 |
| 0.000  | 0.000  | 0.000  | 0.000   | 0.000  | 0.000 |
| DATA POINT 2   |        |        |         |        |       |
| 58425.000  | 5.000  | 28.000 | 100.500 | 8.200  | 1.425 |
| -3.828   | -2.398 | .120   | 3.600   | 6.850  |       |
| 19460.532  | 0.000  | 3.559  | 27.551  | 4.284  | .827  |
| 2.591  | 1.754  | .099   | 2.472   | 4.319  |       |
| DATA POINT 3   |        |        |         |        |       |
| 61375.000  | 7.500  | 38.575 | 119.250 | 12.275 | 1.525 |
| -4.428   | -2.708 | .133   | 4.148   | 13.600 |       |
| 20743.669  | 0.000  | 3.478  | 30.880  | 4.681  | .929  |
| 2.610  | 1.781  | .100   | 2.491   | 8.739  |       |
| DATA POINT 4   |        |        |         |        |       |
| 61757.500  | 10.000 | 46.000 | 133.750 | 16.725 | 1.850 |
| -4.733   | -2.788 | .133   | 4.438   | 6.100  |       |
| 20617.726  | 0.000  | 2.345  | 34.603  | 6.713  | 1.405 |
| 2.783  | 1.819  | .100   | 2.656   | 15.375 |       |
| DATA POINT 5   |        |        |         |        |       |
| 49543.333  | 15.000 | 59.600 | 136.333 | 10.167 | 2.600 |
| -6.607   | -3.907 | .193   | 6.207   | 21.900 |       |
| 22922.206  | 0.000  | 1.514  | 55.694  | 8.978  | 1.686 |
| 3.109  | 1.938  | .102   | 2.972   | 14.042 |       |
| DATA POINT 6   |        |        |         |        |       |
| 63657.500  | 5.000  | 28.000 | 100.250 | 8.200  | 1.275 |
| -4.275   | -2.540 | .120   | 3.985   | 8.950  |       |
| 20408.907  | 0.000  | 3.559  | 29.044  | 4.284  | .914  |
| 2.665  | 1.784  | .099   | 2.541   | 4.594  |       |

DO YOU WANT TO AVERAGE MORE DATA SETS (Y OR N)

? N

.777 CP SECONDS EXECUTION TIME.

Figure 13. Example printout of results computed using the averaging program discussed in text. Each data point vector represents a different pump speed/flow rate. Results are expressed as average change from the baseline value of the variables studied.

The averaging program may be used on either the baseline-subtracted or original data sets. Corresponding variables from several experiments are averaged and the error-of-the-mean is computed using the standard formulas [13]

$$\bar{X} = \frac{1}{N} \sum_{i=1}^N X_i \quad (5)$$

and

$$\sigma_{\mu} = \sqrt{\frac{1}{(N-1)N} \sum_{i=1}^N (X_i - \bar{X})^2}, \quad (6)$$

where N is the number of points,  $X_i$  is the i'th measurement point,  $\bar{X}$  is the mean, and  $\sigma_{\mu}$  is the error-of-the-mean. The mean and error-of-the-mean for the measurement vectors are stored in a separate file as a new data set in a format similar to the original data sets except that each average measurement vector has a corresponding error vector. An example output from this program is shown in Figure 13.

The last program in this series calculates the linear correlation coefficient and a number indicative of the probability for correlation for pairs of variables. This program may use raw, baseline-subtracted, or averaged data sets as input. If averaged data sets are used, there is an option to include the errors in the calculation of the correlation coefficient. The linear correlation coefficient is computed as [13,14]:

$$r = \frac{N \sum X_i Y_i - \sum X_i \sum Y_i}{\left[ N \sum X_i^2 - (\sum X_i)^2 \right]^{1/2} \left[ N \sum Y_i^2 - (\sum Y_i)^2 \right]^{1/2}} \quad (7)$$

where each sum extends over the N measurements,  $X_i$  is the i'th measurement of the independent variable,  $Y_i$  is the i'th measurement of the dependent variable, and r is the linear correlation coefficient. This parameter can range from -1 to +1 with the extreme values corresponding to complete correlation of the variable pair (X,Y) and a value of 0 (zero) corresponding to no correlation. To aid in the interpretation of the correlation

variables. All programs are currently implemented on the Georgia Tech CYBER 70/74 computer system. These programs were used to obtain the data in Table III, presented in Section IV (Experimental Investigations).

The first of this series of programs allows for interactive entry of data and storage on permanent disk files. Data sets are organized by experiment where one experiment consists of a series of measurements on a given dog's left or right kidney, either cortex or medulla. For each measurement, eleven variables are observed: time of measurement, pump speed, flow rate, pressure, kidney weight, temperature, permittivity, conductivity, reflection coefficient amplitude and phase, and probe contact force. These variables are recorded as an eleven component measurement vector in the data set. Typically, there are six measurement vectors in each data set corresponding to pump speeds of 1.0, 5.0, 7.5, 10.0, 15.0, and 5.0 rpm (repeated).

The data normalization program in this series may be used to subtract a measurement vector for a particular pump speed (i.e., flow rate) from all of the measurement vectors within a given data set in order to reduce variations resulting from differences between dogs, without affecting the variability in responses to changing flow rate. This method of normalizing data sets allows measurements from a number of experiments to be averaged and thus determines more accurately the correlations of parameters such as permittivity and conductivity with flow rate. The program rewrites the baseline-subtracted data sets on a new permanent disk file. It should be noted that the time, pump speed, and flow rate values are not altered by the normalization program. Thus, what is obtained in these data sets are changes in pressure, weight, temperature, permittivity, conductivity, reflection coefficient amplitude and phase, and probe contact force from the baseline values (usually pump speed 1.0). An option in this program is the facility to correct the measured kidney weight for the probe contact force in order to record the true weight (measured weight minus probe contact force at each flow rate).

Sixteen conditioned parallel output channels are provided on a multi-pin connector. The event marker, the three temperature measurement circuit outputs, and the four pressure transducer signal outputs are wired to front-panel switches which permit direct connection of these signals to the buffer amplifiers. In this manner, 15 of the sixteen buffer amplifier inputs may be made available for external input signals, but by providing for direct switch selected wiring of seven inputs (temperature and pressure), patch cords for these signals are eliminated. The arrangement just described provides sufficient flexibility for all anticipated experimental configurations and for use with various data acquisition and processing systems in addition to the present one.

Output signals from the signal conditioning system are inputted to an HP 6940B multiprogrammer. The multiprogrammer performs the analog signal multiplexing and analog-to-digital conversion functions. It also converts the data from parallel format to IEEE-488 bus format. This bus is connected to an IEEE-488 bus on the Zenith/Heathkit WH-89 microcomputer system. Other network analyzer system components are also connected to this bus.

Programs for data processing and analysis using the WH-89 microcomputer system will be developed during the fourth year renewal of this research effort. During the third year, computer programs were developed for data analysis using the CYBER 70/74 large mainframe computer system. These programs are discussed in the following subsection. It is anticipated that these analysis programs also will be utilized in fourth-year research efforts, with data being transferred from the WH-89 to the CYBER 70/74 via a modem/telephone link.

#### D. Data Analysis

Several computer programs have been written to aid in the analysis of the data resulting from the experimental investigations. These include programs to interactively enter data and store it on disk for subsequent analysis; subtract baseline values to normalize data from different experiments; average data from different experiments; and compute linear correlation coefficients and correlation probabilities for pairs of

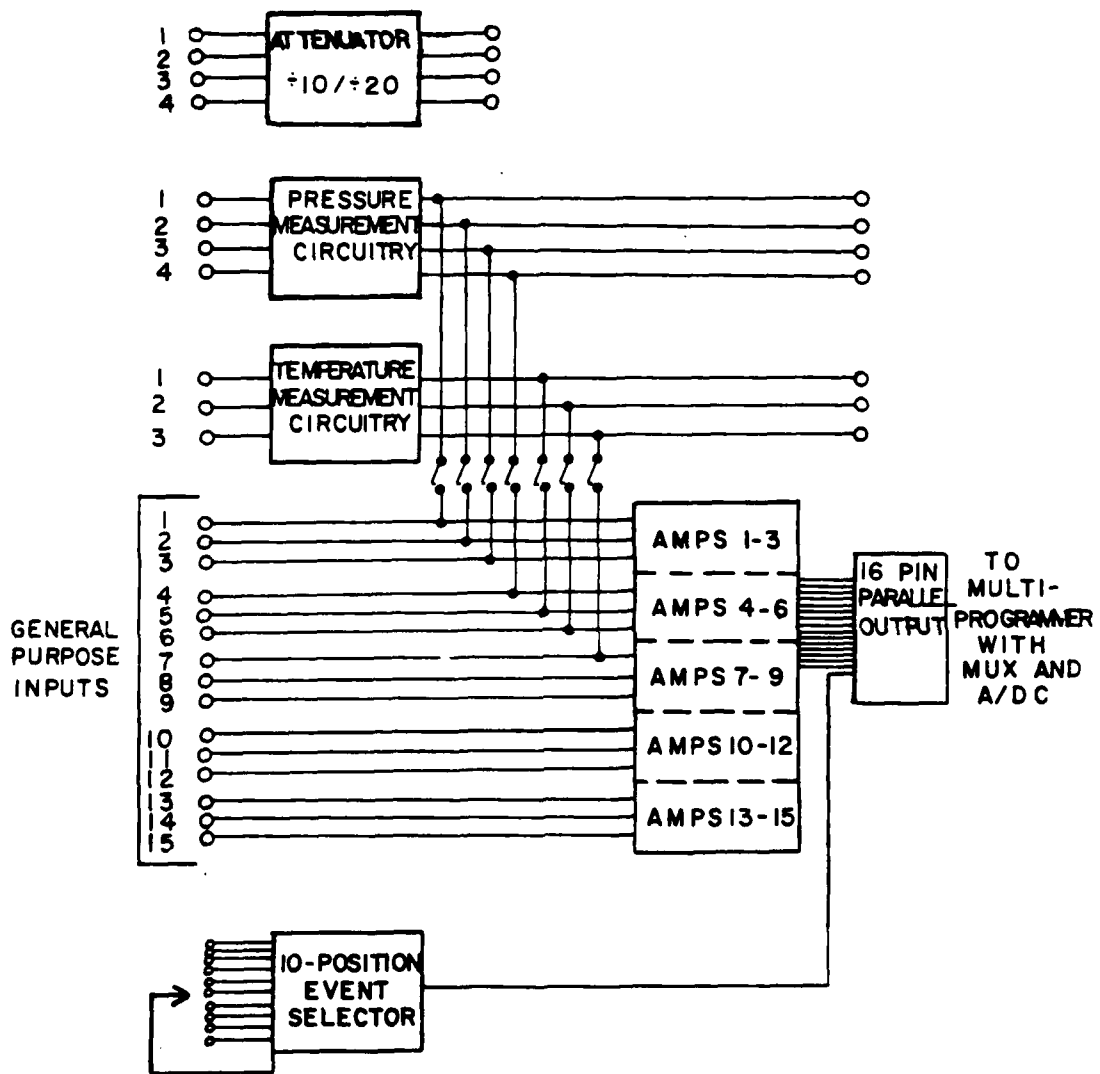


Figure 12. Block diagram of the signal conditioning hardware used to convert various transducer outputs into uniform inputs to the data processing system.

coefficient), but also signals which reflect various physiological data pertinent to the experimental investigations (systemic blood pressures, renal perfusion pressure, organ and systemic temperatures, flow rate, ECG, etc.).

It was determined that conditioning of the signals from the various transducers/instrumentation was required in order to keep all electrical input signals to the A/D converter within a single input voltage range (-5 to 5 volts), which can be digitized, stored, and later processed by the data analysis programs. The signal conditioning hardware consists of a 16-channel analog signal buffering/temperature measurement system. A block diagram of this system is shown in Figure 12. Of the sixteen available input channels, fifteen may be connected to analog signals in the -5 volt to 5 volt range through general-purpose amplifiers. Each amplifier uses an LM358 operational amplifier for buffering and has a variable gain control for setting any desired gain between 1 and 100. They provide a positive analog voltage output for input signals of either polarity (+ or -), with offsets of up to 5 VDC. Three of the signals to be conditioned and buffered have amplitudes which exceed 5 VDC. These analog signal channels may be routed through attenuator stages for reduction by a factor of either 10 or 20. The attenuated signals are then fed into one of the general-purpose amplifier stages.

Three of the sixteen input channels may be connected through front-panel switches to temperature measurement circuits for use with conventional commercially-available plug-in thermistor probes. The probes may be plugged directly into the signal processing system without a requirement for any additional temperature measurement instrumentation. Temperature information from a thermistor sensor is converted to an analog voltage in the 0-5 volt range for digitizing by the A/D converter. One of the sixteen channels is reserved for an event marker which consists of a ten-position switch for selection of one of ten discrete DC voltage levels. Thus, ten different measurement conditions may be distinctly labelled in each experiment.

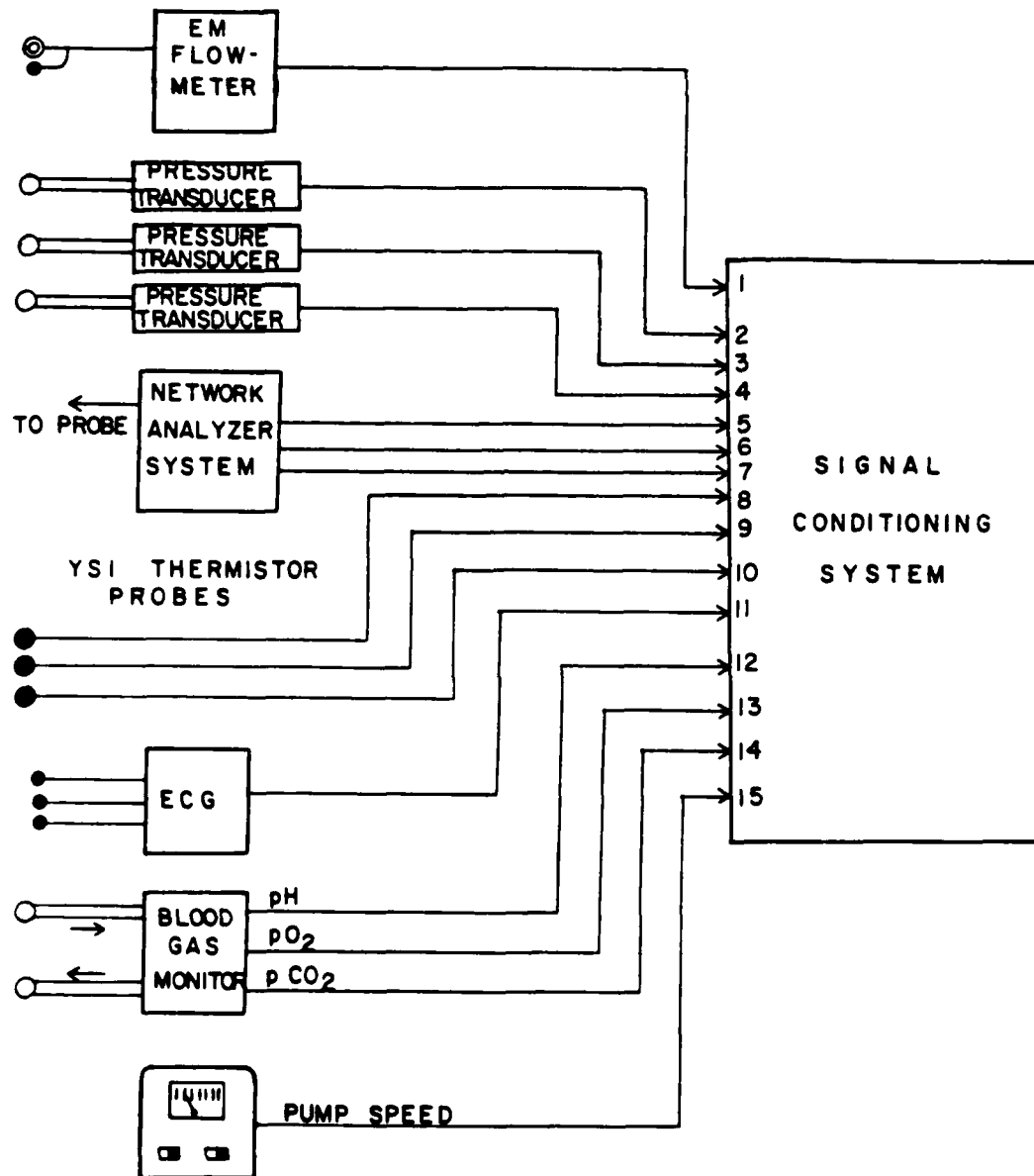


Figure 11. Typical input signals to be monitored during an experiment with the new data acquisition system.

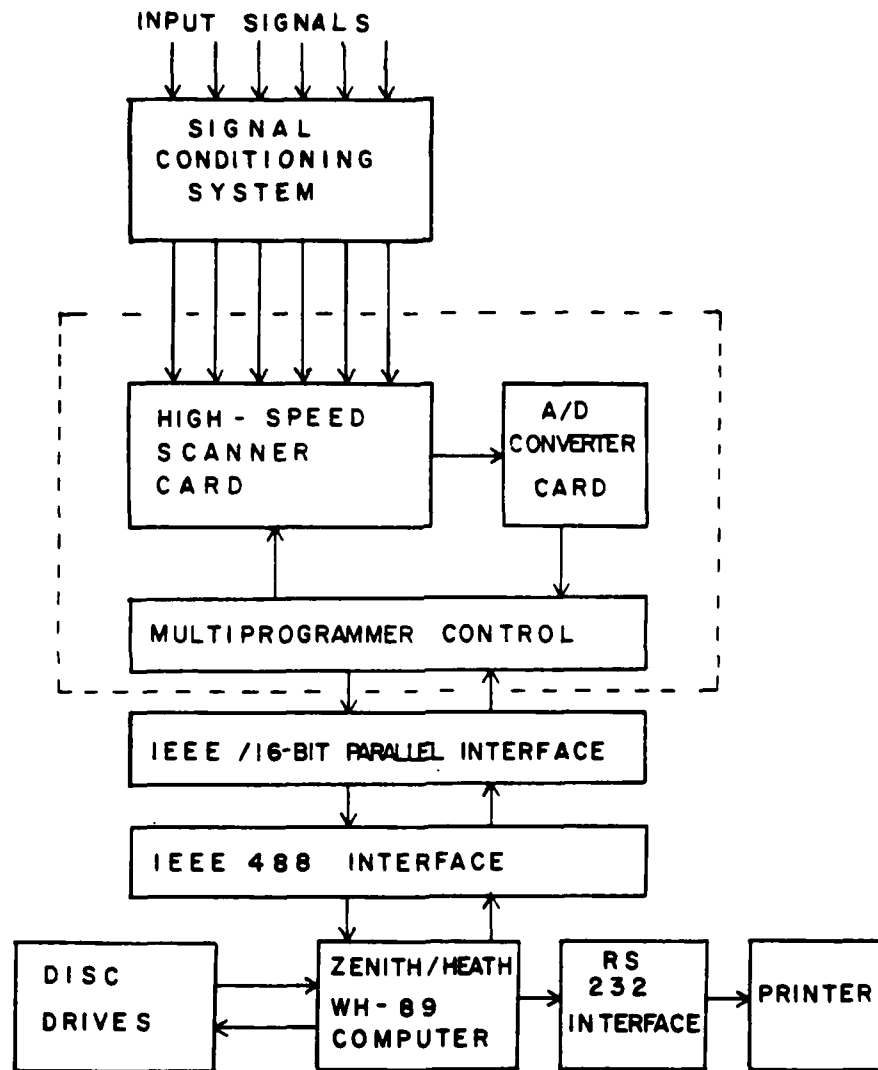


Figure 10. Block diagram of the new Zenith/Heath WH89-based data acquisition and processing system to be used in subsequent experiments.

4. 8-bit parallel port
5. RS-232 serial port
6. 48 line by 80 column CRT

The A/D converter chosen for use with the Intecolor 8052 was an ANALOGIC MP 6812 module. This module was selected because of previous laboratory experience with that device and the availability of an existing module.

The A/D and Intecolor 8052 were interfaced and software was developed for data acquisition. However, because of the lack of an accessible clock in the Intecolor 8052, it was necessary to set up software loops for timing which required that the data acquisition software be inefficient and cumbersome. A hardware problem with the A/D later developed which required sending the module to the manufacturer for a period of approximately two months. During this period, it was decided to purchase the Zenith/Heathkit WH-89 with a combination of funds from this program and internal funds. This new microcomputer system was purchased to be shared between this project and general use with a new network analyzer system. A Hewlett-Packard 6940B Multiprogrammer with high-speed 16-channel multiplexer and high-speed A/D converter cards was also purchased. An IEEE-488 interface board was designed and made available through a local vendor, specifically for our application. The current data acquisition and processing system incorporating the Zenith/Heathkit WH-89, the Hewlett-Packard Multiprogrammer, IEEE-488 interface board, and signal conditioning electronics is described in the following subsection.

#### C. Current Data Acquisition System Design

The current data acquisition and processing system consists of a 16-channel signal conditioning system, a HP 6840B Multiprogrammer (16-channel multiplexer, high-speed A/D converter, I/O electronics, and power supplies), and a Zenith/Heathkit WH-89 microcomputer system with three 5 1/4" floppy-disk drives and an IEEE-488 interface. A block diagram of the data acquisition/processing system is shown in Figure 10 and the various signal input sources to the data acquisition/processing system are shown in Figure 11. This system (Figure 10) permits acquisition of not only probe dielectric measurements data (amplitude and phase of complex reflection

1. Microprocessor-based CPU
2. 48 to 64 kBytes RAM
3. 300 kBytes disk storage
4. CRT terminal
5. Parallel interface for A/D data transfer
6. 16 channel, multiplexing A/D converter with throughput rates up to 20 kHz.
7. RS-232 serial interface for communication with the Georgia Tech CYBER 70/74 computer
8. IEEE-488 interface for network analyzer control
9. Sufficient software for adequate system control.

B. Microcomputer-Based Data Acquisition System Investigation

In order to meet the cost and desired configuration constraints, four microcomputers were investigated: the Commodore PET, APPLE II, Zenith/Heathkit WH-89, and Intecolor 8052. It was determined that the Heathkit WH-89 would be the most suitable choice for this data acquisition system. It utilizes two Zilog Z80 microprocessors (one which functions as the controller for the smart terminal, the other as the CPU) compared to a single Mostek MCS-6502 for the PET and APPLE computers, and an 8080A for the Intecolor computer. In addition, the WH-89 has a great deal of versatility in input/output functions. A disadvantage of the WH-89 is the present lack of availability of an IEEE-488 interface as opposed to the PET and APPLE. However, an IEEE-488 interface board is being developed for the WH-89, although this interface is not presently available on the commercial market.

Although the WH-89 was determined to be the best choice for the data acquisition and processing system with respect to cost/capability effectiveness, it was decided initially to use the Intecolor 8052 micro-computer because this computer already belonged to the Division. Characteristics of the Intecolor 8052 computer are listed below:

1. Intel 8080A based CPU
2. 48K RAM
3. Dual 5-1/4" floppy disks (180 kBytes each)

### SECTION III DATA ACQUISITION AND ANALYSIS

During the third year of this research program, the tradeoffs between developing an analog computer for direct recording of dielectric property data or developing a 16-channel multiplexed data acquisition system having a programmable sampling rate were evaluated. Because of the limitations placed on data processing and analysis by the analog approach, the second approach was selected. Efforts were then directed toward the implementation of a microcomputer-based data acquisition, storage, and processing system. The new system replaces the manual system used during all earlier studies (Years 1-2), in which physiological signals and complex reflection coefficient data were recorded on stripchart recorders and dielectric property information from the Hewlett-Packard semi-automated network analyzer was printed out. Using this method, data must be tabulated by hand on a point-by-point basis and transcribed to computer cards for further processing on the Georgia Tech CYBER 70/74 computer. The nature of this manual system makes data storage and retrieval cumbersome and hence forms a practical limitation to the extent of the data analysis. A new microcomputer-based system for data acquisition and control has been designed which will be ready for use during the fourth-year studies.

#### A. Data Acquisition - Technical Considerations

Several factors had to be considered in the design of a new data acquisition system including budget limitations which restricted the choice to microprocessor-based designs. It was desired to be able to sample up to 16 data channels at a maximum rate of 20 kHz. The digitized information for the data channels, along with their sampling time, should be stored on magnetic disk without operator intervention. This requirement necessitated that roughly 300 kBytes of disk storage be available for one experiment. Additionally, it was desired to be able to perform some real-time processing, control the network analyzer from the system, and have the capability of directly transferring data from the microcomputer to the Georgia Tech CYBER 70/74 large mainframe computer for more detailed analysis. A summary of the desired system configuration is listed below.

### 1. In-Vitro Renal Preparation

Following the femoral cannulations, the surgical procedure for isolating the kidney was begun. The left kidney (as viewed dorsally) was always approached first since it lies lower in the abdomen than the right and is less difficult to surgically expose. An electrosurgical unit was used to make the initial incision (8-10 cm in length) just below the last rib on the left side. The subdermal fascia and fatty tissue were separated by blunt dissection, using hemostats. In a similar manner, the several layers of abdominal wall muscle were each separated until the peritoneal cavity was opened. Then the left kidney was located and the surrounding fascia and fatty tissue were separated from the kidney. The renal blood vessels and ureter were isolated and the renal artery traced from the renal pelvis to its junction with the aorta. Ligatures were tied loosely around the vessels and the ureter was severed. The renal artery was next tied, cannulated distal (with respect to the heart) to the tie, and cut between the tie and the cannula. Next, the renal vein was tied and cut distal to the tie, at which point the kidney was free to be removed from the animal and placed on the external perfusion circuit illustrated in Figure 15. The period between the time at which arterial flow was first cut off and the time when perfusion on the external circuit was begun for each kidney was five to ten minutes. Similar surgical procedures were followed when isolating the right kidney.

Once a kidney was set up on the flow-controlled supply from the perfusion circuit, it was allowed to stabilize while the calibration of the network analyzer system and strip-chart recorders used in conjunction with the dielectric measurement probe was checked. Following the check and recalibration, which usually required approximately 20 minutes, a series of measurements relating perfusion pressure, kidney weight, and flow rate were performed. The organ chamber in which the kidney rested was placed on an electronic balance scale and tared to zero. Then the kidney was placed in the chamber and venous output was collected over a timed period (usually 60 seconds) from the drain tube on the organ chamber. Weight and perfusion pressure were recorded for various flow rates, and

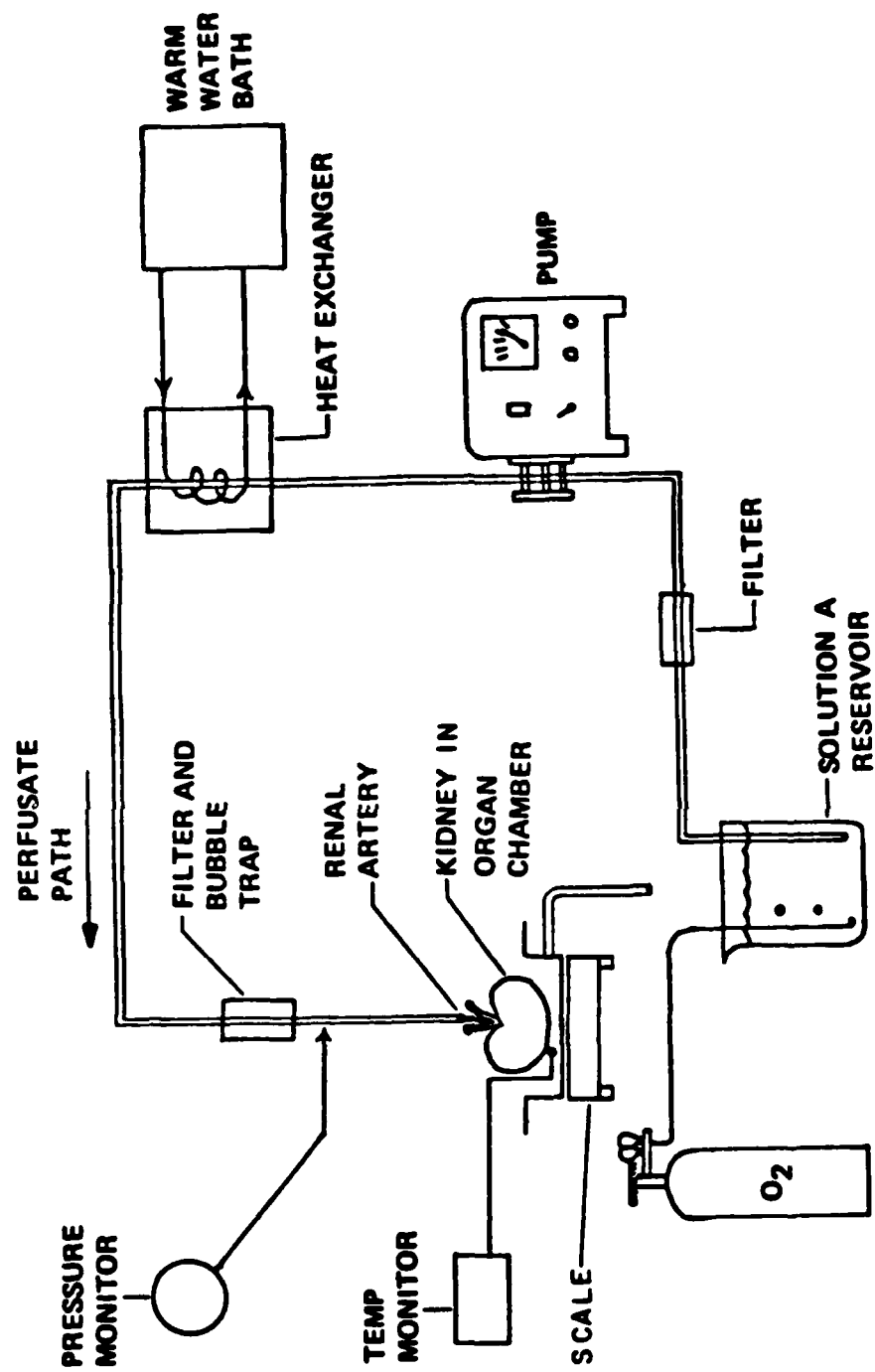


Figure 15. Diagrammatic illustration of experimental setup used for perfusion during *in-vitro* renal dielectric measurements.

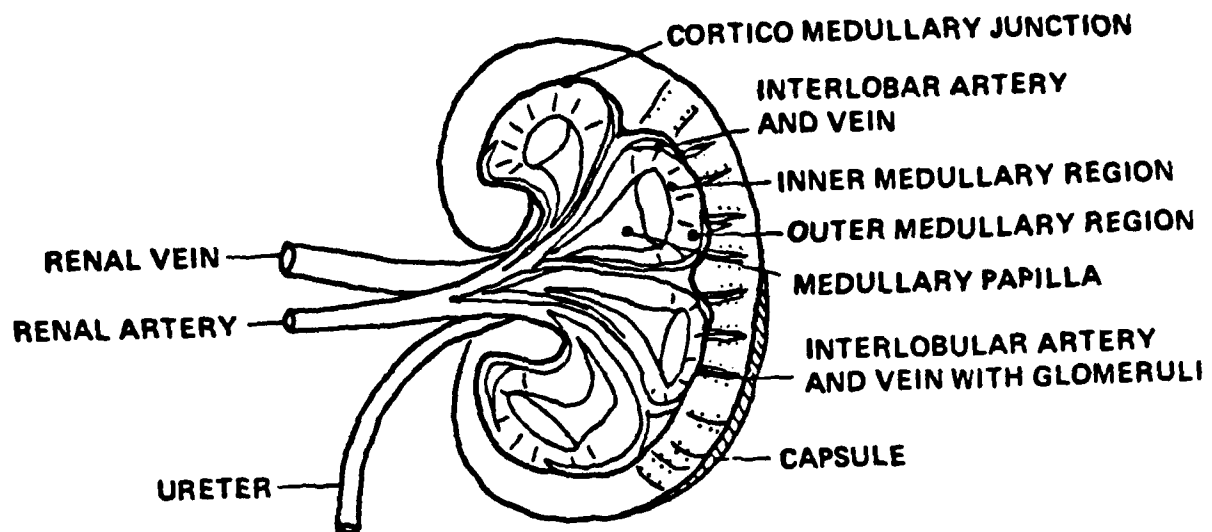
curves showing their relationships are presented in the next subsection of this report.

Once the initial flow/pressure/weight information had been gathered, a small section of the renal capsule was separated and cut away and the dielectric measurement probe was placed in contact with the renal cortex. Initially, data were taken until the dielectric properties had reached a steady state. The flow rate was then increased in sequential steps by increasing the speed of the perfusion pump, allowing both pressure and dielectric properties to reach a steady state condition before incrementing pump speed. Data were recorded for each of five different flow rates. Following the cortex measurements, a 15 ga. trochar needle was used to enter the kidney and the probe was inserted into the medullary region. The measurement sites in the kidney are indicated in Figure 16. An effort was made to place the probe at the same measurement sites in each of the experiments. Data collection in medullary tissue was performed at the same five flow rates used for cortex measurements.

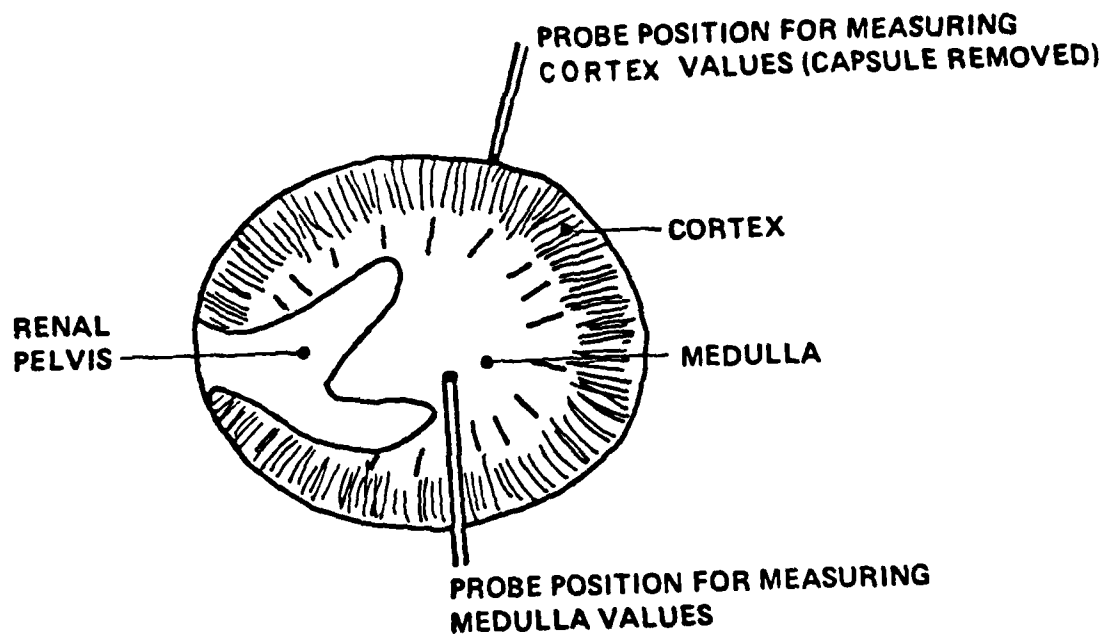
Six kidneys were measured in this fashion. After consideration of the results from the first four kidneys, it was decided to use larger diameter catheters and tubing in the perfusion circuit in order to reduce the total resistance of the circuit and increase flow rates. Thus, the last two kidneys measured in-vitro were perfused under different experimental conditions with respect to pressure and flow. These factors are considered in the following subsection (IV.B) of this report which describes the experimental results.

## 2. In-Situ Renal Preparation

In order to determine if the relationship between renal flow and measured dielectric properties which was observed in-vitro also existed in-vivo, a second series of experiments was performed wherein the dielectric measurements were made in-situ. The surgical procedure for these investigations was similar to that used in the in-vitro experiments. Two dogs were anesthetized with 30 mg/kg body weight pentobarbital sodium and maintained using this same agent. The other dogs were initially anesthetized with 50 mg/kg body weight  $\alpha$ -chloralose administered IV. One dog was maintained with  $\alpha$ -chloralose and occasional supplemental



(a) Renal anatomy in longitudinal cross-section



(b) Transverse cross-sectional view of dielectric property measurement sites

Figure 16. Two anatomical views of kidney. Sites where dielectric property measurements were performed are shown on transverse view of kidney.

doses of pentobarbital sodium as needed. Another two were maintained with  $\alpha$ -chloralose IV, and nitrous oxide ( $N_2O$ ) gas delivered by a Foregger Model Foretrend 100 anesthesia machine. The different forms of anesthesia were dictated by their availability, rather than by experimental requirements.

The femoral vessels were again cannulated and the left (and subsequently, the right) kidney and renal vessels located and isolated. Each dog was then given 2-3 cc heparin and 5 cc anti-coagulant citrate dextrose (ACD) IV, which were allowed to circulate and mix in the bloodstream for several minutes. Ligatures were then tied loosely around the renal arteries, and, in one dog, around the renal vein. In that dog, the left femoral vein was cannulated prior to cannulation of the renal vein. The cannulae were connected to two branches of a Y-shaped tube, of which the third branch was clamped off. Renal venous blood flow was thus directed to the femoral vein so that it could be maintained within the animal, while still allowing for momentary diversion to measure renal flow rates when desired. The left femoral artery was next cannulated and its output directed to the pump which drove the extracorporeal perfusion circuit illustrated in Figure 17. The blood delivered by the circuit perfused the kidney through the renal artery, which was cannulated next. Just prior to this cannulation, 1 cc of heparin was injected directly into the cannula. The perfusion pressure at the renal artery was monitored with a Narco Biosystems pressure transducer via a sidearm branch between the bubble trap and the renal arterial catheter (Figure 17).

After allowing 15-20 minutes for the system to stabilize, a series of measurements was made using a protocol which corresponded to that used in the in-vitro experiments. Problems with the surgery prevented the in-situ series of experiments from being as successful as the in-vitro series. Data from the second dog used in the in-situ experimental series were not collected since, apparently, air bubbles had significantly reduced flow in the left kidney. Although an attempt was made to measure the right kidney, blood clotting became a problem at the time the measurements were begun, because blood flow in the perfusion circuit had been

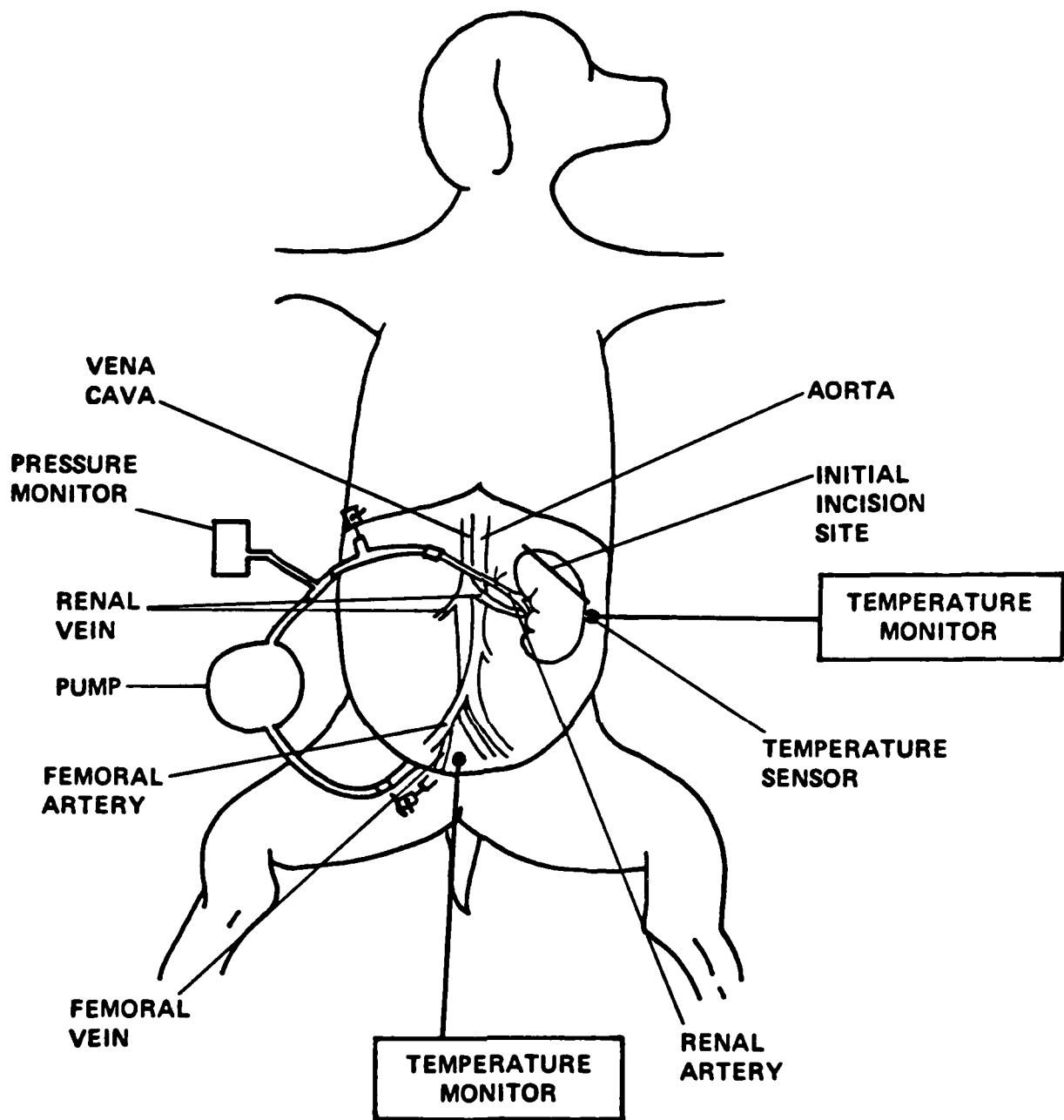


Figure 17. Diagram of extracorporeal perfusion circuit used for control of renal blood flow during in-situ renal dielectric property measurements. Note site of initial surgical incision.

shut off for too long a period. This experiment indicated that the two problems most likely to hinder normal renal blood flow in these in-situ experiments were blood clots and air bubbles. In later experiments, utmost care was taken to prevent clot formation and to prevent air bubbles from entering the kidney via the renal artery.

#### B. Perfusion Pressure, Renal Flow, and Kidney Weight Measurements

After each kidney had been surgically isolated and was being perfused, an attempt was made to characterize the pressure-flow relationship for the organ. In this way, it would be possible to obtain an indication of how well the kidney was functioning with respect to a normal flow/pressure relationship and how well the measured data reflected normal physiological conditions. The kidney was perfused at a set of discrete pump speeds. At each pump speed, pressure was recorded and total renal flow was measured by collecting the renal output in a graduated cylinder during a timed interval. The results are plotted in Figures 18-22.

It can be seen in Figures 18-20 that results from three of the first four kidneys in this series of six in-vitro experiments (no data are available from kidney # 2) do not extend above flow rates of 60-70 ml/min. At the time of these experiments, it was believed that higher flow rates would produce excessive renal perfusion pressures. As noted in the previous subsection of this report, in later experiments (kidneys 5 and 6) larger diameter tubing was used in the perfusion circuit. This resulted in a lower-resistance circuit (less pressure drop in the renal artery catheter) so that a pressure measurement in the revised circuit more accurately reflected the true pressure in the renal artery. With this circuit used for kidneys 5 and 6, flow rates of 150 ml/min were achieved without excessively high renal arterial pressure levels. Thus, the latter two kidneys measured in-vitro (5 and 6) were observed under conditions of pressure and flow which more accurately reflected actual in-situ conditions than did the first four.

In each case, flow rate is plotted as a function of both pump speed and renal perfusion pressure. For each experiment, the measured data were entered into a curve-fitting program which computed functional polynomial fits of various orders to the data. The lowest-order fit

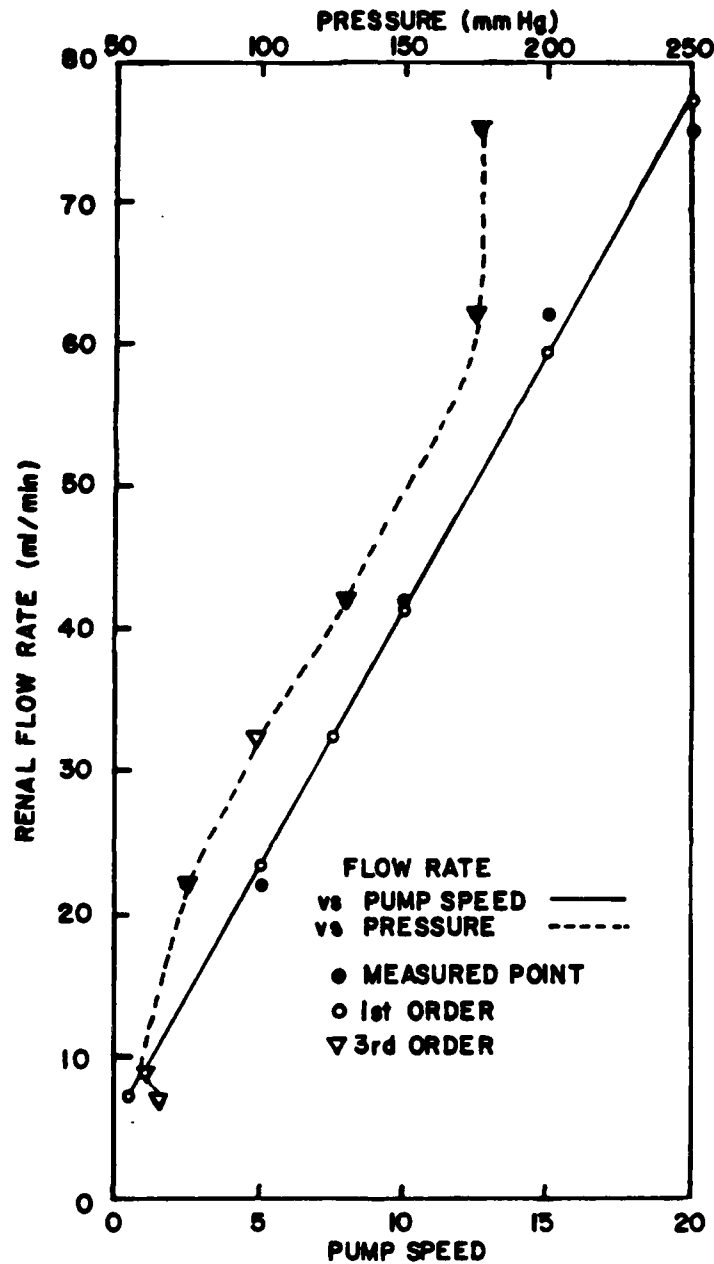


Figure 18. Flow rate vs. perfusion pressure and vs. pump speed for Kidney # 1. Curves connecting computed points (open symbols) represent a "best fit" approximation to measured data (solid symbols).

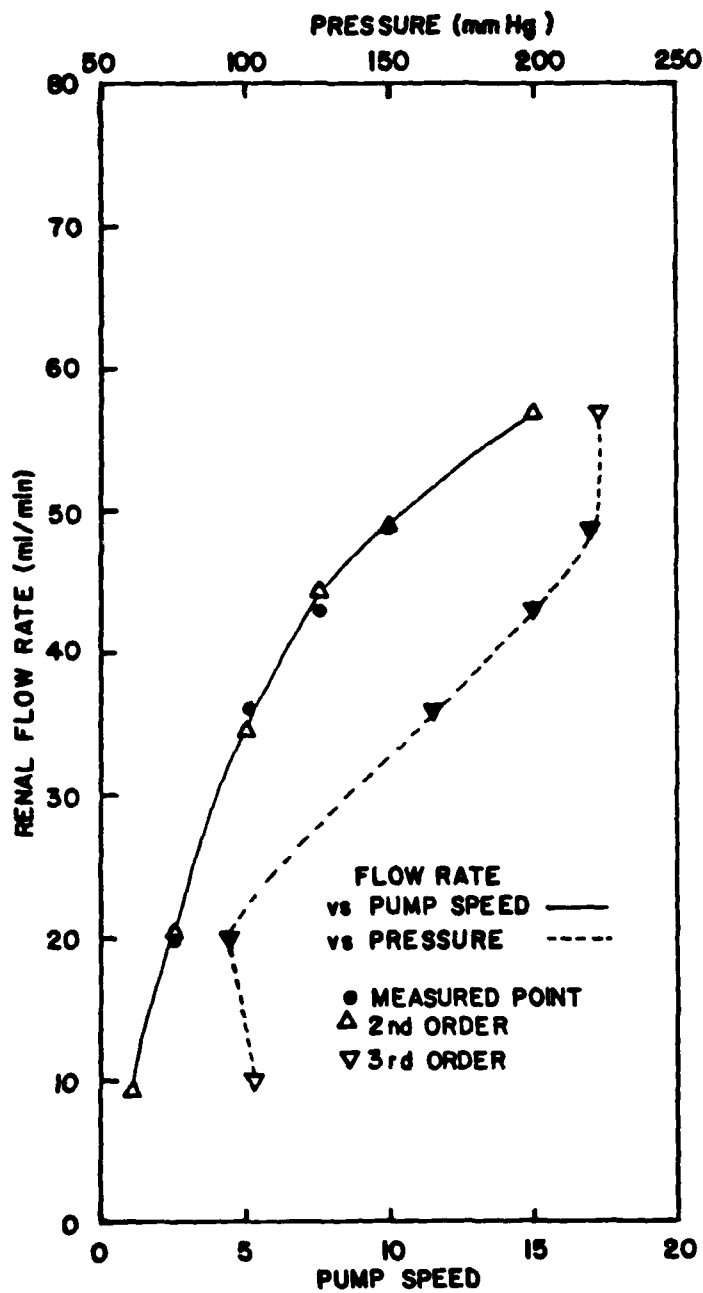


Figure 19. Flow rate vs. perfusion pressure and vs. pump speed for Kidney # 3. Curves connecting computed points (open symbols) represent a "best fit" approximation to measured data (solid symbols).

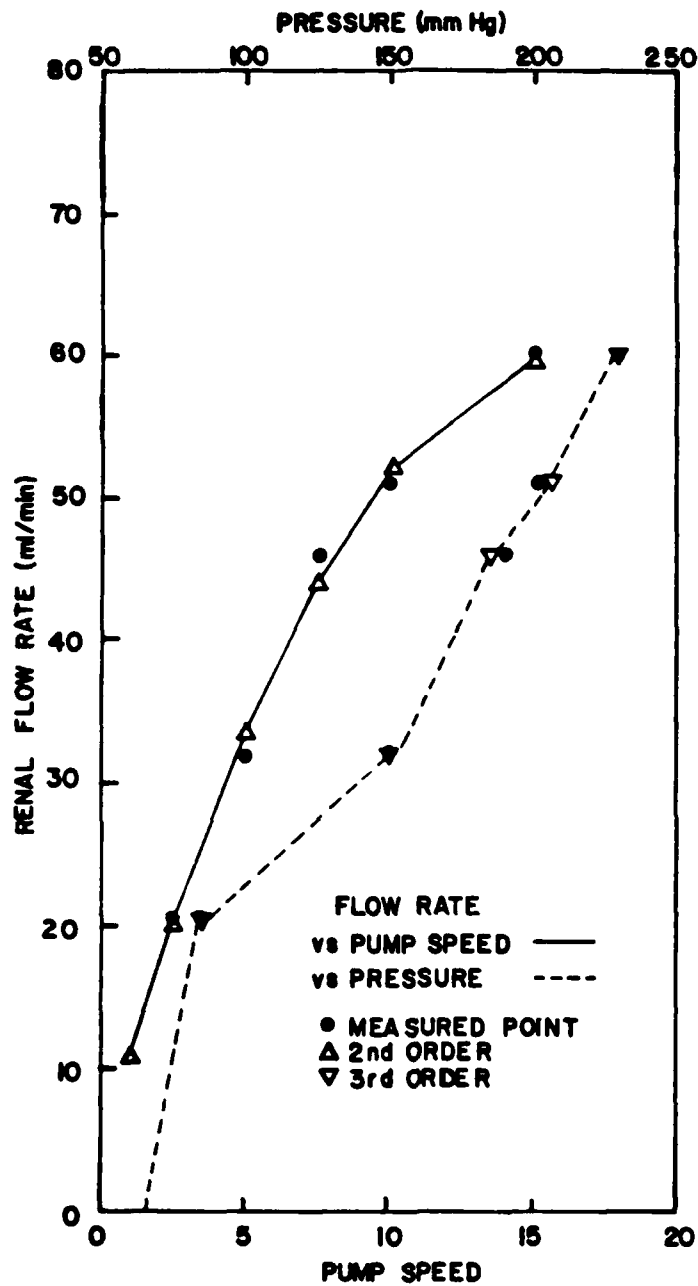


Figure 20. Flow rate vs. perfusion pressure and vs. pump speed for Kidney # 4. Curves connecting computed points (open symbols) represent a "best fit" approximation to measured data (solid symbols).

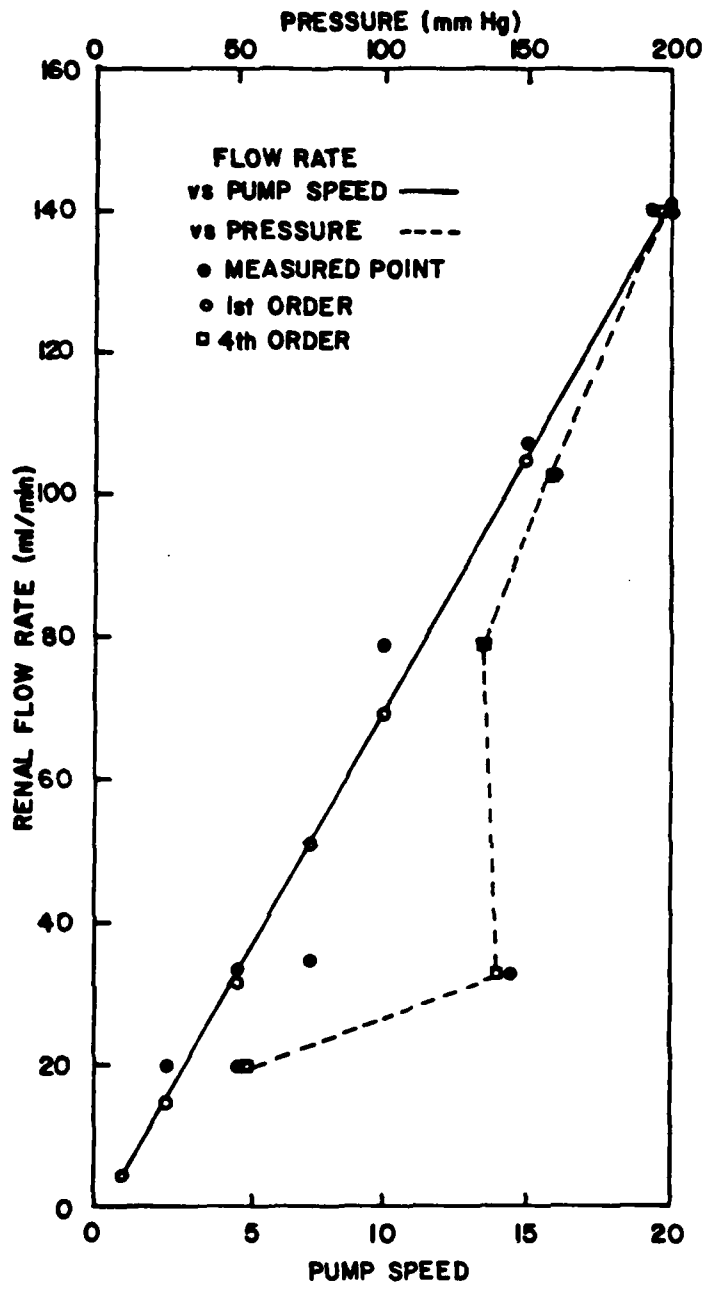


Figure 21. Flow rate vs. perfusion pressure and vs. pump speed for Kidney # 5. Curves connecting computed points (open symbols) represent a "best fit" approximation to measured data (solid symbols).

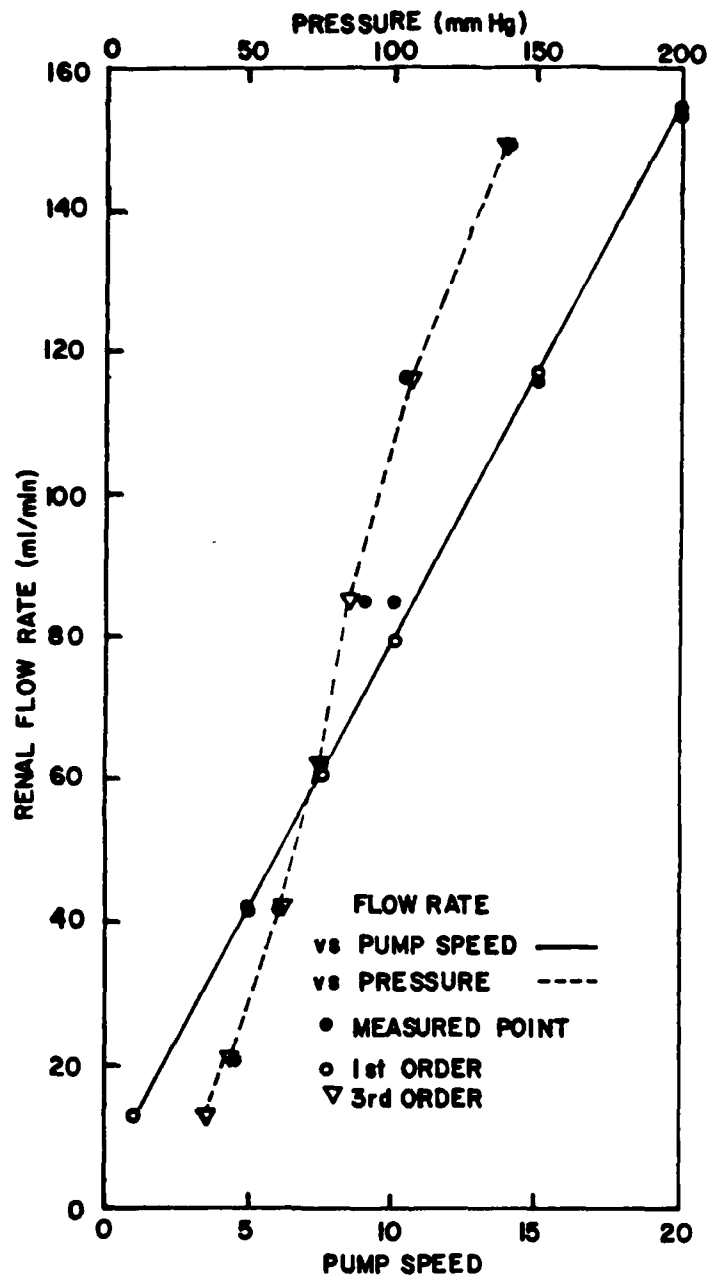


Figure 22. Flow rate vs. perfusion pressure and vs. pump speed for Kidney # 6. Curves connecting computed points (open symbols) represent a "best fit" approximation to measured data (solid symbols).

with acceptably low deviations from the measured data is plotted together with the measured data (Figures 18-22). The relationship between pump speed and flow rate for each kidney was adequately characterized by a 1st or 2nd order equation. Flow rate and perfusion pressure most frequently exhibited a 3rd order relationship (roughly sigmoid-shaped curve).

### C. Renal Dielectric Property Studies

During the last reporting period (Annual Technical Report No. 2 [9]), preliminary data were collected relating dielectric properties of renal tissue to varying conditions of renal flow. At that time, dielectric properties were examined as a function of pump speed. Pump speed was used as a surrogate parameter for renal flow rate in these experiments. Prior to initiating the series of experiments which are described in detail in this report, the earlier experiments were reconsidered with perfusion pressure treated as the independent variable. Figure 23 shows the relationship between the relative dielectric constant ( $K$ ) and conductivity ( $\sigma$ ) of renal tissues in an isolated kidney and perfusion pressure measured in the renal artery. The renal vein and ureter were free so that any back pressure resulted solely from the renal tissue itself. During the dielectric measurements of each tissue type (medulla, cortex, and cortical surface), the flow rate was varied pseudo-randomly so that the pressure was neither monotonically increasing nor decreasing. The most distinct trend showed up in the medullary measurements, where a decreased perfusion pressure was clearly associated with higher values for  $K$  and  $\sigma$ . Similar patterns were detected in the cortical and surface measurements, although they were not as distinct. These results suggested that, at lower perfusion pressures, the fluid tends to "pool" in the kidney, since the presence of an increased amount of bulk water could account for the higher dielectric values.

Figure 24 illustrates a striking illustration of this effect. The figure shows a 2-channel stripchart recording of complex reflection coefficient ( $\Gamma$ ) amplitude and phase taken from the analog output of the microwave network analyzer system. The recorded amplitude and phase

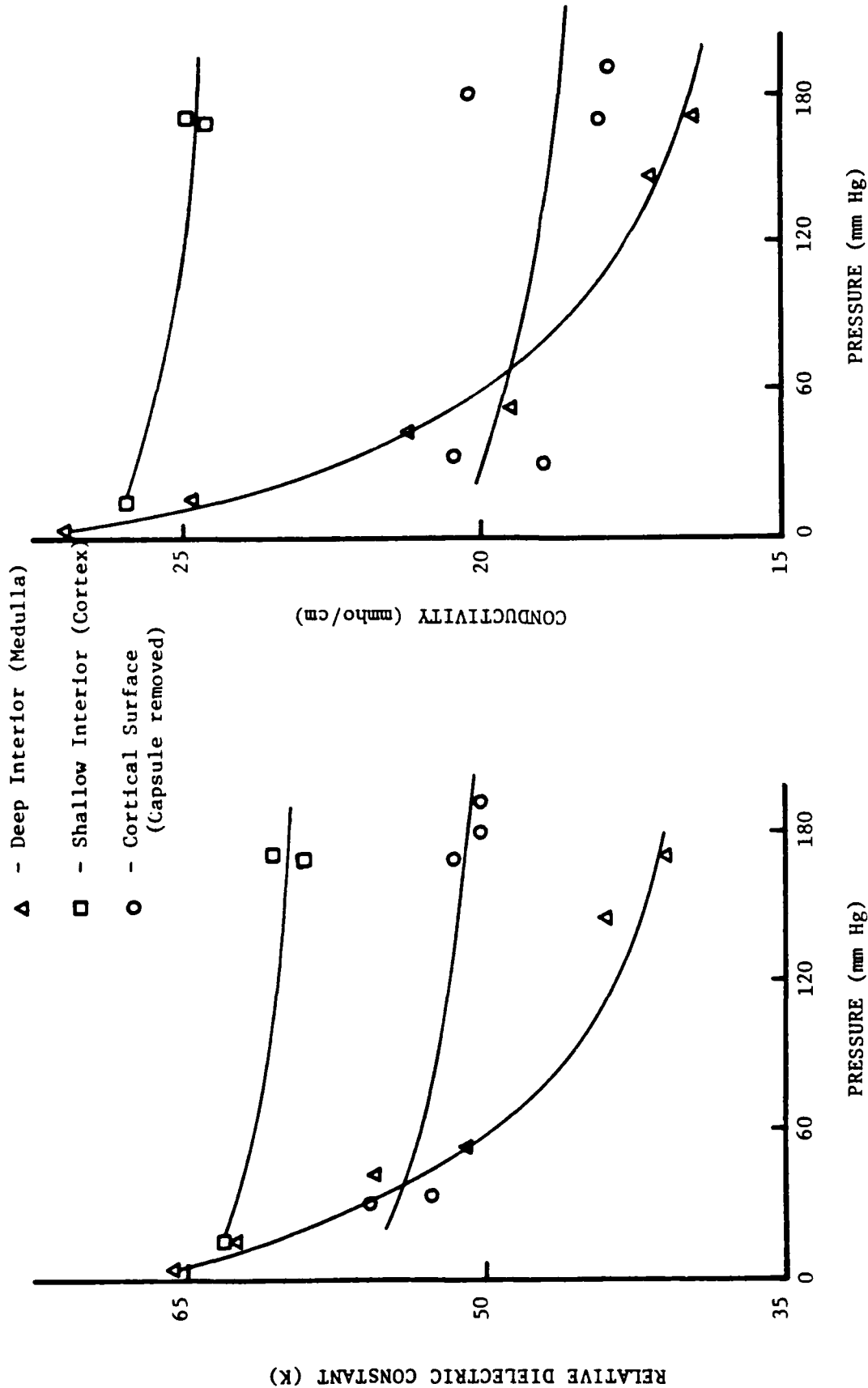


Figure 23. Relative dielectric constant and conductivity of renal tissue measured as a function of perfusion pressure. Isolated kidney perfused with a  $Mg^{2+}$  -  $K^{+}$  rich solution.

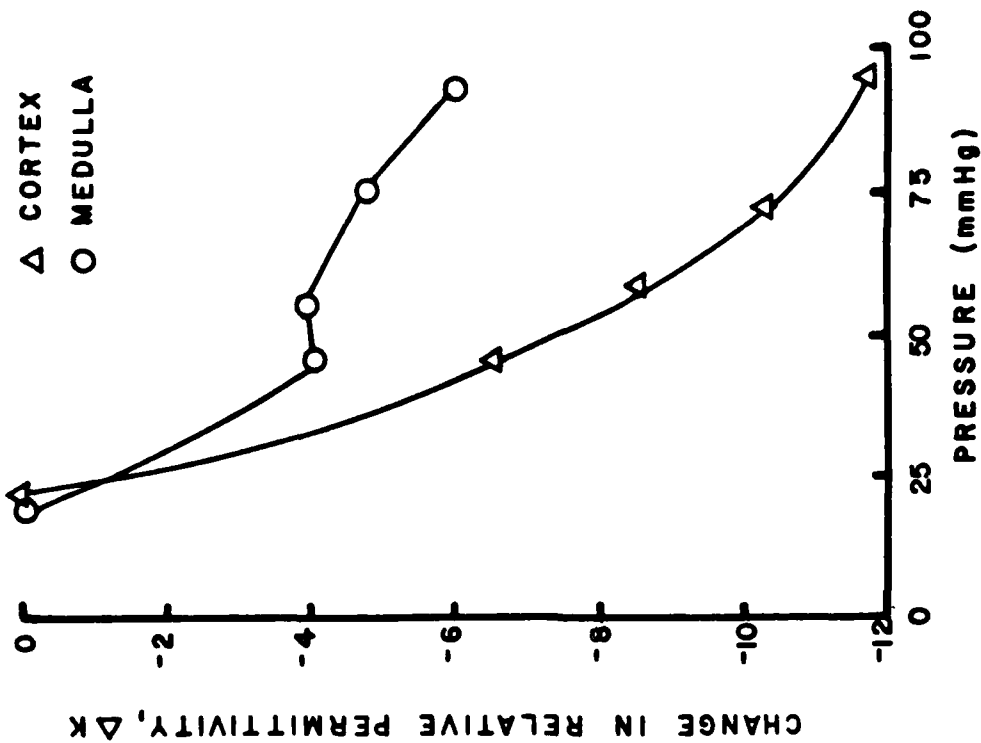
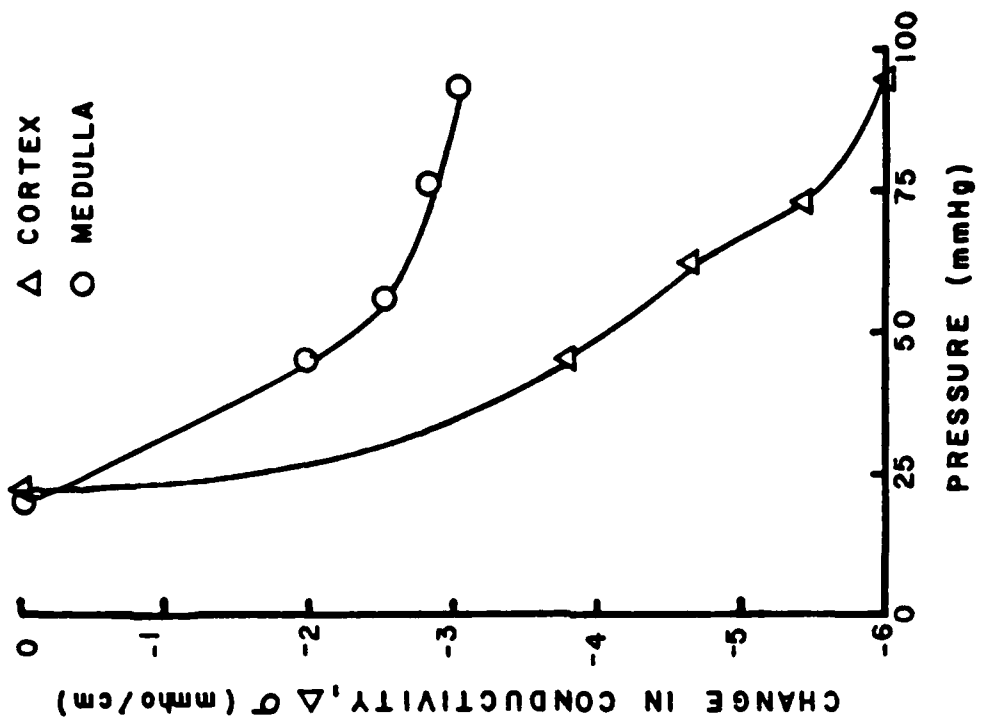


Figure 29. Baseline-subtracted dielectric properties as a function of perfusion pressure in Kidney #6. Correlation coefficients ( $r$ ) and probabilities for correlation ( $P_c$ ) are listed in Table III.

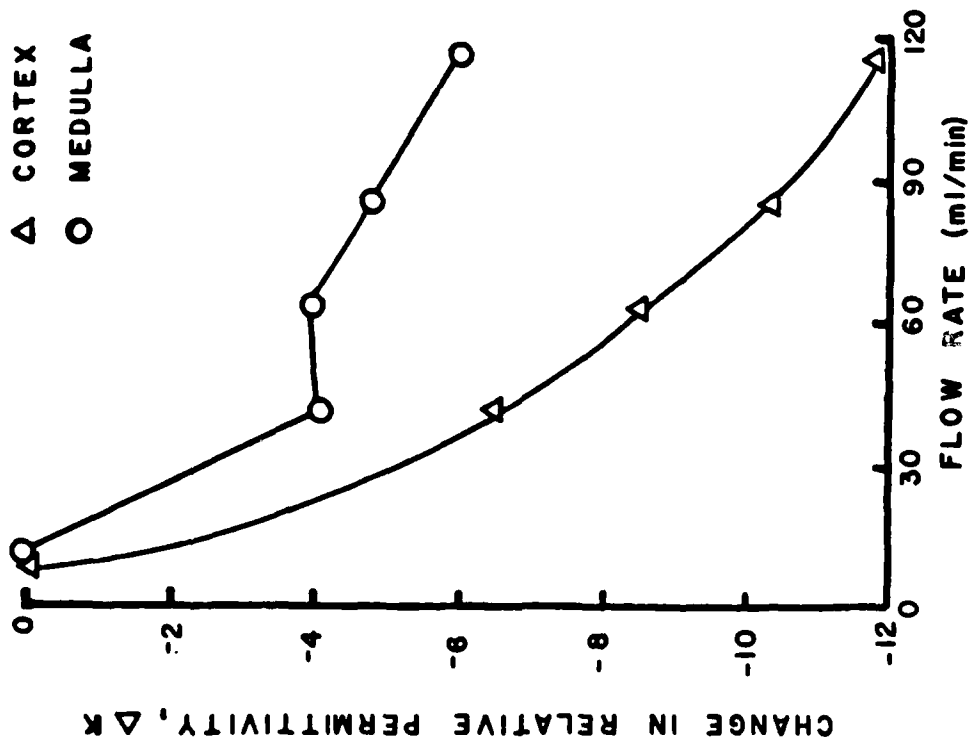
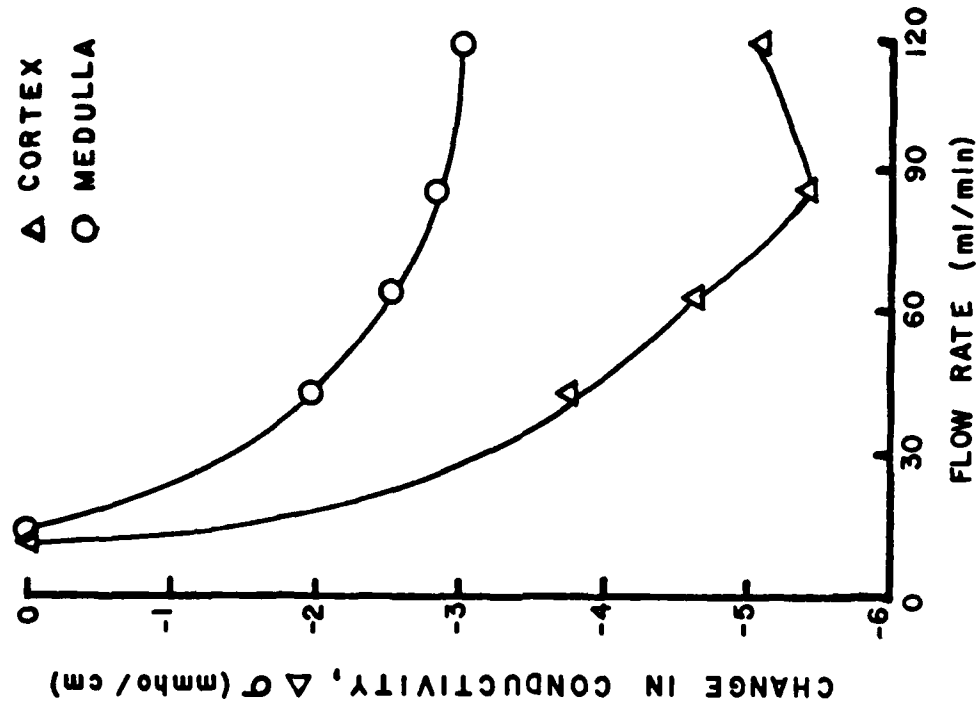


Figure 28. Baseline-subtracted dielectric properties as a function of flow rate in Kidney #6. Correlation coefficients ( $r$ ) and probabilities for correlation ( $P_c$ ) are listed in Table III.

TABLE III Concluded

## CORRELATION COEFFICIENT AND PROBABILITIES FOR CORRELATION

| Independent Variable | Dependent Variable                                | Correlation Coefficient (r) | Probability for Correlation ( $P_c$ ) | Remarks       |
|----------------------|---|-----------------------------|---------------------------------------|---------------|
| Flow Rate            | $\Delta K$ in Normal Cortex                       | -0.695                      | 0.875                                 | See Figure 31 |
|                      | $\Delta K$ with Phenoxybenzamine                  | -0.945                      | 0.945                                 |               |
|                      | $\Delta\sigma$ in Normal Cortex                   | -0.678                      | 0.861                                 |               |
|                      | $\Delta\sigma$ with Phenoxybenzamine              | -0.963                      | 0.963                                 |               |
| Perfusion Pressure   | $\Delta K$ in Normal Cortex                       | -0.740                      | 0.907                                 | See Figure 32 |
|                      | $\Delta K$ with Phenoxybenzamine                  | -0.993                      | 0.993                                 |               |
|                      | $\Delta\sigma$ in Normal Cortex                   | -0.726                      | 0.897                                 |               |
|                      | $\Delta\sigma$ with Phenoxybenzamine              | -0.979                      | 0.979                                 |               |
| Flow Rate            | $\Delta$ Perfusion Pressure for Normal Kidney     | 0.996                       | 1.000                                 | See Figure 33 |
|                      | $\Delta$ Perfusion Pressure with Phenoxybenzamine | 0.963                       | 0.963                                 |               |
|                      | $\Delta$ Kidney Weight for Normal Kidney          | 0.931                       | 0.993                                 |               |
|                      | $\Delta$ Kidney Weight with Phenoxybenzamine      | 0.962                       | 0.962                                 |               |

TABLE III Continued

CORRELATION COEFFICIENT AND PROBABILITIES FOR CORRELATION

| Independent Variable | Dependent Variable                                      | Correlation Coefficient (r) | Probability for Correlation (P <sub>c</sub> ) | Remarks       |
|----------------------|---|-----------------------------|---|---------------|
| Perfusion Pressure   | ΔK in Cortex, Kidney # 6                                | -0.961                      | 0.998   | See Figure 29 |
|                      | ΔK in Medulla, Kidney # 6                               | -0.888                      | 0.982   |               |
|                      | Δσ in Cortex, Kidney # 6                                | -0.931                      | 0.993   |               |
|                      | Δσ in Medulla, Kidney # 6                               | -0.887                      | 0.981   |               |
| Flow Rate            | ΔPerfusion Pressure for Cortex Measurement, Kidney # 6  | 0.997                       | 1.000   | See Figure 30 |
|                      | ΔPerfusion Pressure for Medulla Measurement, Kidney # 6 | 0.999                       | 1.000   |               |
|                      | ΔKidney Weight for Cortex Measurement, Kidney # 6       | 0.994                       | 1.000   |               |
|                      | ΔKidney Weight for Medulla Measurement, Kidney # 6      | 0.994                       | 1.000   |               |

Continued

TABLE III Continued

CORRELATION COEFFICIENT AND PROBABILITIES FOR CORRELATION

| Independent Variable | Dependent Variable  | Correlation Coefficient (r) | Probability for Correlation (P <sub>c</sub> ) | Remarks       |
|----------------------|---|-----------------------------|---|---------------|
| Flow Rate            | Avg. ΔPerfusion Pressure for Cortex Measurements, Kidneys 1-4.  | 0.970                       | 0.999   | See Figure 27 |
|                      | Avg. ΔPerfusion Pressure for Medulla Measurements, Kidneys 1-4. | 0.896                       | 0.984   |               |
|                      | Avg. ΔKidney Weight For Cortex Measurements, Kidneys 1-4.       | 0.942                       | 0.995   |               |
|                      | Avg. ΔKidney Weight for Medulla Measurements, Kidneys 1-4.      | 0.772                       | 0.928   |               |
| Flow Rate            | ΔK in Cortex, Kidney # 6  | -0.935                      | 0.994   | See Figure 28 |
|                      | ΔK in Medulla, Kidney # 6                                       | -0.869                      | 0.975   |               |
|                      | Δσ in Cortex, Kidney # 6  | -0.900                      | 0.985   |               |
|                      | Δσ in Medulla, Kidney # 6                                       | -0.876                      | 0.978   |               |

Continued

TABLE III

## CORRELATION COEFFICIENT AND PROBABILITIES FOR CORRELATION

| Independent Variable | Dependent Variable                          | Correlation Coefficient (r) | Probability for Correlation ( $P_c$ ) | Remarks       |
|----------------------|---|-----------------------------|---------------------------------------|---------------|
| Flow Rate            | Avg. $\Delta K$ in Cortex, Kidneys 1-4      | -0.790                      | 0.939                                 | See Figure 25 |
|                      | Avg. $\Delta K$ in Medulla, Kidneys 1-4     | -0.939                      | 0.995                                 |               |
|                      | Avg. $\Delta\sigma$ in Cortex, Kidneys 1-4  | -0.732                      | 0.902                                 |               |
|                      | Avg. $\Delta\sigma$ in Medulla, Kidneys 1-4 | -0.930                      | 0.993                                 |               |
| Perfusion Pressure   | Avg. $\Delta K$ in Cortex, Kidneys 1-4      | -0.876                      | 0.978                                 | See Figure 26 |
|                      | Avg. $\Delta K$ in Medulla, Kidneys 1-4     | -0.959                      | 0.997                                 |               |
|                      | Avg. $\Delta\sigma$ in Cortex, Kidneys 1-4  | -0.840                      | 0.964                                 |               |
|                      | Avg. $\Delta\sigma$ in Medulla, Kidneys 1-4 | -0.962                      | 0.998                                 |               |

Continued

permittivity and conductivity from baseline values as a function of flow rate and as a function of pressure are presented. These results are from in-vitro kidneys 1-4, where measured renal arterial pressures were higher than in-situ pressures at similar flow rates. Figure 27 illustrates this observation. Note that the dielectric properties (relative permittivity and conductivity) have a strong negative correlation with flow rate and pressure (Figures 25 and 26). Also, unlike the overall average values shown in Tables I and II, little difference was observed between measured dielectric changes in cortex and medulla. Measured changes in pressure and kidney weight with changing flow rate had a strong positive correlation, the opposite result from that obtained for the dielectric properties. Linear correlation coefficients and probabilities for these and subsequent data are presented in Table III.

Results for a single kidney (#6) are presented in Figures 28-30. Once again, the inverse (negative) correlation between dielectric properties and pressure/flow rate is observed. However, two important differences exist between these data and the data displayed in Figures 25-27. First, prior to the experiment involving kidney #6 in this series, the perfusion circuit had been modified to reduce its resistance to flow and thus, more physiologically normal flow rates were obtained for a given perfusion pressure. Second, both the relative permittivity and conductivity measured as functions of total renal flow rate or as functions of pressure exhibit factors of 2 to 3 larger changes in the renal cortex than in the renal medulla. This result is in agreement with the trend in overall average values shown in Tables I and II. Further, as would be expected, the changes in pressure and weight as a function of flow rate, which are parameters measured for whole kidney, are the same for permittivity measurements in both cortex and medulla (Figure 30). Again in Figure 30, a strong positive correlation between pressure/weight and flow rate was observed. These results (different dielectric changes in cortex and medulla) are interesting because, if they can be correlated with shifts in regional blood flow or compartmental water shifts in the kidney, the probe impedance measurement technique could provide information useful to better understanding the role of the kidney in hypertension -- or to

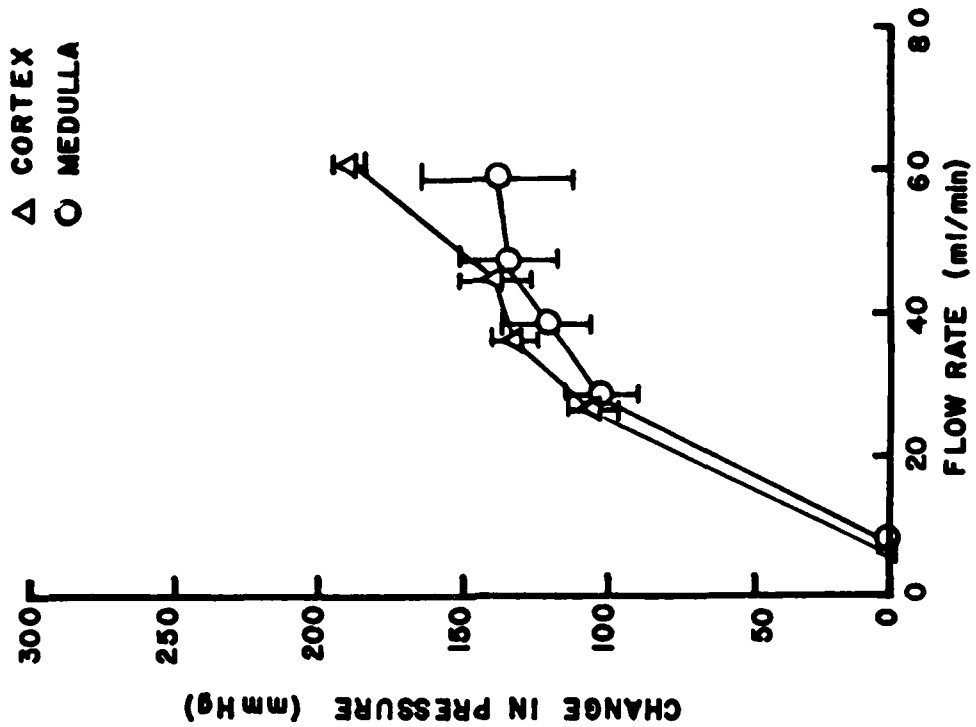
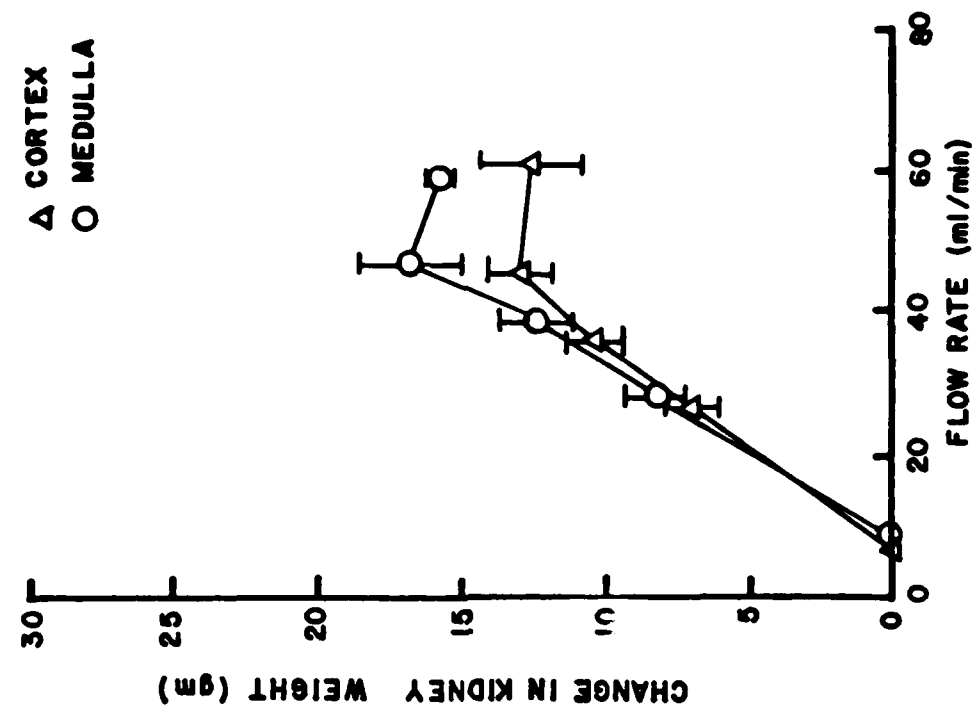


Figure 27. Average changes in perfusion pressure and kidney weight as functions of flow rate while measuring dielectric properties of cortex and medulla tissues in kidneys 1-4.

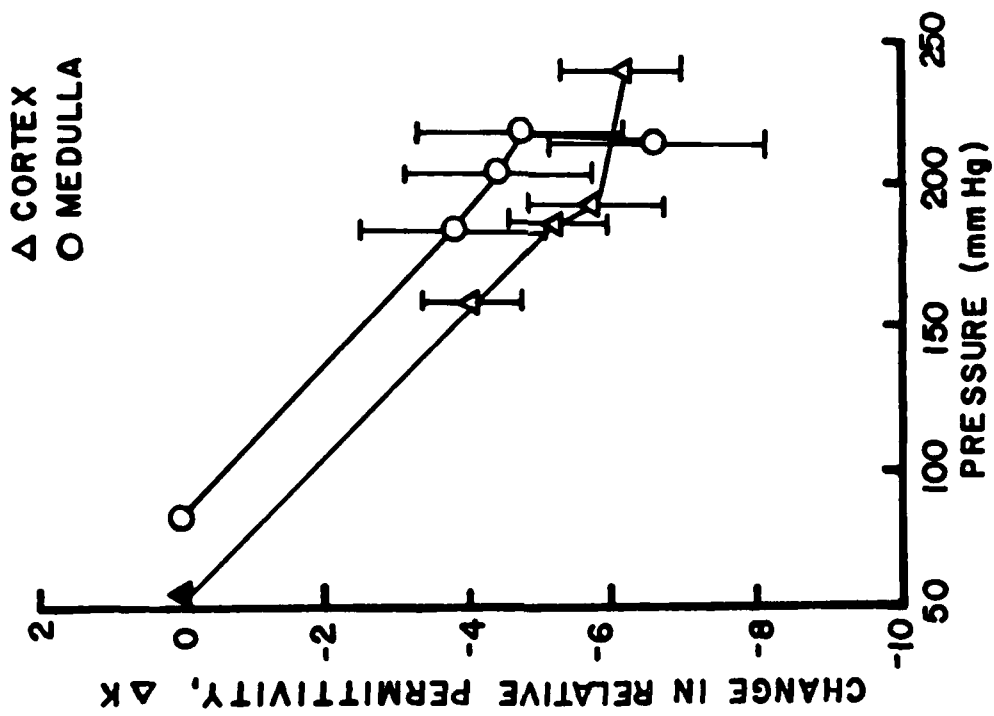
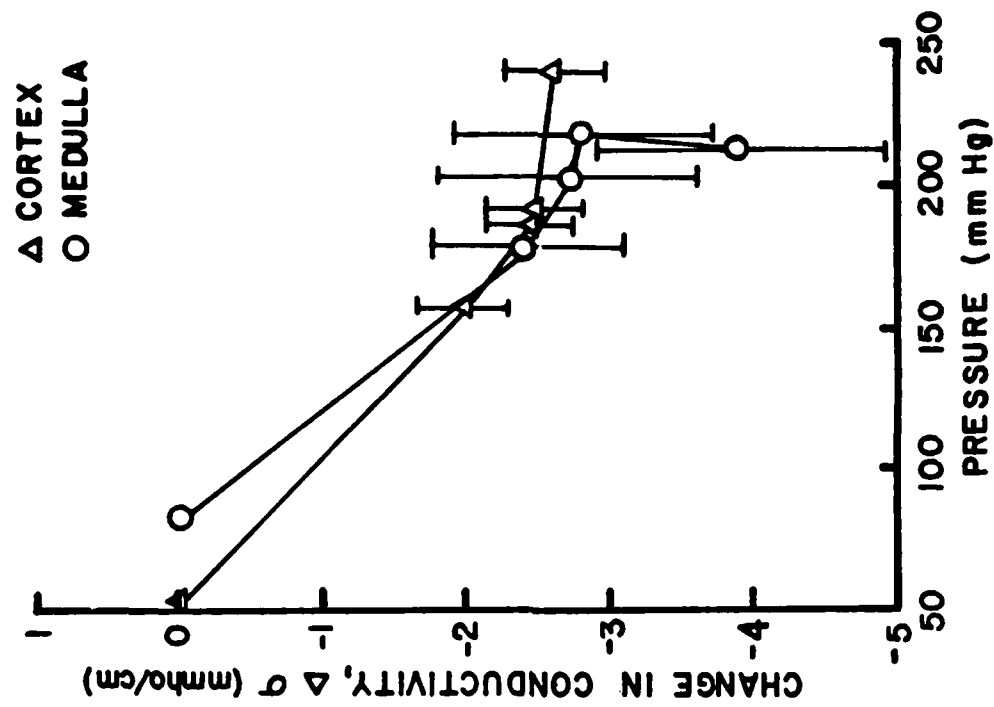


Figure 26. Averaged, baseline-subtracted dielectric properties as a function of perfusion pressure in Kidneys 1-4. Correlation coefficients ( $r$ ) and probabilities for correlation ( $P_c$ ) are listed in Table III.

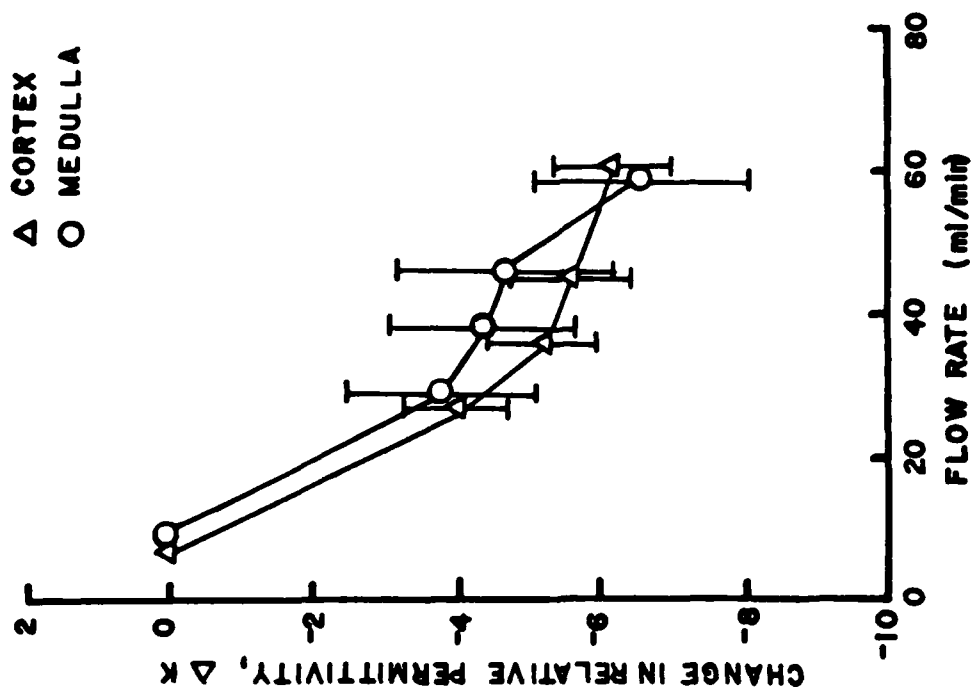
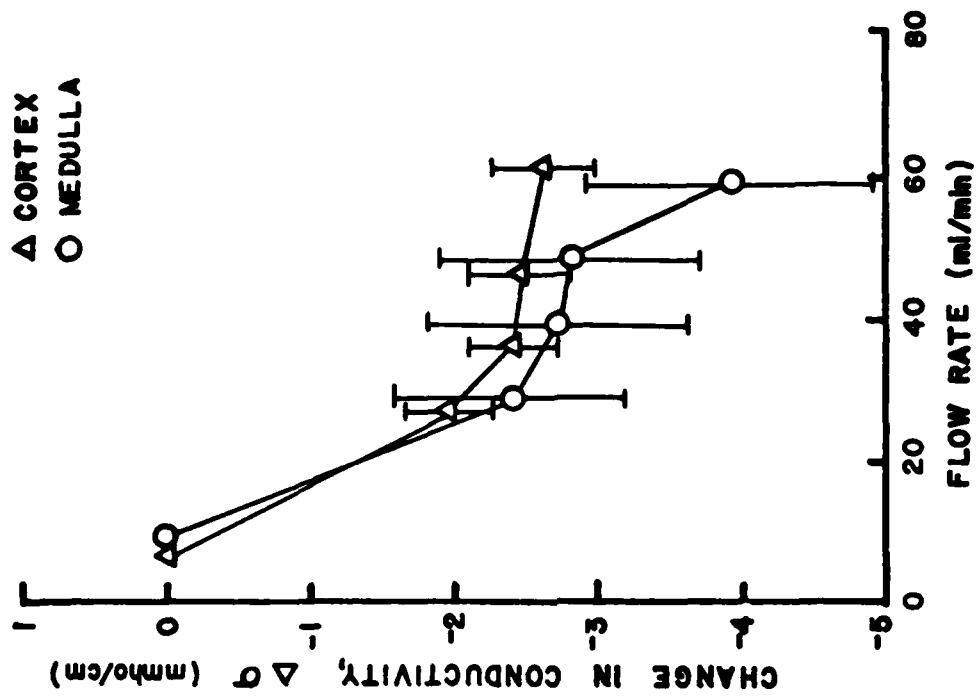


Figure 25. Averaged, baseline-subtracted dielectric properties as a function of flow rate in Kidneys 1-4. Correlation coefficients ( $r$ ) and probabilities for correlation ( $P_c$ ) are listed in Table III.

TABLE II  
RENAL MEDULLA PROPERTIES VS. FLOW RATE\*

| RENAL FLOW<br>(ml/min)    | 8.5   | 28.0  | 38.6  | 46.0  | 59.6  |
|---------------------------|-------|-------|-------|-------|-------|
| MEASURED<br>PARAMETERS    |       |       |       |       |       |
| Pressure<br>(mm Hg)       | 83.8  | 184.3 | 203.0 | 217.5 | 213.0 |
| Relative<br>Permittivity  | 58.94 | 55.37 | 54.79 | 54.53 | 55.81 |
| Conductivity<br>(mmho/cm) | 27.29 | 25.61 | 25.36 | 25.41 | 26.92 |
| Weight<br>(g)             | 66.3  | 74.5  | 78.6  | 83.0  | 75.2  |
| Temperature +<br>(°C)     | 37    | 37    | 37    | 37    | 37    |

\* Dielectric property measurements performed at 2450 MHz.

+ Temperature coefficients of  $-0.3\%/^{\circ}\text{C}$  for Relative Permittivity and  $-2.0\%/^{\circ}\text{C}$  for Conductivity were used to normalize tissue temperatures to  $37^{\circ}\text{C}$ . Temperatures of measured tissue ranged from  $34.0^{\circ}\text{C}$  to  $37.1^{\circ}\text{C}$ .

TABLE I  
RENAL CORTEX PROPERTIES VS. FLOW RATE \*

| RENAL FLOW<br>(ml/min)    | 7.3   | 28.0  | 36.0  | 46.0  | 60.2  |
|---------------------------|-------|-------|-------|-------|-------|
| MEASURED<br>PARAMETERS    |       |       |       |       |       |
| Pressure<br>(mm Hg)       | 53.8  | 156.5 | 185.3 | 190.8 | 242.5 |
| Relative<br>Permittivity  | 53.41 | 49.56 | 48.49 | 48.24 | 47.71 |
| Conductivity<br>(mmho/cm) | 22.27 | 20.77 | 20.55 | 20.57 | 21.01 |
| Weight<br>(g)             | 69.9  | 76.9  | 79.9  | 82.9  | 82.5  |
| Temperature †<br>(°C)     | 37    | 37    | 37    | 37    | 37    |

\* Dielectric property measurements performed at 2450 MHz.

† Temperature coefficients of  $-0.3\%/^{\circ}\text{C}$  for Relative Permittivity and  $-2.0\%/^{\circ}\text{C}$  for Conductivity were used to normalize tissue temperatures to  $37^{\circ}\text{C}$ . Temperatures of measured tissue ranged from  $34.2^{\circ}\text{C}$  to  $37.5^{\circ}\text{C}$ .

values are subsequently used to determine the tissue's dielectric properties. The recordings in Figure 24 are real-time recordings of complex reflection coefficient amplitude and phase measured as a function of perfusion rate and pressure. In every instance where perfusion rate was changed, a rapid corresponding change in the recorded components of the complex reflection coefficient ensued. An increase in perfusion rate (and pressure) caused a decrease in the components of  $\Gamma$  (and in the computed dielectric properties), while decreasing the rate of perfusion caused the component values to increase.

The observed phenomenon was investigated further with in-vitro experiments performed during this reporting period. Results using isolated, perfused kidneys are presented in Tables I and II. In these tables, the values shown for each of the measured variable parameters as a function of renal flow rate are the average values of six kidneys. Note that the data has been collected so that either perfusion pressure or rate of perfusion (renal flow) may be used as the independent variable. Increasing flow rate, and thus pressure, results in an increase in kidney weight. However, it is noted that the observed kidney weight gain is relatively small in proportion to the changes in pressure and flow rate. Also, at higher flow rates, changes in weight with changes in pressure/flow were proportionately even smaller. An inverse relationship between pressure/flow and dielectric properties, i.e., an increase in pressure/flow producing a decrease in relative permittivity and conductivity, was observed for both cortex and medulla. However, the magnitude of the measured changes was less in the medulla than in the cortex, and at increased flow rates, mean changes in dielectric parameters in the medulla were not statistically significant. These results may well indicate a regional shift in renal flow with changes in total renal flow and/or perfusion pressure. By relating the measured changes in renal dielectric properties to changes in regional flow rate or volume by another independent method, it may be possible to use the probe dielectric measurement technique as a tool for also measuring regional shifts in renal blood flow. In Figures 25-27, the mean measured changes (and standard errors) in relative

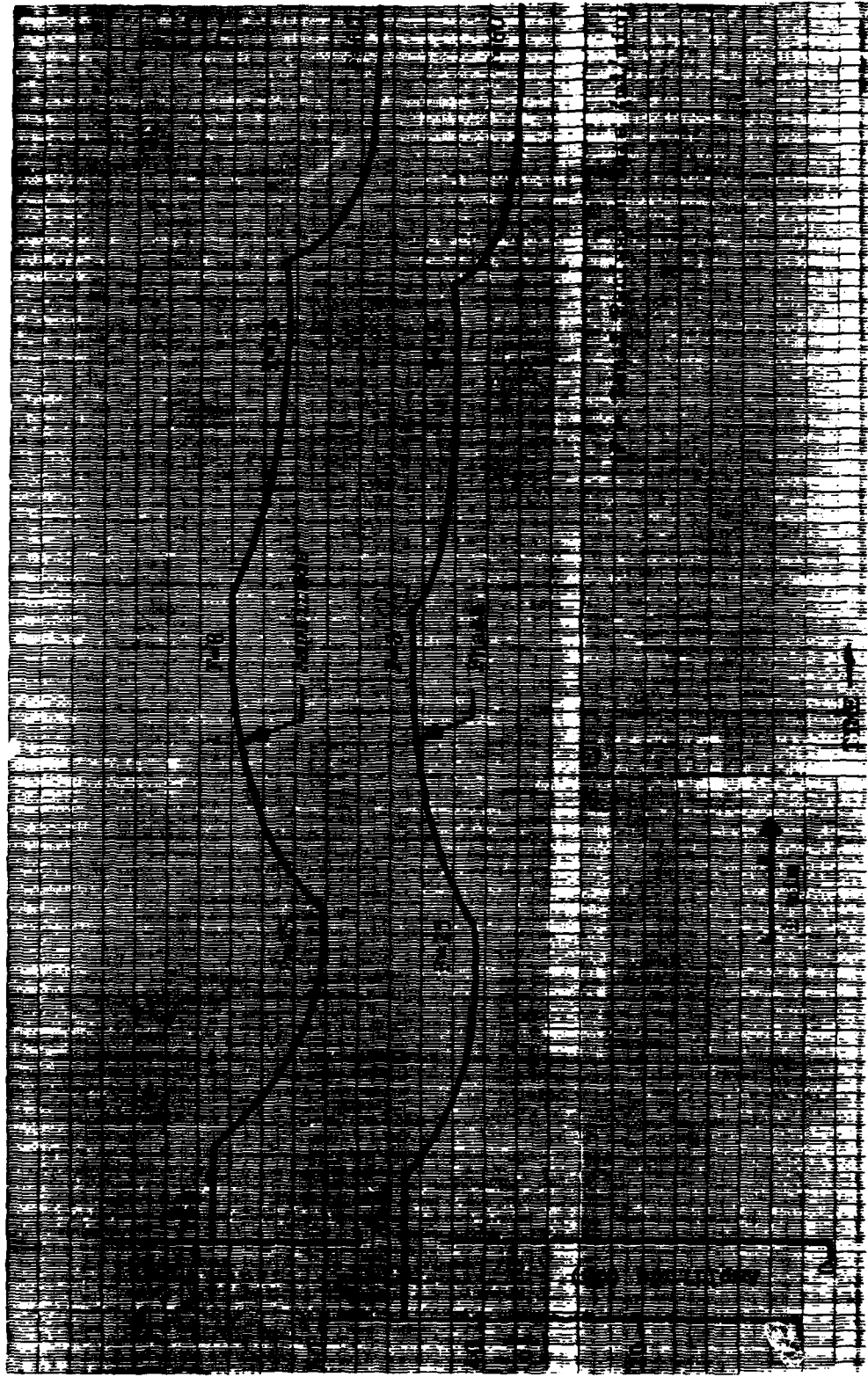


Figure 24. Amplitude and phase of complex reflection coefficient of medulla tissue measured in-vitro in isolated, perfused kidney.

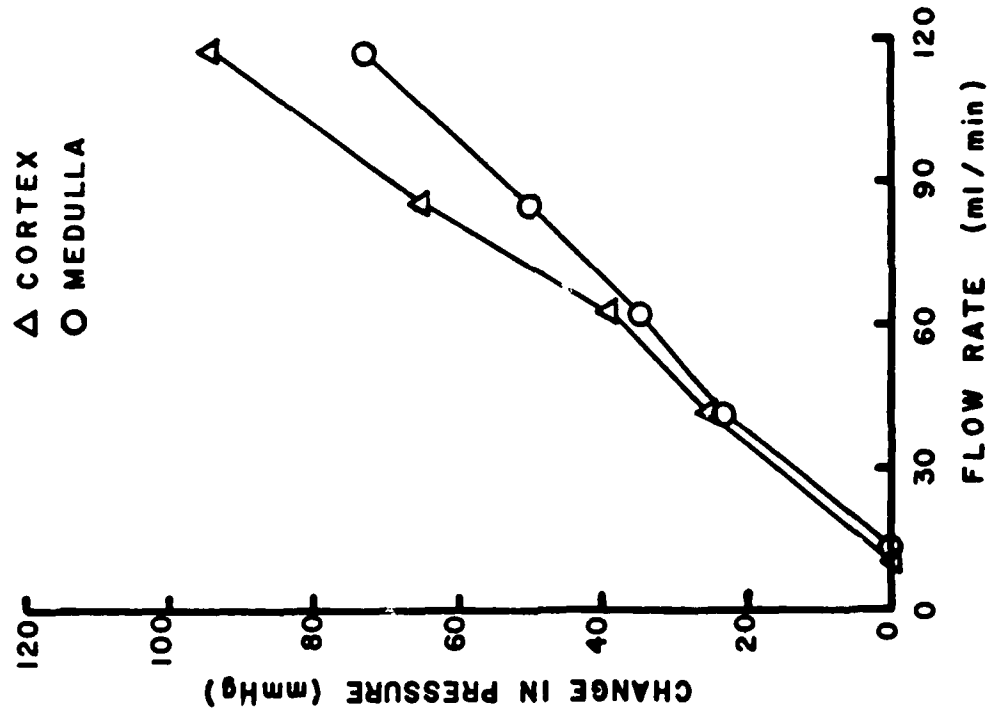
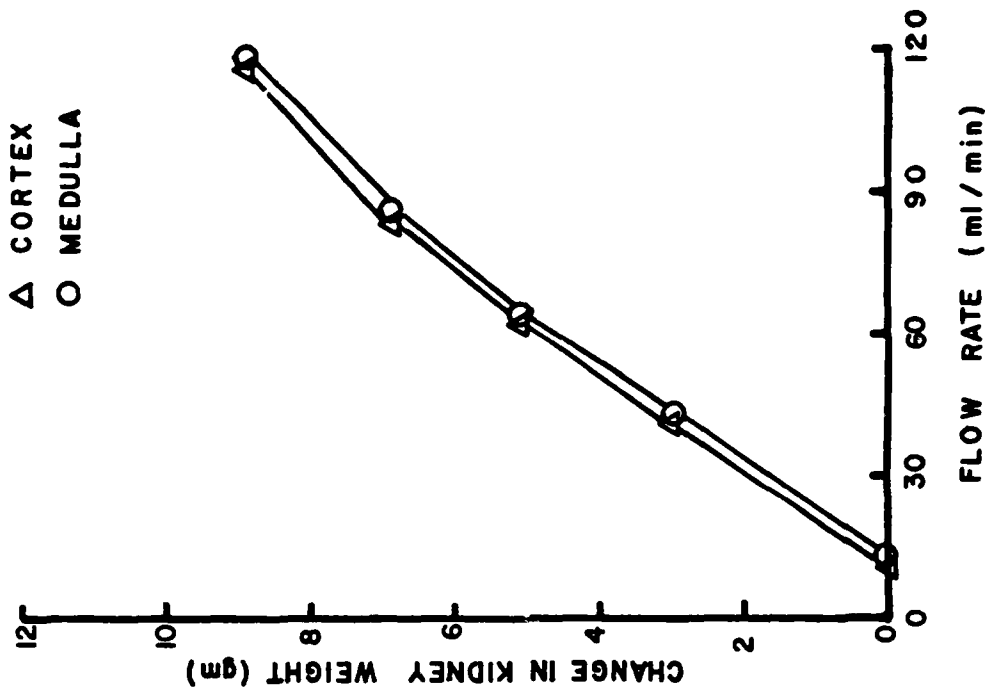
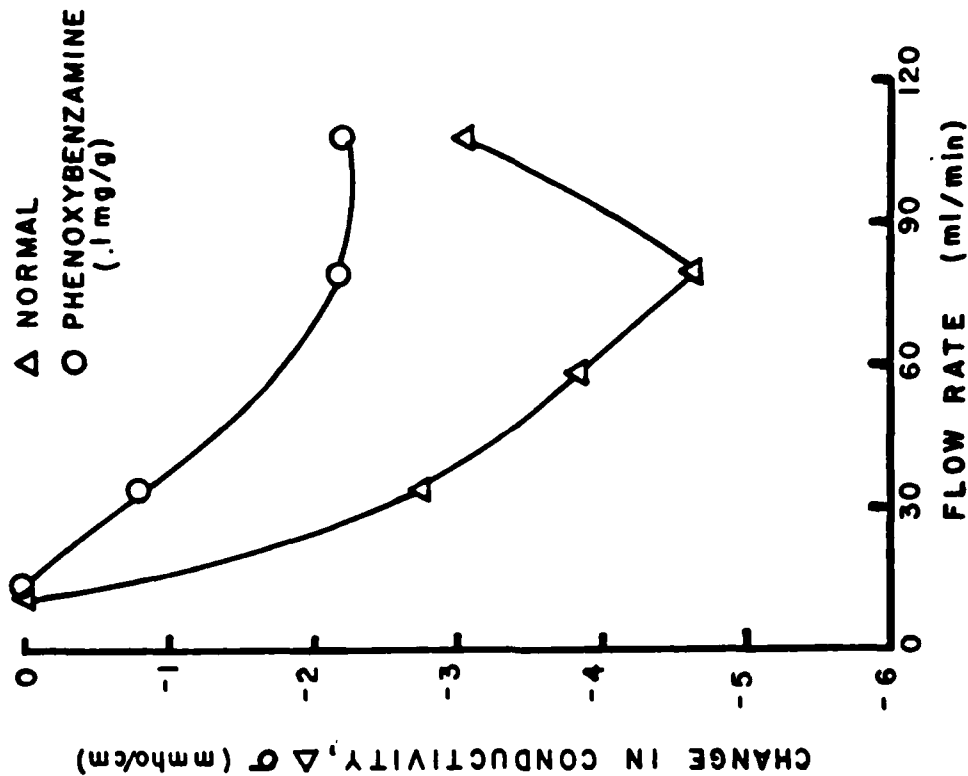


Figure 30. Changes in perfusion pressure and kidney weight as functions of flow rate while measuring dielectric properties of cortex and medulla tissues in Kidney #6.

better understanding the kidney's autoregulation mechanism. Even more exciting, if problems with attaining adequate sensitivity and resolution can be solved, is the possibility of using microwave imagery to interrogate the organ non-invasively for the purpose of studying renal flow distribution/redistribution. From such studies, it may be possible to better determine the kidney's role in hypertension and to observe how the kidney autoregulates flow under conditions of changing renal arterial pressure by redistribution.

In Annual Technical Report No. 2 [9], we speculated that the negative correlation between renal dielectric properties and total renal flow rate may in part be due to the kidney's autoregulation mechanism. Thus, the kidney acts as a system whose transfer function changes as a function of its input. In order to better study the possible active role of the kidney with respect to the observed negative dielectric property/flow correlation, it is necessary to force the kidney's transfer function to remain "constant" as a function of its input, i.e., make the transfer function itself independent of the input (within reasonable physiological limits). One method would be to "shut down" the renal autoregulation mechanism. In one experiment, after control data for each flow rate had been measured, phenoxybenzamine (0.1 mg/g) was added to the perfusate and each of the flow conditions repeated. Phenoxybenzamine was selected because of its  $\alpha$ -receptor blocking properties, which results in relaxation of vascular smooth muscle (and dilation of the vessels). The results of this experiment are shown in Figures 31-33. The major noteworthy point is that the phenoxybenzamine reduced the negative correlation between the dielectric properties and flow rate or pressure parameters (Figures 31 and 32), while having little effect with respect to control values or pressure and weight change brought about by changes in flow rate (Figure 33). Although preliminary, these results suggest that a significant role is played by the kidney's autoregulation mechanism (or vasoconstrictor release) with respect to the inverse relationship which we have repeatedly observed between renal dielectric properties and flow rate.

CORTEX



CORTEX

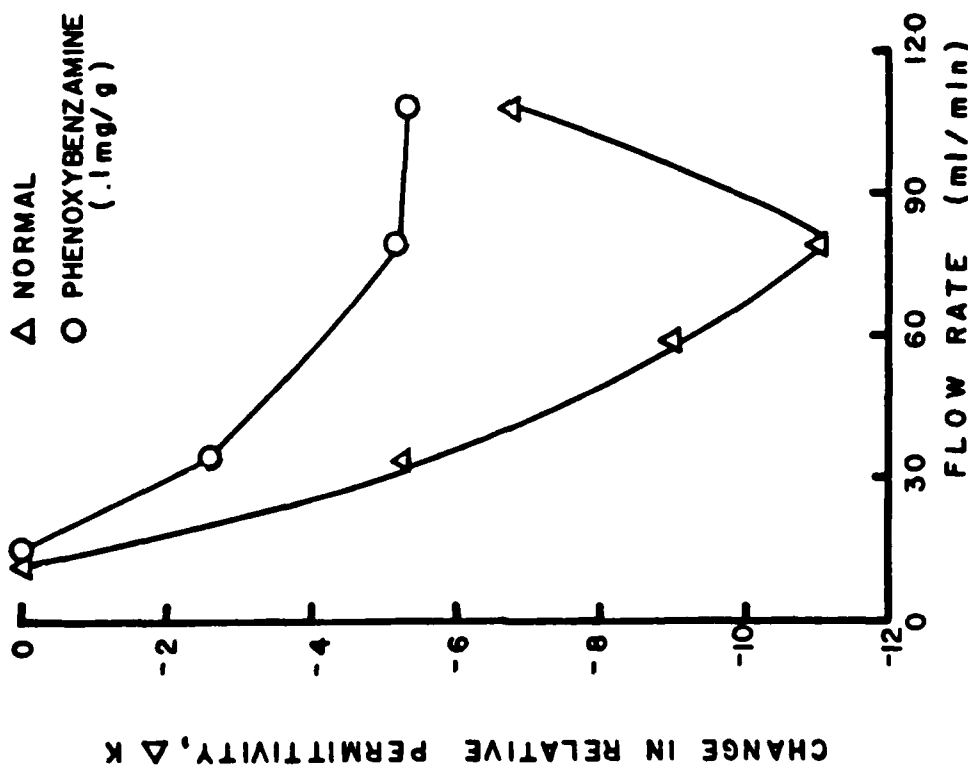


Figure 31. Comparison of baseline-subtracted dielectric properties of renal cortex in Kidney #5 under varying flow conditions, before and after administration of phenoxybenzamine. Correlation coefficients ( $r$ ) and probabilities for correlation ( $P_c$ ) are listed in Table III.

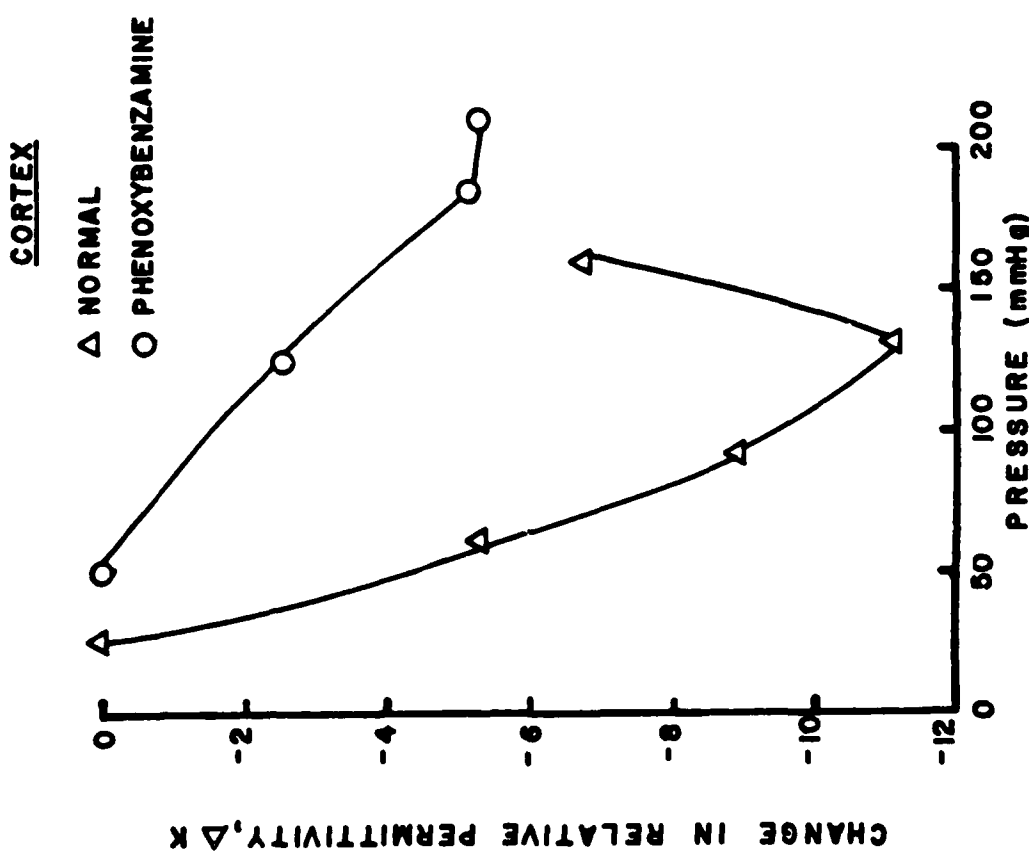
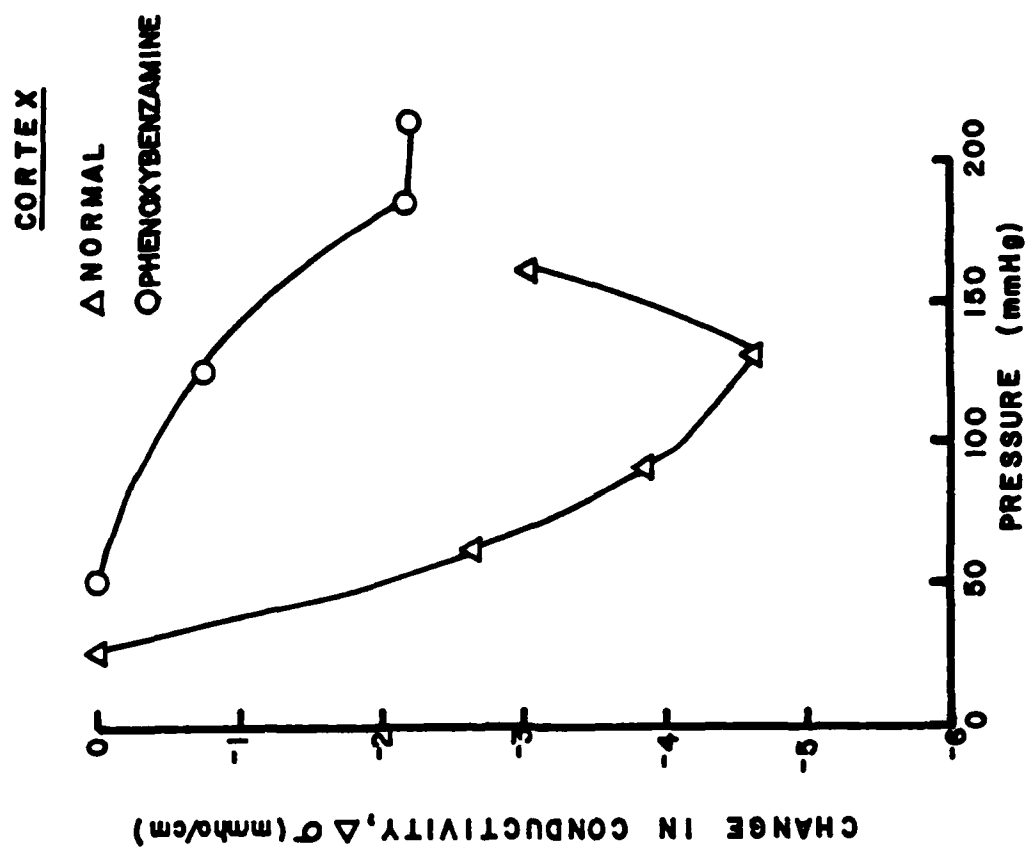
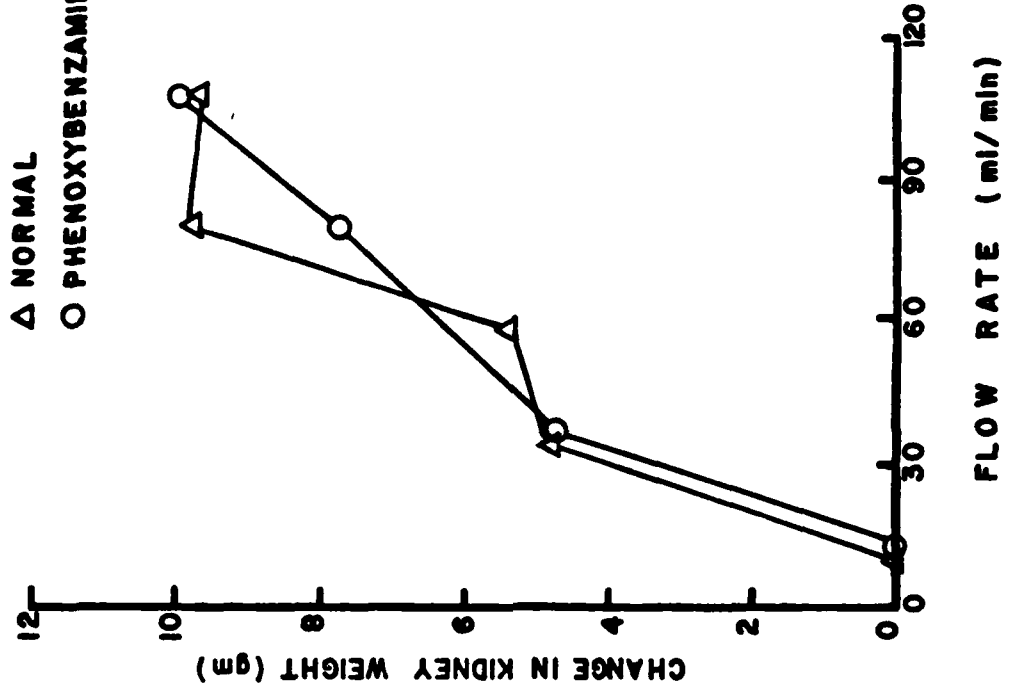


Figure 32. Comparison of baseline-subtracted dielectric properties of renal cortex in Kidney #5 under varying perfusion pressures before and after administration of phenoxybenzamine. Correlation coefficients ( $r$ ) and probabilities for correlation ( $P_c$ ) are listed in Table III.

CORTEX

Δ NORMAL  
○ PHENOXYBENZAMINE



CORTEX

Δ NORMAL  
○ PHENOXYBENZAMINE

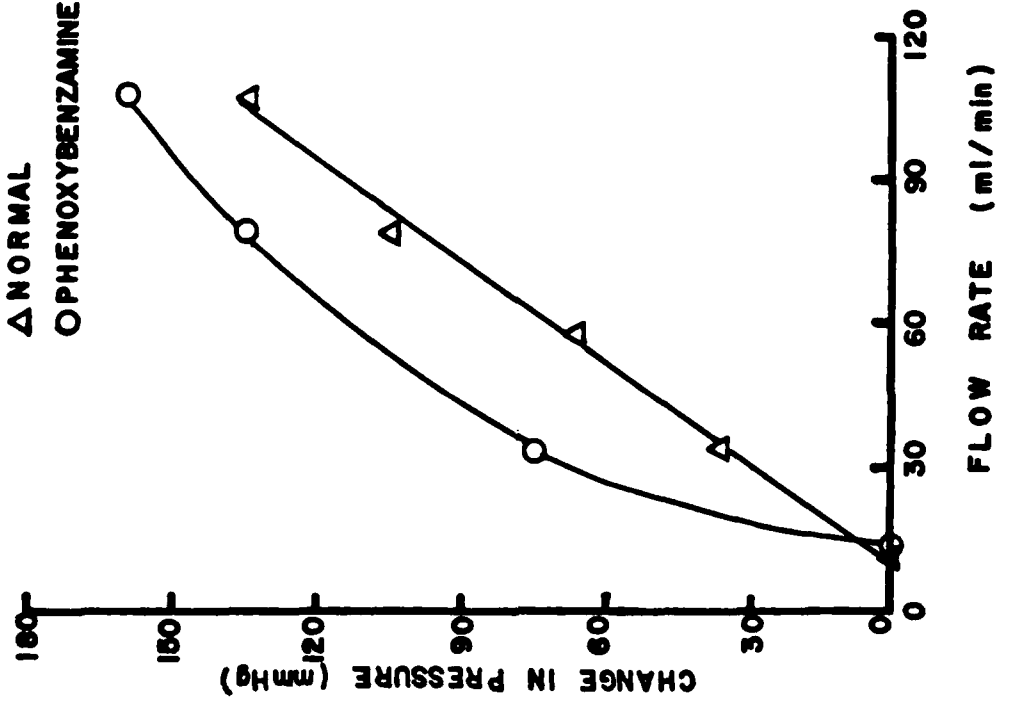


Figure 33. Changes in perfusion pressure and kidney weight as functions of flow rate in Kidney #5, before and after administration of phenoxybenzamine.

It is possible that the inverse dielectric property/flow relationship referred to above may be further decoupled by judicious choice of pharmacological agents whose actions on the kidney's "transfer function" are known. Experiments are planned to further investigate the observed phenomena described above and to hopefully determine the mechanism(s) responsible for the measured changes in dielectric properties with varying flow rate/pressure.

In-situ measurements of renal dielectric properties under controlled-flow conditions were also performed; however, the present results are preliminary because of the small number of successful experiments. It is important to know if the response of in-situ dielectric properties to flow changes are similar to observed responses in-vitro, or if cardiovascular and/or renal control mechanisms present only in-situ cause a different response in the measured permittivity as a function of flow rate and perfusion pressure. Unfortunately, several of the in-situ experiments met with surgical difficulties that precluded any data collection. Data collected from one in-situ experiment is presented in Table IV, although problems existed even in this experiment. The clear trends evident in the later in-vitro experiments did not develop here. Part of the problem was caused by noise on the analog signal from which the dielectric properties were computed. In addition, while the measurements were being made, the kidney began to bleed from a puncture wound inflicted by the probe as a result of spasms by the dog. Further efforts to measure renal dielectric properties under more desirable in-situ conditions are planned. Earlier problems with blood clotting and air bubbles in the lines have been solved, and more judicious use of anesthesia should help to prevent problems such as the one above from recurring.

TABLE IV  
IN-SITU RENAL DIELECTRIC PROPERTIES\* UNDER VARIED PERFUSION CONDITIONS

| <u>Region</u> | <u>Pump Speed<br/>(rpm)</u> | <u>Temperature†<br/>(°C)</u> | <u>Pressure<br/>(mm Hg)</u> | <u>Relative<br/>Permittivity</u> | <u>Conductivity<br/>(ms/cm)</u> |
|---------------|-----------------------------|------------------------------|-----------------------------|----------------------------------|---------------------------------|
| Surface       | 10                          | 34.0                         | 220                         | 49.75                            | 20.69                           |
| Cortex        | 10                          | 34.0                         | 170                         | 54.88                            | 24.15                           |
|               | 1                           | 34.0                         | 25                          | 56.85                            | 25.97                           |
|               | 5                           | 34.0                         | 80                          | 59.25                            | 26.06                           |
| Medulla       | 5                           | 34.0                         | 80                          | 69.47                            | 32.00                           |
|               | 7.5                         | 34.0                         | 125                         | 58.47                            | 25.24                           |
|               | 10                          | 34.0                         | 181                         | 56.11                            | 24.22                           |
|               | 15                          | 34.0                         | 256                         | 58.40                            | 25.74                           |
|               | 1                           | 34.0                         | 47                          | 56.10                            | 24.83                           |

\* Measurements made at 2450 MHz.

† Temperature Coefficients of  $-0.3\%/^{\circ}\text{C}$  for Relative Permittivity and  $-2.0\%/^{\circ}\text{C}$  for Conductivity were used to normalize tissue temperatures to  $34.0^{\circ}\text{C}$ . Temperatures of measured tissue ranged from  $32.2^{\circ}\text{C}$  to  $34.8^{\circ}\text{C}$ .

SECTION V  
CONCLUSIONS AND RECOMMENDATIONS

The research efforts performed during the third year of this four-year research program have been successfully completed. The primary third-year objectives of (1) further development of the existing measurement probe for measuring dielectric characteristics and possibly blood flow changes in-situ, (2) evaluation of data recording methods, (3) development of hardware for a multi-channel data acquisition and logging system, (4) development of software for statistical analysis of experimented results, (5) studying effects of changing renal blood flow and pressure on renal dielectric properties, and (6) preliminary investigation of the influence of pharmacological agents on renal dielectric properties were achieved. In this section, conclusions based on results of the third year's efforts are first discussed, followed by recommendations for the fourth-year efforts. The tasks reflected in these recommendations are those included in our renewal proposal for the fourth-year investigations.

A. Conclusions from Results

The dielectric probe measurement technique was further improved during the third-year efforts by modification of the spring-loaded probe holder developed during the second year for maintaining more uniform contact pressure between the probe and the tissue under study. The spring-loaded probe holder reduced probe contact related errors from 4-6% to approximately 1% of the measured dielectric constant and conductivity values. The spring-loaded probe holder allowed the probe to track minor tissue movements while maintaining good electrical contact with the tissue. Furthermore, the movement of the probe when the tissue moved prevented major interference by the probe to local blood flow.

Use of the probe for in-vivo kidney measurements involved more pronounced movements due to respiration. This necessitated modification of the spring-loaded probe holder to allow a greater range of movement.

Data were obtained in both analog and digital form, with each having advantages and disadvantages. The problem with the analog data collection is that processing of the data required a great deal of manual effort. This was a slow and tedious process. However, analog data recording did provide a continuous record of experimental events. The digital data acquisition system did a great deal of the data processing automatically; however, it permitted sampling only dielectric property data. Its major drawback was a slow sampling rate. All physiological data were recorded in analog form using stripchart recorders.

Various alternative data recording techniques were evaluated. These included analog and digital methods. From the experimental investigations, it was determined that a need existed to increase the sampling rate in order to follow rapid changes (both dielectric and physiological) and to permit accurate temporal data correlation. It was determined that the optimal solution would be the use of a digital recording system with a high data sampling rate that is gated on and off via software control. Such a system would also be automatically gated "on" at the onset of physiological change.

To meet the need for improved data acquisition and logging, a system was designed and fabricated which included 15 buffered analog data input channels plus a 10-position event marker. The buffered analog signals are routed through a multiplexing 20 kHz A/D converter to a Zenith/Heath WH-89 for recording in digital form on floppy disk. The WH-89 will also be used to control the network analyzer - based probe measurement system. Although the hardware design is complete, system control software has yet to be written. This task is included in the recommended fourth-year efforts.

The in-vitro renal dielectric property studies consistently showed an inverse relationship between changes in total renal flow (or perfusion pressure) and dielectric properties (permittivity and conductivity). The negative correlation was stronger in cortex than in medulla. Similar results were obtained for in-situ measurements. Measured changes in pressure and kidney weight with changing flow rate had a strong positive correlation, the opposite result from that obtained for the dielectric properties.

The different dielectric changes in cortex and medulla may possibly be indicative of redistribution of regional blood flow or compartmental water shifts in the kidney, information which could be useful to understanding the role of the kidney in hypertension. Renal dielectric changes measured using the in-situ probe technique suggest that the pressure-flow-volume relationship in the kidney is not a simple one, and that regional flow redistribution influences the local renal dielectric properties. Further, bulk water shifts may not be the only influencing factor in the measured dielectric changes. It is possible that measured changes reflect operation of the kidney's autoregulation mechanism. From a systems viewpoint, the kidney's transfer function changes as a function of its input, i.e., an active "feedback" pathway exists. Decoupling the feedback from the system such that the kidney's transfer function does not vary with input would make possible better study of the possible active role of the kidney with respect to the observed dielectric property/flow correlation. Use of  $\alpha$ -blocking drugs to relax vascular smooth muscle can effectively "decouple" much of the feedback process with respect to renal autoregulation. Partial success in doing this was achieved using phenoxybenzamine, as described in Section IV, Experimental Investigations. It is possible that further decoupling of the inverse dielectric property/flow relationship can be achieved with other pharmacological agents which have known effects on autoregulation. Phentolamine is one possible candidate.

Another method of examining the renal dielectric property/flow relationship would be to inject radiolabeled microspheres under several different perfusion conditions and study their distribution. Also, the use of chromium-labeled red cells, from which an Angor camera could provide a blood flow image, is an attractive method for studying renal flow distribution which was suggested by Col. L. E. Larsen, Contracting Officer's Technical Representative. Future experiments using pharmacological agents and radiolabeled tracers to further investigate the relationship described above and in Section IV are planned for the fourth-year studies.

## B. Recommended Future Efforts

Although major advancements in the realm of dielectric measurements were accomplished during the third year of this program, a number of questions of physiological significance remain. Further, the results raise additional questions that should be investigated to provide significant information to the Army in terms of EM field interaction with living tissues.

During the discussions between the Army Contracting Officer's Technical Representative and project personnel from Georgia Tech, additional tasks were identified which would require additional resources and time to accomplish. Because of the detailed experimental nature of these investigations, it is recommended that resources be allocated to perform additional tasks in fourth-year efforts. Specifically, the following additional tasks are recommended:

### Task 1. Develop Multiple-Probe Data Multiplexing System

Develop a microcomputer-controlled multiplexing system to permit simultaneous recording of information from multiple probes located at different measurement sites. The multiplexer will couple with the data processing system to provide the capability for obtaining a spatial distribution of data that reflects dynamic changes in measured properties on a real-time basis.

### Task 2. Characterize Renal Electrical Properties with Changes in Blood Flow, JGA, and GFR

Measure in-situ renal dielectric properties as a function of pharmacologically-induced changes in the juxtaglomerular apparatus and glomerular filtration rate, and as a function of renal blood flow. The influence of changes in each of the above parameters on dielectric properties will be evaluated independently and interactively in separate experiments.

Task 3. Investigate Dielectric Changes in Brain During Auditory Stimulation

Perform studies to determine the effects of auditory stimulation on in-situ dielectric properties of the auditory cortex (under halothane anesthesia). Correlate measured changes in dielectric properties with neural electrical recordings and with blood flow changes.

Task 4. Investigate Effects of Hypercapnia and Anoxia on Brain Dielectric Properties

Perform experiments under known hypercapnic and anoxic conditions (monitoring blood gases under halothane anesthesia) to determine effects of regional cerebral blood flow on in-situ dielectric properties of dog brain.

Task 5. Develop True Needle Probe for Tissue Mapping

Develop a true needle probe to permit "mapping" in-situ tissue dielectric characteristics within an organ. This development will involve the investigation of the biocompatibility of materials for probe fabrication, the design of special coaxial probes (with the outer conductor being effectively a hypodermic needle), and the design of tooling and fabrication of special connectors.

Task 6. Perform Dielectric Mapping of In-situ Brain Tissues

Characterize brain tissue as a function of depth beneath the pial surface by performing dielectric measurements using the needle probe.

SECTION VI  
REFERENCES

1. L.E. Larsen and J.H. Jacobi, "Microwave interrogation of dielectric targets. Part I: By scattering parameters", Med. Phys., Vol. 5, No. 6 pp. 500-508, 1978.
2. J.H. Jacobi and L.E. Larsen, "Microwave interrogation of dielectric targets. Part II: By microwave time delay spectroscopy", Med. Phys., Vol. 5, No. 6, pp. 509-513, 1978.
3. L.E. Larsen and J.H. Jacobi, "Microwave scattering parameter imagery of an isolated canine kidney", Med. Phys., Vol. 6, No. 5, pp. 394-403, 1979.
4. J.H. Jacobi and L.E. Larsen, "Microwave time delay spectroscopic imagery of isolated canine kidney", Med. Phys., Vol. 7, No. 1, pp. 1-7, 1980.
5. E.C. Burdette, F.L. Cain, and J. Seals, "In-Vivo Determination of Energy Absorption in Biological Tissue," Final Technical Report, Project A-1755, U.S. Army Research Office Grant No. DAAG29-75-G-0182, January 1979.
6. E.C. Burdette, F.L. Cain, and J. Seals, "In-Vivo Probe Measurement Technique for Determining Dielectric Properties at VHF Through Microwave Frequencies," IEEE Trans. Microwave Theory Tech., Vol. 28, No. 4, pp. 414-428, 1981.
7. E.C. Burdette, F.L. Cain, and J. Seals, "In-Situ Permittivity Measurements: Perspective, Techniques, Results," Electromagnetic Dosimetric Imagery Symposium, 1980 IEEE MTT-S International Symposium, Washington, D.C., May 1980 (IEEE Press, New York).
8. E.C. Burdette, R.L. Seaman, J. Seals, and F.L. Cain, "In-Vivo Techniques for Measuring Electrical Properties of Tissues," Annual Technical Report No. 1, Project A-2171, U.S. Army Medical Research and Development Command, Contract No. DAMD17-78-C-8044, July 1979.
9. E.C. Burdette, P.G. Friederich, and F.L. Cain, "In-Vivo Techniques for Measuring Electrical Properties of Tissues," Annual Technical Report No. 2, Project A-2171, U.S. Army Medical Research and Development Command, Contract No. DAMD17-78-C-8044, September, 1980.
10. A.R. Von Hippel, Dielectric Materials and Applications, M.I.T. Press, Cambridge, Mass., 1954.

11. J.D. Kraus, Antennas, McGraw-Hill Book Company, New York, 1950.
12. I.J. Bahl and S.S. Stuchly, "Effect of Finite Size of Ground Plane on the Impedance of a Monopole Immersed in a Lossy Medium," Electronics Letters, Vol. 15, No. 22, p. 728-729, 1979.
13. W.J. Dixon and F.J. Massey, Introduction to Statistical Analysis, McGraw-Hill Book Company, New York, 1969.
14. P. R. Bevington, Data Reduction and Error Analysis for the Physical Sciences, McGraw-Hill Book Company, New York, 1969.